

Doctoral theses at NTNU, 2023:51

Stefanie Tomasch

Application and development of dissipation based combustion models for conventional and unconventional combustion processes

ISBN 978-82-326-5305-8 (printed ver.)
ISBN 978-82-326-6513-6 (electronic ver.)
ISSN 1503-8181 (printed ver.)
ISSN 2703-8084 (electronic ver.)

Doctoral theses at NTNU, 2023:51

NTNU
Norwegian University of
Science and Technology
Thesis for the degree of
Philosophiae Doctor
Faculty of Engineering
Department of Energy and Process Engineering

 **NTNU**
Norwegian University of
Science and Technology

 NTNU

 **NTNU**
Norwegian University of
Science and Technology

Stefanie Tomasch

Application and development of dissipation based combustion models for conventional and unconventional combustion processes

Thesis for the degree of Philosophiae Doctor

Trondheim, March 2023

Norwegian University of Science and Technology
Faculty of Engineering
Department of Energy and Process Engineering



Norwegian University of
Science and Technology

NTNU

Norwegian University of Science and Technology

Thesis for the degree of Philosophiae Doctor

Faculty of Engineering

Department of Energy and Process Engineering

© Stefanie Tomasch

ISBN 978-82-326-5305-8 (printed ver.)

ISBN 978-82-326-6513-6 (electronic ver.)

ISSN 1503-8181 (printed ver.)

ISSN 2703-8084 (electronic ver.)

Doctoral theses at NTNU, 2023:51



Printed by Skipnes Kommunikasjon AS

Abstract

Concepts for burner operation have manifolded under the influence of increasing performance demands for combustion processes. This is to support the global effort to reduce pollution and greenhouse gas emissions radically. The trend to more efficient, environment-friendly process design has also led to increasingly complex burner-operating conditions and the growing importance of finite-rate chemistry phenomena such as flame thickening, local extinction etc.

Computational Fluid Dynamics has the potential to effectively complement experimental research to achieve a higher level of understanding of the combustion process. However, the complex turbulence-chemistry interaction in modern combustion processes challenges the fundamental assumption of (infinitely) thin reaction zones (flamelets), which many turbulent combustion models build upon. The focus of this thesis is the application and development of dissipation-based combustion models that are capable of including finite-rate chemistry effects and relaxing the limiting thin flame assumption. One merit of dissipation-based models with finite-rate chemistry is their flexible applicability under a broad range of flame and flow conditions.

The first part of the thesis deals with the application of the well-known Eddy dissipation concept (EDC) with finite-rate chemistry calculation to turbulent flames under varying conditions. Following some preliminary studies of the EDC in the RANS framework for conventional combustion, the main work was the modelling of a lab-scale MILD burner using the EDC with Large eddy simulation (LES). The aims of the corresponding Paper I are the evaluation of the EDC and a second dissipation-based combustion model, the Partially stirred reactor model (PaSR) in LES using measurements for the MILD burner, their direct comparison in terms of modelling performance and the discussion of the observed reacting flow to gain insights into this operational mode. An important conclusion from this study is that dissipation-based combustion models show competitive

performance in predicting the reacting flow under MILD conditions when compared to other modelling approaches in the literature. Potential challenges arise, however, for the choice of proportionality constants in the context of LES, which is especially relevant for the EDC.

An algebraic dissipation-based combustion model was developed and evaluated in a second comprehensive study within the thesis. The new combustion model addresses some of the challenges observed in the previous part. Motivations were to reduce computational expenses, improve compatibility with LES theory, relax presumptions on the flame structures, and avoid the necessity to adjust proportionality constants. The key output of this study is a new combustion model evaluated using measurements and numerical results from sophisticated, well-documented combustion models found in the literature for two different premixed flames. Papers II and III provide promising results concerning the applicability of the new model to complex premixed reacting flows showing competitive performance to capture moderate flame thickening and local extinction. Another advantage of the model is the strong coupling between the modelled heat release and reaction rate.

Following the successful application of the new dissipation-based combustion model to two premixed air-methane flames, the results of a preliminary study investigating an oxy-methane flame are shown. Compared to the previous studies, the complexity increased considerably due to the non-unity Lewis number of the fuel in the investigated O_2/CO_2 oxidiser, the altered chemical activity, and the changed thermal behaviour of the oxidiser. Satisfactory results were achieved for predicting the reacting flow field. However, they also indicated that the characteristics of the oxy-fuel set-up need to be better taken into account by the modelling approach.

Preface

The subsequently presented doctoral thesis was conducted at the Norwegian University of Science and Technology (NTNU), Department for Energy and Process Engineering (EPT) under the supervision of Prof. Ivar S. Ertesvåg, Dr. mont. Christoph Spijker and Dr. Eng. Dmitry Lysenko. The PhD work was part of the OxyFUN project (project No. 268369) headed by SINTEF Energy Research and was funded by the Research Council of Norway through the national research program for CCS technologies CLIMIT.

Acknowledgements

Many people have provided support and guidance on the sometimes challenging way to complete this thesis. I would like to express my sincere gratitude to them, knowing that I would have never come this far without their help. First and foremost, I would like to thank Professor Ivar S. Ertesvåg for the chance to do my Ph.D. under his supervision, for his patience, and continuous support, and for always being there when needed. I sincerely thank Professor Nedunchezian Swaminathan for welcoming me as a visitor to his group at the University of Cambridge and for his invaluable advice and guidance during the last few years. His interest in and commitment to this work have been a great motivation for me.

Also, my gratitude goes to my co-supervisor Dr. Christoph Spijker, who, together with Dr. Werner Pollhammer has always had an open ear and good advice for me. I am very glad for their continuous support since I started to work with them as a Master student. I would also like to acknowledge the support from the Research Council of Norway and the excellent IT support I received from the IT Staff at the Norwegian Research Infrastructure Services (NRIS) and Sigma 2 and from Mr. Peter Benie at the University of Cambridge.

I would also like to thank all my colleagues for the good collaboration and for the eventful and enjoyable time together. Silje, Ehsan, Knut, thank you for "adopting" me into your group and for all the fun game nights, and skiing trips, and dinners that were a welcome distraction from the daily fights with the Ph.D. work. Zhiyi, Zhi, James, Dimitrios, thank you for making my stay in Cambridge a time I like to think back to. To my colleagues from Leoben, Christian, Gregor, Renata, Mario, Werner, thank you for your friendship and the fun times we have together.

Finally, I would like to thank my wonderful family. Elisabeth and Wolfgang, you are the best, most generous acquaintances/ parents-(not)-in-law one can have. Melanie, thank

you for being such a great sister, study colleague, housemate, travel companion, and friend. Daniela and Manfred, I am so entirely grateful to have such wonderful parents, there are no words that could express what your everlasting support means to me. Last but not least, thank you Felix for your love and support, for trusting in me when I don't, for always pushing me to do my best, and for your heartfelt honesty.

Contents

Part I Thesis Background

1	Introduction	3
1.1	Combustion as energy supply and its perspective in the 21 st century	3
1.2	Combustion concepts	3
1.3	Combustion Computational fluid dynamics	4
1.4	Knowledge gap in literature	5
1.5	Aims, scope	11
1.6	Summary of work	12
2	Modelling	14
2.1	Turbulence modelling	14
2.2	RANS modelling	14
2.3	Turbulent combustion modelling and the EDC	15
2.4	LES	18
2.5	Differences between the LES combustion models applied in Papers I-III	18
2.6	Implementation of the algebraic dissipation-based combustion model	19
3	Preliminary Results	21
3.1	General	21
3.2	Cold flow unsteady RANS simulations	21
3.3	Reacting jet flame RANS-EDC simulations	26
3.4	Transferring Paper III's numerical setup to an oxyfuel flame	31
3.5	Insights from the preliminary studies	37
4	Contributions to the research output	38

4.1	Overview	38
4.2	List of papers	39
5	Conclusion and outlook	40
References		43
 Part II Research Output		
	Paper I	55
	Paper II	67
	Paper III	89
 Part III Appendix		
A	Supplementary data	123
A.1	Cold Sydney swirl burner velocity variations	123
A.2	Sandia Flames D	124
A.3	Swirl-stabilised oxy-fuel flame velocity variations	128

List of publications

Peer-reviewed journal publications

- * Zhiyi Li, Stefanie Tomasch, Zhi X. Chen, Alessandro Parente, Ivar S. Ertesvåg, Nedunchezian Swaminathan, *Study of MILD combustion using LES and advanced analysis tools*, Proceedings of the Combustion Institute, Volume 38, Issue 4, 2021, Pages 5423-5432, ISSN 1540-7489, DOI: 10.1016/j.proci.2020.06.298.
- * Stefanie Tomasch, Nedunchezian Swaminathan, Christoph Spijker, Ivar S. Ertesvåg *Development of a turbulence dissipation based reaction rate model for progress variable in turbulent premixed flames*, Combustion Theory and Modelling, 26:5, 896-915, 2022, DOI: 10.1080/13647830.2022.2083525

Submitted manuscripts

- * Stefanie Tomasch, Nedunchezian Swaminathan, Christoph Spijker, Ivar S. Ertesvåg *A numerical study of flow structures and flame shape transition in swirl-stabilized turbulent premixed flames subject to local extinction*. Submitted to a journal Dec. 2022

Additional publications

- * S.Tomasch, I. Ertesvåg, *CFD Simulation of an Axisymmetric Sudden Duct Expansion*. The Joint meeting of the Polish and Scandinavian-Nordic Sections of the Combustion Institute. Krakow September 6-7, 2018. (Conference proceeding / Oral presentation)

- * S.Tomasch, I. Ertesvåg, *Towards a better understanding of oxy-fuel combustion - An approach using CFD for natural gas SCGT/CC*. CLIMIT PhD and PostDoc Seminar 2019. Oslo January 18, 2019. (Visual presentation)
- * S. Tomasch, I. Ertesvåg, *The influence of the reactor model on EDC's mean reaction rate - A study on the relevance of choice*. 9th European Combustion Meeting. Lisboa April 14-17, 2019.

Nomenclature

Acronyms

CCS	Carbon capture and storage
CFD	Computational fluid dynamics
DNS	Direct numerical simulation
EDC	Eddy dissipation concept
FVM	Finite volume method
GHG	Greenhouse gases
IEA	International Energy Agency
LES	Large eddy simulation
MILD	Moderate or intense low-oxygen dilution
ODE	Ordinary differential equation
OpenFOAM	Open-source field operation and manipulation software
PaSR	Partially stirred reactor
PDF	Probability density function
PFR	Plug flow reactor
PSR	Perfectly stirred reactor
RANS	Reynolds-averaged Navier-Stokes
RMS	Root mean square

RSM	Reynolds stress models
SAS	Scale-adaptive simulation
SGS	Subgrid-scale
SST	Shear stress transport
UN	United Nations
URANS	Unsteady Reynolds-averaged Navier-Stokes

Roman letters

Symbol	Definition	Formula	Dimension
c	Progress variable		
C_{D1}	EDC model constant		
C_{D2}	EDC model constant		
c_P	Constant pressure specific heat capacity		J/kg/K
D	Diameter		m
Da	Damköhler number	t_f/t_c	
D_{mix}	Diffusion coefficient of mixture		m^2/s
D_r	Diffusion coefficient of reactants mixture		m^2/s
k	Turbulence kinetic energy	$1/2(\overline{u'_i u'_i})$	m^2/s^2
Ka	Karlovitz number	t_c/τ_{Kol}	
k_{SGS}	Subgrid-scale turbulence kinetic energy		m^2/s^2
L'	Turbulence macro length scale	$\propto u'^3/\epsilon$	m
Le	Lewis number	$\alpha_{\text{th}}/D_{\text{mix}}$	
L_{EDC}^*	Length scale of EDC reacting structure		m
L_F	Laminar flame thickness	D_{mix}/S_L	m
m	(Reactor) Mass		kg
\dot{m}	Mass flow rate		kg/s

\dot{m}^*	EDC normalized fine structure mass flow rate	$1/\tau^*$	1/s
\dot{m}_k'''	Species production rate		kg/s
r	Radial position		m
R	Radius		m
R_O	Outer radius		m
R_i	Volumetric reaction rate of species i		kg/m ³ /s
Re	Reynolds number	UD/ϑ	
Re_t	Turbulence Reynolds number	$u' L'/\vartheta$	
Re_ν	Reynolds number (Kolmogorov scales)	$\nu \eta/\vartheta$	
S	Swirl number		
S_L	Laminar flame speed		m/s
$S_{u,0}$	Laminar flame speed		m/s
S_{ij}^*	Mean rate of strain tensor		1/s
t_{EDC}^*	Time scale of the EDC reacting structure		s
T_{ad}	Adiabatic temperature		K
T_0	Initial temperature		K
t_c	Chemical time scale		s
t_f	Turbulence macro time scale		s
TI	Turbulence intensity	u'/U	
u_{EDC}^*	Velocity of the EDC reacting structure		m/s
$U_{B(ulk)}$	Bulk velocity		m/s
u'_i	Fluctuating velocity		m/s
U_e	Velocity air co-flow		m/s
U_j	Jet velocity		m/s
U_s	Axial velocity component of the swirling inflow		m/s
W_s	Tangential velocity component of the swirling inflow		m/s
x	axial position		m

Y_k Mass fraction of species k

Z Mixture fraction

Greek letters

Symbol	Definition	Formula	Dimension
α_{th}	Thermal diffusion coefficient	$\lambda_{\text{th}}/(\rho c_p)$	m^2/s
γ^*	EDC fine structure mass fraction		
δ_{ij}	Kronecker delta		
δ_{L}	Laminar flame thickness		m
δ_{r}	Reaction layer thickness		m
ϵ	Turbulence kinetic energy dissipation rate		m^2/s^3
ϵ_{SGS}	SGS turbulence kinetic energy dissipation rate		m^2/s^3
η_{Kol}	Kolmogorov length scale	$(\vartheta^3/\epsilon)^{1/4}$	m
ϑ	Kinematic viscosity		m^2/s
ϕ	Equivalence ratio		
ϑ_{t}	Kinematic eddy viscosity	μ_{t}/ρ	m^2/s
κ	Wave length		$1/\text{m}$
λ_{th}	Heat conductivity		$\text{W}/\text{m}/\text{K}$
μ	Dynamic viscosity		$\text{kg}/\text{m}/\text{s}$
μ_{t}	Dynamic eddy viscosity		$\text{kg}/\text{m}/\text{s}$
ν_{Kol}	Kolmogorov velocity scale	$(\vartheta\epsilon)^{1/4}$	m/s
ρ	Density		kg/m^3
σ_c^2	Progress variable variance		
τ_{res}	Residence time		s
τ^*	EDC fine structure residence time		s
τ_{Kol}	Kolmogorov time scale	$(\vartheta/\epsilon)^{1/2}$	s
τ_{res}	Reactor residence time	\dot{m}/\dot{m}	s
ω	Specific turbulence dissipation rate	$\propto \epsilon/k$	$1/\text{s}$
ω_k	Volumetric reaction rate of species k		$\text{kg}/\text{m}^3/\text{s}$

Functions and Operators

Symbol	Definition
\square'	Fluctuating
$\tilde{\square}$	Favre-averaging/ -filtering
$\bar{\square}$	Reynolds-averaging / LES-filtering
$\langle \square \rangle$	time-averaging
$\nabla \square _{\max}$	maximum gradient

Part I
Thesis Background

1 Introduction

1.1 Combustion as energy supply and its perspective in the 21st century

Combustion has constituted a driving force of human evolution for thousands of years [1]. In this course, it underwent a remarkable development in its application from simple bonfires providing heat and light to high-tech rocket engines used in space flights. Fossil fuels as key sources of energy have become inextricably linked to industrialisation. In this context, they have facilitated social, political, and economic upheavals [1]. Their usage is indisputably related to pollution and emission of greenhouse gases (GHG) [1], and broad agreement exists among experts that these emissions are contributing to the anthropogenic climate change [2, 3]. The effort to act against the incipient climate crisis has increased recently. Attracting attention worldwide, 2015's UN climate change convention in Paris achieved to reach international commitment to the aim of keeping the anthropogenic global temperature increase considerably below 2 degrees Celsius [4]. In contradiction to this mark, there is agreement among relevant reports, e.g. [5], that the global energy demand will continue to increase over the next decades. The necessary successive transformation of the energy generation sector towards emission neutrality is in progress, but, as has been stated for example by Swaminathan [6], will be too slow to be able to reduce the share of combustion considerably within the coming decades. To put the importance of fossil fuels for energy supply into perspective, the 2019 World Energy Outlook from the International Energy Agency [7] documented that in 2018 more than 81% of the primary energy demand was still covered by oil, coal, and gas. Consequentially, combustion continues to play a considerable role in the global energy supply in the nearer future, and efficiency enhancement and emission reduction of combustion processes are of utmost importance to contribute to the global effort to cut down greenhouse gas emissions.

1.2 Combustion concepts

Within the last years, concepts for burner operation have manifolded under the influence of increasing performance demands concerning thermal efficiency and emissivity behaviour. An overview of relevant research topics can be found in [8]. Novel technologies try to access adverse aspects of combustion such as heat loss, material wear out, and emission formation from different angles. Very lean premixed flames exhibit a modest

temperature increase which, together with the perfect mixing and a large oxygen excess suppress extensive emissions. The so-called moderate or intense low-oxygen dilution (MILD) combustion is targeted at reducing the peak temperatures and promoting an almost homogeneous reaction and composition field and has the potential to increase the process efficiency while concurrently reducing emissions [9]. Its onset is connected to well-defined conditions, as will be discussed in Section 1.4. Finally, oxyfuel combustion, as part of the carbon capture and storage (CCS) technology, aims to decouple the combustion process completely from emissions by collecting flue gases and supplying them for subsequent use or deposition. In terms of thermal and reactive properties, oxyfuel can deviate strongly from conventional air-fuel combustion.

The drawback of lean premixed flames, potentially operating close to the lean blow-out limit, is the tendency to dynamic behaviour [10, 11] and the danger of flashback. As stated in [9], the MILD operational mode can be categorised as a separate combustion regime. It is characterised by distributed heat release and small temperature gradients, a feature that distinguishes MILD from conventional combustion taking place in thin high-temperature layers [6]. Oxyfuel combustion, implying the burning of fuel with pure oxygen instead of air, results in substantially lower mass streams and higher temperatures, an undesirable condition in light of the influence of temperature. To deal with this problem, composition and mass flow in oxyfuel flames are commonly controlled by adding a diluent, a circumstance that changes combustion conditions considerably in terms of kinetics, radiation, etc. [12]. The main combustion products CO_2 and H_2O are popular to imitate recirculated flue gas [13]. The variation of diluents as well as flexible compositions described in the literature combine highly diverse combustion conditions under the generic term of oxyfuel combustion. All emergent, unconventional operational modes, devised to meet future requirements, have in common that they are presently still at an early stage of development. However, a comprehensive picture of the combustion process is indispensable for the successful implementation of any new technology [14].

1.3 Combustion Computational fluid dynamics

In this context, effective complementation of experimental research by numerical modelling of combusting flows using Computational Fluid Dynamics (CFD) methods is desirable but requires reliable and validated tools. The fast advance in computing power that has taken place over the last few decades has promoted the development towards this aspired goal [15]. The strength of CFD is that data for several quantities are accessible

in a high resolution of space and for transient simulations also time. This is particularly important for a better understanding of the combustion process, as temperature distribution, gas composition, and flow patterns all affect the reaction pathways and control the output of a burner in a highly non-linear manner. CFD simulations of combustion processes use, to a varying degree, models of the real processes to describe chemistry, turbulence, and their interaction observed over a large spectrum of scales. The easier access to powerful computational resources enables us to use methods with continuously strengthened relation to the real fluid-dynamical/chemical problem but also raises the bar concerning modelling performance [15]. The trend to more efficient, environmentally-friendly process design also leads to increasingly complex operating conditions to be tackled by combustion modelling.

1.4 Knowledge gap in literature

Turbulent flames occur in different configurations, facilitated by the strong non-linearity of both turbulence and chemical kinetics [16] interacting to shape them. Many models and sub-versions of models are available to describe turbulent flames. A comprehensive overview is given by Swaminathan et al. [17]. Many of these models show similarities or conceptual links, as was shown by Veynante and Vervish [18].

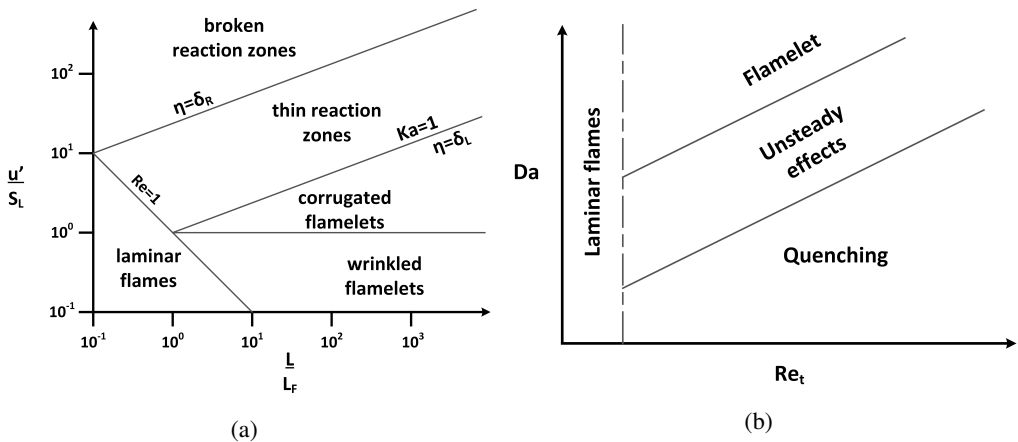


Fig. 1 Turbulent combustion regime diagrams for (a) premixed and (b) non-premixed flames based on [19] and [18], respectively.

From the first efforts in the 1970s onward, it was tried to organise flames based on their expected behaviour, or more precisely, their structure. Diagrams of flame regimes determined from global flame and flow quantities were developed by several authors inde-

pendently and are still an important tool to estimate a turbulent flame's global behaviour. The main idea is to classify flames through two independent groups of dimensionless quantities composed of chemistry and turbulence scales. Peters' [19] version, shown in Figure 1a, is one of the best-known regime diagrams for premixed turbulent combustion. Under premixed conditions, the combustion process is dependent on the mixing of fresh and burnt gases, controlled by turbulence at sufficiently high Reynolds numbers. In Figure 1a, turbulence is represented by (large) turbulence velocity and length scales u' , L' and chemistry by the intrinsic flame speed and thickness S_L , L_F . The intrinsic laminar flame speed S_L is governed by the interaction of chemistry, diffusion, and heat release. The ratio of scales between laminar flame and turbulence controls the structure, as suggested by the regime diagram in Figure 1a.

Flame regimes for turbulent non-premixed flames are commonly assessed through the global position of the flame in a Re_t - Da -diagram [18], as shown in Figure 1b. One aspect of this choice is that no intrinsic velocity can directly be related to the non-premixed flame. Non-premixed flames are governed by the two interacting processes of reaction and fuel-oxidiser mixing. The ratio of the related time scales is referred to as Damköhler number Da and plays an important role in the assessment of the flame structure [20]. Turbulence speeds up the mixing process by increasing the flame surface. Quantitatively, this can be assessed using the turbulence Reynolds number Re_t , which gives information on the strength of the prevailing turbulence. For combustion CFD, these regime diagrams provide an important orientation for the choice of the modelling approach, as not only the flame structure but also most combustion models and their assumptions can be connected to specific regimes, which becomes clear from the analysis in [18].

Both non-premixed and premixed combustion shows a combustion regime characterised by thin flamelets. In this regime, the flame surface is deformed by turbulence, but due to fast chemistry, even the smallest eddies are too large to enter and change the approximately laminar and undisturbed flame structure. This regime has been investigated thoroughly in experimental studies of premixed [21] and non-premixed turbulent flames, see the analysis in [22] and the references therein. Most combustion models were designed to operate close to this flamelet regime, which is underpinned by the review of Veynante and Vervish [18]. First, in many simple flame configurations, such as jet flames, chemical time scales are expected to be small enough for reaction zones to be undisturbed by turbulence [22]. Second, it is convenient to omit the spatial extent of flame structures or approximate them to behave like undisturbed laminar flames, which are straightforward to solve. However, many studies have emerged that report on the limits of the thin flame assumption. Meneveau and Poinso [23], for example, stated

that the quenching of chemistry through turbulence is an important aspect controlling the validity of the flamelet assumption. Also, flame thickening, which has been studied using high-fidelity experimental and numerical methods for instance in [24, 25], opposes the thin flamelet assumption. The emergence of new operational concepts aimed at improving the performance and control of combustion processes has been accompanied by the increased importance of chemistry [26]. This was stated in [27] specifically for lean premixed combustion and in [6] for MILD combustion. The focus of the thesis was on the investigation and development of combustion models capable of including finite-rate chemistry effects, relaxing the thin flamelet assumption by which many combustion models are limited. Most turbulent flames undergo chaotic transitions between different kinetic and flame regimes [9] and the applicability of a combustion model in a broad range of conditions is therefore highly beneficial.

Especially the alternative operation mode of flameless combustion [28] is characterised by slow kinetics and distributed reaction zones and heat release [6]. Cavaliere and Joanon [9] introduced the MILD operation mode as a clearly defined sub-category of flameless combustion, which makes it well comparable and reproducible and has led to considerable interest both from the experimental [29–31] as well as simulation side [32–34]. Mixing-based finite-rate chemistry combustion models have played a major role in the simulation of MILD burners from the beginning. Christo and Dally [35] noted in a very early numerical study of MILD combustion an improved performance of the Eddy dissipation concept (EDC) with finite-rate chemistry calculation, developed by Magnussen and co-workers [36–39], over a classical flamelet model. Subsequently, several studies, among others [40–42], investigated the performance of the closely related EDC and Partially stirred reactor (PaSR) models to investigate MILD burners. These studies were performed in the RANS modelling framework.

Flow control in modern combustion systems involves multiple highly complex flow structures that influence the flame beneficially in terms of efficiency, emissivity, etc. Phenomena such as rotation, separation, curvature, and interacting shear/boundary layers, to name a few examples, are commonly observed in realistic combusting flows. However, these flow features are well-known to cause anisotropy, inhomogeneity, and three-dimensionality in the flow [43]. Many studies have previously stressed the shortcomings of RANS eddy-viscosity based approaches to model these flows correctly, e.g. [44, 45]. The strong dependence of the flame structure on prevailing turbulence conditions makes combustion CFD very sensitive to inaccuracies connected to the choice of the turbulence model. Studies in literature providing direct comparisons of RANS and LES, among others [46, 47], commonly conclude that improved capture of the flow physics is achieved

using LES. However, for combusting flows, it has been stated by Lysenko et al. [48] that discrepancies between the approaches can be a consequence of the used turbulence closure but also of the sub-models applied to capture turbulence-chemistry interaction. Especially the effect of the latter is difficult to assess objectively as most combustion models, among them also the popular EDC and PaSR, were developed for the RANS framework, which distinguishes itself considerably from the LES methodology. The key assumption that considerable parts of the chemical processes take place in the unresolved spectrum of scales is expected to hold for LES, as has been stated in many studies before [48–51]. The filter scale in LES is commonly located in the inertial range, while reactions are connected to micro-mixing mainly taking place in the viscous range of the turbulence spectrum. For the EDC, different paths have been followed to apply it within the LES framework. To give a short overview of existing approaches in an order of increasing deviation from the original formulation, a direct transfer of the EDC model into the LES framework was chosen in [48–50]. Panjwani et al. [50] adjusted the constants included in the cascade model to take into account the part resolution of the turbulence spectrum. Chen et al. [51] revised the cascade model to adjust it to LES and derived relations between the SGS turbulence kinetic energy k_{SGS} , its dissipation rate ϵ_{SGS} , and the respective total quantities k , and ϵ . Jella et al. [52] applied double-filtering of the flow field to analyse the cascade and used EDC constants that were adjusted to the local flow conditions. Panjwani et al. [50] and Lysenko et al. [48] investigated a non-premixed turbulent jet flame, Chen et al. [51] investigated a hot pool fire, and Jella et al. [52] a swirl-stabilised partially premixed flame. Jella et al. provided a comparison with RANS-EDC results but the investigated flame was stabilised by a strong swirling flow with a swirl number of $S = 1.3$, under which conditions RANS two-equation turbulence models are known to perform poorly. The application of LES per se is expected to improve results considerably under these conditions, independent of the combustion model. Issues as outlined in [51, 52] undoubtedly exist for a direct transfer of the EDC into the LES framework, nevertheless, the connection of this approach to the original formulation of the EDC has merit for the evaluation of changes from RANS to LES, but also reformulations of the LES-EDC cascade model.

The discussion of literature from above has underpinned the merit of dissipation-based models with finite-rate chemistry calculation, especially their broad applicability and relevance for modern combustion systems. Knowing the challenges of existing LES combustion models is highly conclusive for further developments. One major issue that has already been addressed is the role of proportionality constants in the EDC. The difficulty is to adjust them to a certain flame, or even more so to local conditions in the

flame. An analysis of the scientific discussion on this topic is given by Ertesvåg [53]. Model constants originally developed in the framework of RANS are highly challenging to adjust to LES. This is due to the varying part resolution of the turbulent flow field with strong intermittency effects that have to be considered. In addition, on-the-fly stiff chemistry calculations and transport equations for every included species are very limiting for the application in the per se already computationally expensive LES framework.

Lean, turbulent premixed flames can be subject to considerable dynamic behaviour [10, 11] and require stabilisation through flow control to prevent blow-off. Different passive flow control measures were taken in [54–56]. For this type of combustion, the transient LES is highly relevant to capture the dynamic combustion process satisfactorily. A large number of LES studies of premixed flames exists in the literature. Some recent ones are given subsequently. Finite-rate chemistry effects are broadly observed due to the comparatively larger chemical time scales in lean combustion [27]. The deviation of the flame structures from the thin flamelet assumption in lean premixed combustion [27] also leads to the growing importance of resolved contributions to micro-mixing and reactions under these conditions. Dunstan et al. [57] showed through DNS analysis that qualitative disagreement between the behaviour of reaction and dissipation rate existed for increasingly resolved flame structures, related to a significant contribution of the burning mode PDF (probability density function). From this, it becomes clear that flexible LES combustion models are required to cope with local finite-rate chemistry effects and partial flame resolution.

A lean premixed turbulent flame, stabilised behind a bluff body undergoing flame thickening, was simulated using an unstrained laminar flamelet model in [58, 59]. Modelling of partially premixed and premixed flames with local extinction was carried out by Chen et al. [60] and Wang et al. [27], both using a presumed probability density function approach. The former used unstrained steady laminar flamelets, the latter a reaction-diffusion manifolds approach. The influence of the equivalence ratio on the flame shape and structure in a sudden duct expansion with swirling flow was investigated in [61] using a Thickened flamelet approach. All of these studies used LES turbulence modelling.

The burner investigated in [61] was also part of a study on oxyfuel combustion of methane, detailed in [62] and described in several articles [56, 63, 64]. Oxyfuel combustion is another unconventional operation mode, which has raised interest in combination with carbon capture and storage (CCS) technology. Suitable experimental studies that can be used for evaluating simulation results are scarce, as has been stated by Glarborg and Bentzen [65], describing that most oxyfuel studies deal with solid fuels or operate at a semi-industrial scale. In [62], extensive measurements, primarily of the axial,

radial, and tangential velocity components in the flames, are available for comparison. While oxyfuel combustion originally describes combustion with oxygen instead of air, a diluting component is commonly added [62] to reduce negative side effects such as high peak temperatures. This changes the combustion process by affecting the collision frequency of reactants, the thermal conditions due to altered heat capacities and radiation properties, and interference of the chemically-active diluent with the reaction process, as was described in [12]. Among the studies dealing with single-phase gaseous oxyfuel combustion, many introduced pure non-preheated CO_2 as diluent [66, 67]. Especially where the comparison with air-fuel combustion mode was intended, this approach prevailed [56, 63, 64]. The influence of the level of preheating of the oxidiser was included in [68]. To the author's knowledge, the usage of recirculated flue gas as a diluent, highly relevant in MILD operation [69], has not played an important role for lab scale oxyfuel flames so far. In their experiments, Sundkvist et al. [70] observed that the dilution with recirculated flue gas reduced the laminar flame speed. Watanabe et al. [56] carried out measurements in a turbulent flame in a $\text{CH}_4/\text{CO}_2/\text{O}_2$ and CH_4/air mixture. They observed that despite lower laminar flame speeds in the oxyfuel system, the flame was shorter and more intense. From this they concluded that the differences in flame structure between the oxyfuel and air-fuel cases could not be derived from the laminar flame properties, such as the laminar flame speed. They suggested that the below unity Lewis-number Le of the oxyfuel case, in comparison to $Le \approx 1$ for the air-fuel case, caused finer wrinkling of the flame and led to a higher flame surface density. These considerations of Watanabe et al. [56] agree well with the findings of Aspden et al. [71], who investigated flames characterised by below-unity Lewis numbers and stated that Damköhler and Karlovitz numbers based on laminar flame properties were not able to capture the impact of turbulence on the reacting structures. Lewis number effects are well-known to strongly influence the shape and behaviour of flames. In a recent study on premixed non-unity Lewis number flames, Potnis et al. [72] could show experimentally how $Le < 1$ counter-flow flames became stronger for increased strain before promptly being quenched. In their study, Kim et al. [73] provided a simplified relation supporting the influence of the Lewis number on the extinction strain rate. Lee and Kim [74] described non-unity Lewis numbers as the important cause for non-uniform thermal energy distribution. They further stated that due to the strong non-linearity of the system, even small perturbations in the thermal energy field have considerable effects on characteristics such as flame speed, extinction, and ignition phenomena. From these studies, it becomes clear that the comparison of oxyfuel and air-fuel conditions raises highly relevant and complex questions also for the general understanding of combustion, e.g. the role of Lewis number.

1.5 Aims, scope

This thesis aims to use, evaluate and progress combustion modelling in CFD for the simulation of conventional and modern combustion processes. The main task was to investigate the closure of the mean/filtered reaction rate $\bar{\omega}_i$ for Reynolds-averaged Navier-Stokes (RANS) modelling and Large Eddy Simulation, a core element of successful combustion CFD. The main methodology for turbulence treatment was LES, which reflects a general development in combustion CFD, facilitated by the broad accessibility of powerful computational resources, advanced numerical methods and, satisfactory subgrid-scale (SGS) closures. The focus was on the application and further development of a sub-category of combustion models best described as dissipation-based reaction rate models connecting the chemical reaction to turbulent mixing but concurrently allowing for the inclusion of finite-rate chemistry effects. A more thorough description will be given in Section 2.5. In this context, the existing, well-investigated EDC was applied first in conventional and unconventional combustion in RANS and later in LES. An approach was followed, where the original RANS formulations were transferred directly into the LES framework, with the advantage that the results can be used as starting point for further work on the EDC in LES. On basis of the experience gathered in the previous step, a new simple algebraic dissipation model was developed, aiming to address some challenges observed in the application of the EDC.

The multi-disciplinary nature of CFD, involving several different stand-alone fields of research, requires a clear definition of scope. In this thesis, single-phase gaseous combustion modelling of short-chain hydrocarbons is investigated. Among the different numerical solution methods (finite-element, finite-difference, finite-volume) available for CFD, the Finite Volume Method (FVM) was used for all flow studies within this thesis. For the simulations, the finite-volume open-source CFD-software OpenFOAM [75] was used, more specifically versions 2.4.1, 4.1, 5.0 and 6.0. Numerical methods play an important role within FVM and are crucial for the stability of simulations and the accuracy of results. However, the topic was only managed from a user perspective within this thesis. Also, turbulence modelling, thermal radiation, and chemical kinetics are important aspects of successful combustion modelling, but at the same time, they constitute independent fields of research. In this thesis, they were addressed relying on the extensive work and findings of others.

1.6 Summary of work

The structure of the thesis reflects the increasingly complex simulation setups that were investigated in the course of the PhD work. The starting point was the unsteady RANS simulation of cold flow, followed by the RANS simulation of hot flow. The cold flow simulations were carried out for the cold Sydney swirl burner benchmark case [76], consisting of a central fuel jet and a swirling annulus separated by a bluff body. The main aim of the cold flow simulations was to investigate the performance and suitability of RANS in common burner geometries and to get a good understanding of the setup for more advanced studies. The results were presented at the joint meeting of the Polish and Scandinavian-Nordic Sections of the combustion institute 2018 and the CLIMIT PhD and PostDoc Seminar 2019.

The RANS combustion simulations presented in this thesis were based on the Eddy dissipation concept [38] with the inclusion of finite-rate chemistry [37] using a GRI-3.0 mechanism [77] with 53 species and 325 reactions. For the simulations, the edcSMOKE library from [78, 79] was linked into OpenFOAM. The investigated flames were Sandia flame D and E [80, 81], two non-premixed piloted jet flames at different inlet velocities. The geometry was reduced to a 2-d wedge form considering the symmetry in the burner geometry. The main aim of this study was to get familiar with the code and study the difference between the two commonly used zero-dimensional reacting structures used for including finite chemistry effects in the simulations. The results were presented at the 9th European Combustion Meeting.

LES was used as the main approach within the thesis work and in the included papers. In Paper I, the Eddy dissipation concept and the Partially stirred reactor model were used to model a lab-scale MILD burner from [82]. The burner consisted of a central high-velocity air jet surrounded by a ring of low-velocity fuel jets. The recirculation of hot gases within the burner ensured the dilution of fresh reactants and the onset of MILD conditions. The combustion modelling library used within this paper was again from [80, 81]. Both models included on-the-fly chemistry calculation, and a skeletal mechanism with 17 species and 58 reactions (displayed in [83]) was used for this purpose. The main aspects of this study were to investigate the application of the combustion models, initially developed for RANS, in the LES context, to study their performance in unconventional combustion conditions, including their direct comparison, and to gain more insights into MILD combustion. The study was presented at the 38th Symposium of Combustion and was published in the Proceedings of the Combustion Institute.

Paper II deals with the development and testing of a new dissipation-based model for LES considering finite-rate chemistry effects. The model was applied to a bluff-body stabilised lean premixed flame investigated experimentally by [55, 84]. The comparison of the new model with an existing LES study of [58], using an unstrained flamelet approach with presumed Beta-PDF, was also included. The main differences to the previously investigated Eddy dissipation concept in Paper I are that the new model solves for the progress variable and its variance instead of a large number of species transport equations. Furthermore, finite-rate chemistry effects are included through the deviation of the transported progress variable variance from its maximum at completely mixing controlled combustion conditions and no constants are used/required to adjust the model to a specific combustion problem. The main aim of this study was to show that promising results could be achieved with a simple and computationally inexpensive new algebraic combustion model, including good predictions of the flame structure and flame quantities such as temperature, temperature variance, and main species. The study was published in *Combustion Theory and Modelling*.

Paper III presents the extended work on the new algebraic combustion model and applied it to a turbulent lean premixed swirl-stabilised flame with varying equivalence ratios. The two resulting V- and M- shaped flames were thoroughly investigated in experiments for different conditions [85, 86] and results are available in several journal articles, e.g. [61, 87]. In addition, the flame was studied before through LES using a Thickened Flamelet approach [61, 87]. While Paper II was concerned with the prediction of flame structures, temperature, and mass fractions, Paper III focused on the flow/combustion coupling. Consequentially, it included a close comparison of velocity data in axial, radial, and tangential direction, predicted and measured flow structures such as corner and centre recirculation zones, and the vorticity and shear fields. The main aspects of this study were to further investigate the new algebraic combustion model introduced in Paper II under different, but still lean premixed, turbulent combustion conditions and to evaluate its performance in predicting the flow/combustion coupling. Furthermore, this study was aimed at contributing to a better understanding of the complex arising flow fields in the two investigated V- and M- shaped flames and stress influences on the stabilisation of either form.

In addition to lean premixed air-methane mixtures, the swirl-stabilised flame was also operated with a $\text{CH}_4/\text{O}_2/\text{CO}_2$ mixture at the same inlet Reynolds number and adiabatic temperature as the conventional combustion case. In the last step, the model was also tested for a lean premixed oxyfuel flame in the same burner geometry as is described in Paper III for conventional air combustion. The main aim of this study was to test

a potential extended applicability of the model to oxyfuel conditions, investigate the differences between the air-fuel and oxyfuel cases and evaluate observations in terms of existing literature.

2 Modelling

2.1 Turbulence modelling

RANS and LES modelling, used within the PhD work, are approaches treating the equations of motion for turbulent fluid flows. Turbulence is a multi-scale phenomenon acting on a continuous spectrum of wavelengths /frequencies and requires a numerical solution of the transport equations. Figure 2 sketches the degree of resolution of the turbulence energy spectrum for the two concepts RANS and LES together with Direct Numerical Simulation (DNS), corresponding to a fully-resolved numerical solution of the flow field.

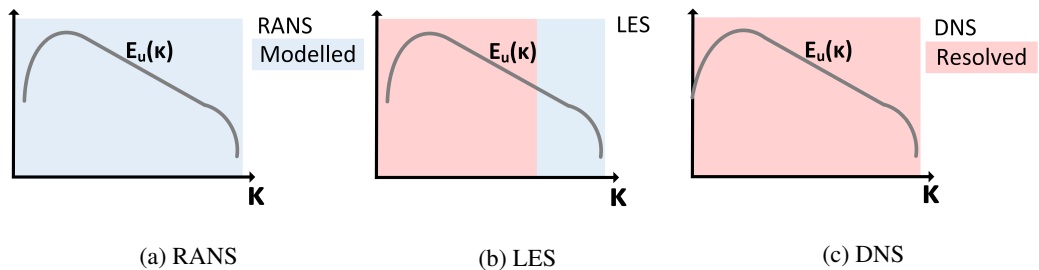


Fig. 2 Comparison of concepts to include turbulence into CFD calculations.

2.2 RANS modelling

RANS is the computationally least expensive approach modelling the full turbulence spectrum. Reynolds [88] lay the foundation for RANS modelling by replacing transported quantities with a two-component formulation consisting of a mean and fluctuating part. The subsequent averaging over large enough times to remove the influence of turbulence on the solution of the Reynolds-averaged transport equations reduces the contribution of turbulence to a single unclosed term describing the turbulence flux of the respective quantity. For the velocity, this unclosed term corresponds to the turbulence (Reynolds)

stress tensor $\overline{\rho u'_i u'_j}$. The most common family of RANS turbulence models uses an eddy viscosity approach based on the Boussinesq hypothesis [89] to close $\overline{\rho u'_i u'_j}$. They assume a proportionality of the Reynolds stresses to the mean rate of strain tensor S_{ij}^* , defined as

$$S_{ij}^* = \frac{1}{2} \left(\frac{\partial \bar{u}_i}{\partial x_j} + \frac{\partial \bar{u}_j}{\partial x_i} \right), \quad (1)$$

and a turbulence (eddy) viscosity ϑ_t .

$$-\overline{u'_i u'_j} = 2\vartheta_t S_{ij}^* - \frac{2}{3} k \delta_{ij} \quad (2)$$

The unknown terms on the right-hand side of Equation 2 are ϑ_t and the turbulence kinetic energy $k = 1/2(\overline{u'_i u'_i})$. Two-equation models solve transport equations for two independent turbulence-related quantities [90] to close ϑ_t . The obvious one is the turbulence kinetic energy k , which appears directly in Equation 2. In addition, a transport equation for the turbulence kinetic energy dissipation rate ϵ or a frequency $\omega \propto \epsilon/k$ is commonly solved, which is related to the mean dissipation process. The latter is used in the family of k - ω models based on the work of Wilcox [91], which is especially relevant for wall-bounded flows. Through the time-averaging operation applied in RANS modelling, transient information is eliminated from the solved flow fields. For unstable flows, persistent unsteady phenomena such as hydrodynamic instabilities play a crucial role and are important to preserve as part of the solution. Unsteady RANS modelling can capture large-scale unsteady structures while being based on RANS arguments [90]. It constitutes an intermediate step between RANS and LES in terms of accuracy and computational effort. The scale adaptive k - ω SST approach [90, 92] from Menter was used within this thesis in the transition to LES methodology. Results are presented in Section 3.

2.3 Turbulent combustion modelling and the EDC

By including combustion in turbulent flow, the complexity of the problem increases sharply due to the introduction of a surge of new, relevant quantities needed to capture the thermo-chemical conditions. Besides composition, the simulation of reacting flows involves solving a form of energy (total/internal energy or total/sensible enthalpy) equation. For systems that are open toward the environment, which was the case for all simulations in this thesis, sensible enthalpy is used. The additional number of transport equations to describe the reacting flow depends strongly on the combustion model applied.

For RANS simulations within this thesis, the Eddy dissipation concept with finite-rate chemistry calculations was used, which requires transport equations for all species occurring in the considered reaction mechanism. The EDC provides an expression for the

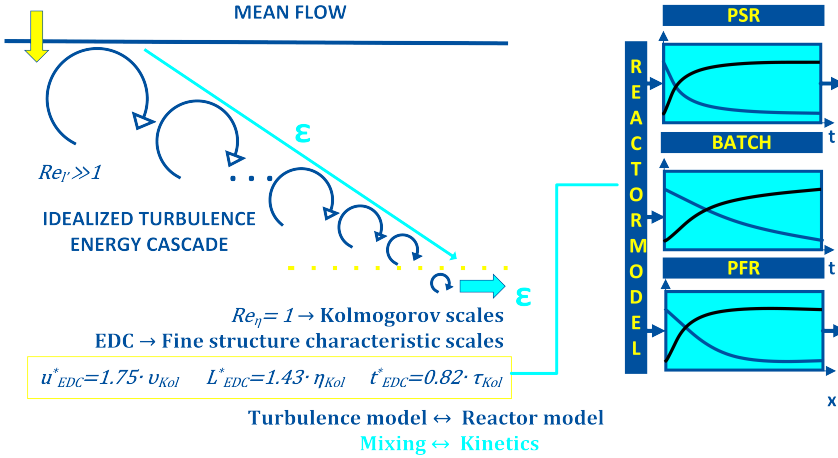


Fig. 3 Overview of the components of the EDC combustion model in RANS .

Reynolds-averaged/filtered reaction rate $\bar{\omega}_i$ that enters the species mass fractions transport equations. The model connects the reaction process to small turbulence structures of the order of Kolmogorov scales, unresolved by both RANS and LES. In a commonly used form, it comprises a turbulence cascade model [36, 38, 39] and a 0-d reactor model [37] for finite-rate chemistry calculations as sketched in Figure 3. The cascade model links the large-scale turbulence quantities explicitly available from the turbulence model to the unknown small scales of the order of Kolmogorov scales. These small scales, connected to chemical activity, are referred to as fine structures within the EDC. The main EDC parameters, determined from the cascade model, are the fine structure mass fraction

$$\gamma^* = \left(\frac{3C_{D2}}{4C_{D1}^2} \right)^{3/4} \left(\frac{\vartheta \epsilon}{k^2} \right)^{3/4} = \left(\frac{3C_{D2}}{4C_{D1}^2} \right)^{3/4} Re_t^{-3/4} \quad (3)$$

and the fine structure residence time

$$\tau^* = \frac{1}{\dot{m}^*} \quad \text{with} \quad \dot{m}^* = \left(\frac{3}{C_{D2}} \right)^{1/2} \left(\frac{\epsilon}{\vartheta} \right)^{1/2}, \quad (4)$$

where C_{D1} and C_{D2} are model constants. Gran and Magnussen [37] included kinetics by treating the smallest eddies as isobaric, perfectly stirred reactors (PSR). The PSR or continuous stirred-tank reactor (CSTR) conserves its mass through a balance of in- and

outflow. Due to chemical conversion, the mass of each species changes following

$$\frac{d m Y_k}{dt} = \dot{m} Y_{k,\text{in}} - \dot{m} Y_{k,\text{out}} + \dot{m}_k''', \quad (5)$$

where \dot{m}_k''' is a production term related to chemical reactions. A residence time $\tau_{\text{res}} = m/\dot{m}$ in the reactor results from the ratio of reactor mass m to through-flow \dot{m} and is connected to the fine structure residence time in [37]. For times $t \gg \tau_{\text{res}}$, the PSR will converge to a steady state, as indicated by the sketched functions of time for the PSR reactor shown in Figure 3. This stiff, time-dependent ordinary differential equation is integrated for every species in the considered chemical mechanism to reach the steady state. Being easier to handle, the ordinary differential equations of plug flow (steady in time) and batch (steady in space) reactors are also often connected to the EDC, as stated in [93]. The batch reactor does not exchange material with its surroundings. The evolution of the mass of each species is described by

$$\frac{d m Y_k}{dt} = \dot{m}_k'''. \quad (6)$$

The batch reactor is transient, but can reach chemical equilibrium. Representative transient profiles expected in a batch reactor are shown together with profiles in the PSR and plug flow reactor in Figure 3. The plug flow reactor is operating in a steady state and develops a characteristic profile in the flow direction. The corresponding conservation equation is expressed as

$$\frac{d m Y_k}{dx} = \dot{m}_k'''. \quad (7)$$

The equation shows similarities with Equation 6 when replacing the dependency on time by space. Assuming a constant flow through, the batch reactor can be recovered from the plug flow reactor (PFR) and vice-versa.

Previous studies have stated that the different reactor types used together with the EDC did not influence the results for the main reaction educts and products noticeably [41, 94]. Both studies mentioned visible but small differences between the reactor models for the minor combustion components. In Section 3, presenting preliminary results, the choice of reactor model used in the RANS-EDC is addressed. The focus is on its influence on the results from an integral point of view. The role chemical time scales have for the reactor differences is addressed too, together with their interaction with the EDC fine structure residence time.

2.4 LES

The idea behind LES is to resolve the instantaneous flow field down to a certain filter width. The turbulence scales that can pass the mathematical filter are removed from the resolved solution, and their influence is commonly included by a subgrid-scale (SGS) model. The theory behind LES has been described in detail in [95], exemplary for comprehensive literature on this topic. Through the filtering operation applied to the transport equations, terms similar to the turbulence stress/flux terms from RANS modelling arise. However, the two approaches provide fundamentally different degrees of resolution of the flow details. Characteristic results of a RANS and an LES of a jet are shown in Figure 4 to underpin this. As a consequence of the resolution of anisotropic large scales, the more homogeneous, direction-independent small scales are modelled in LES. In this thesis, a one-equation SGS model solving a transport equation for the SGS turbulence kinetic energy k_{SGS} was used. The model is based on an eddy-viscosity approximation.

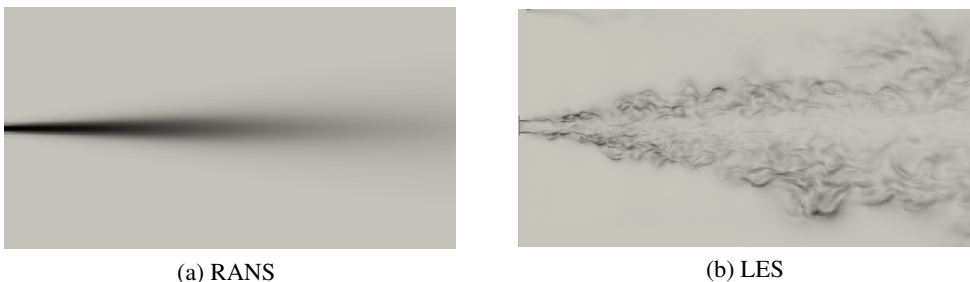


Fig. 4 RANS (Figure 4a) and LES (4b) simulation results for a jet flow showing the strong difference in detail resolution between the two approaches.

2.5 Differences between the LES combustion models applied in Papers I-III

The principles of the EDC (within the RANS methodology) have already been described shortly in Section 2.3. Its formulation within the LES framework for this study is addressed in Paper I. The new finite-rate chemistry dissipation model is thoroughly elucidated in Paper II. In Paper III, the filtered reaction rate expression is complemented by a term considering reactions at resolved scales and a model for local extinction when the SGS mixing time scales become much smaller than the local flame time in the turbulent flame. From this perspective, a repetition of the theory is redundant and a conceptual comparison between the formulations in the papers is of greater value.

Starting with the comparison between the EDC and the new combustion model in Paper II, it should be noted that both are connected to the eddy break-up process, presumably controlling the energy cascade in turbulent flows [96]. This break-up process is a pictorial imagination of turbulence dissipation involved in the transfer of kinetic energy from the largest to the smallest turbulence scales through a continuous spectrum. At high Reynolds numbers, it constitutes the key mixing process. Both models cope with the deviation from the high Damköhler number limit, corresponding to purely mixing-controlled combustion. In the EDC, the inclusion of finite-rate chemistry is commonly realised by introducing a canonical reactor model, as has been discussed in Section 2.3. It involves the on-the-fly calculation of transport and ordinary differential equations (ODE) for all species contained in the applied mechanism. The new model presented and used in Papers II and III does not solve species transport equations but relies on the reduction of the thermo-chemical state to quantities that preserve fundamental information of the combustion problem, such as the mixing state and combustion progress [18]. The transport equations for the filtered progress variable and its variance include all relevant terms to give a detailed description of the flame structure in premixed combustion. Furthermore, the filtered reaction rate expression used in Papers II and III was realised without adjustable constants. For the EDC, proportionality constants in the modelled relation between fine structures and large-scale turbulence (cascade) play an important role, a summary can be found in [53].

It should be noted that the formulation of the filtered reaction rate model in Paper III constitutes a refinement of the expression used in Paper II to consider the contribution of resolved scales. This modification is relevant for partial resolution of the flame structures by the modelling approach, in this case, high-fidelity LES.

2.6 Implementation of the algebraic dissipation-based combustion model

The combustion model presented in Papers II and III was implemented in an OpenFOAM solver for the transient turbulent flow of compressible fluids. This subsection gives a summary of the model structure and calculation process, sketched in Figure 5. The formulation of the dissipation-based reaction rate using the progress variable c results in the main cornerstone/restraint for the combustion model implementation. For a fixed fresh gas composition, thermodynamic and transport properties become functions of c , which avoids to solve the full extent of composition and temperature fields. This influences the application of the thermophysical model, handling energy and heat in OpenFOAM [97]

and providing physical properties such as viscosity to the solver. A new thermophysical model class had to be linked to OpenFOAM to ensure that these properties are determined as functions of the combustion state and passed on correctly for the calculation of the flow field. A probability density function (PDF) approach is used to determine filtered thermodynamic and transport properties based on laminar flamelet calculations. Tables store the PDF data in this code, which the solver loads at the start of the simulation. They can be accessed on-the-fly for each cell at each time step. Linear regression is used to calculate a target value based on the two closest entries in these tables.

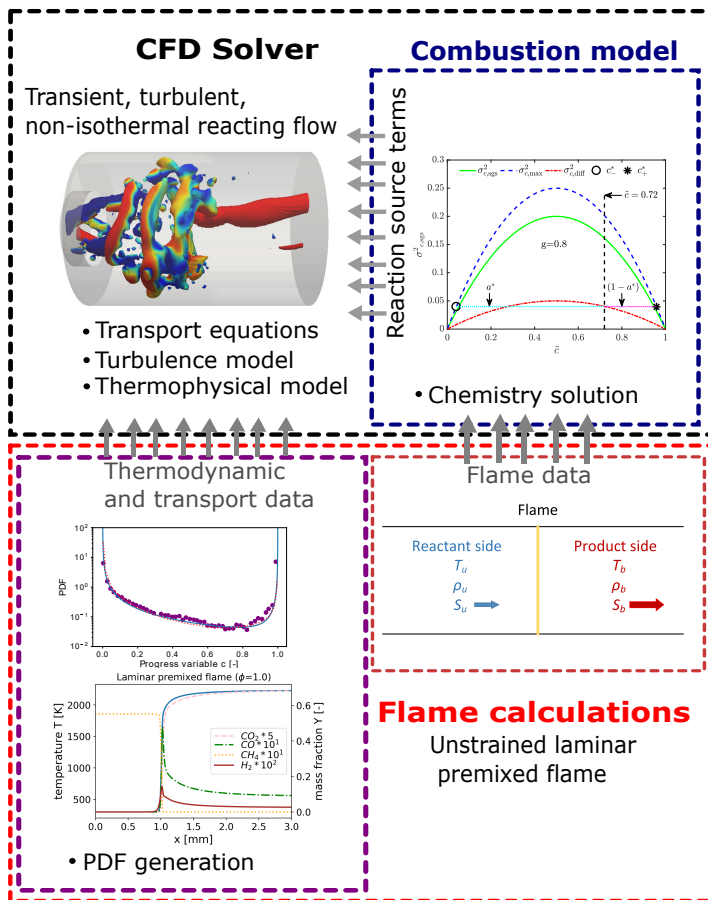


Fig. 5 Graphical overview of the model flow for the algebraic, dissipation-based combustion model applied within a transient, compressible CFD solver.

The second access point to the laminar flame calculations is the combustion model, which requires information on the laminar flame speed, thermal flame thickness, and a global heat release parameter. These data do not enter the filtered reaction rate expression explicitly. However, they enter the algebraic scalar dissipation rate model from Dunstan et

al. [57], used in this study to close the SGS progress variable variance transport equation. Through the strong relation between $\overline{\omega}_c$ and σ_c^2 , these parameters affect indirectly also the reaction rate formulation.

3 Preliminary Results

3.1 General

This section shows unpublished results and pre-works for the manuscripts presented subsequently. First, cold unsteady RANS simulations of a swirl-stabilised benchmark case for combustion modelling, referred to as the Sydney swirl burner [76, 98], are shown. Second, RANS simulations of the two Sandia flames D and E [80, 81] are presented, which used the EDC as combustion closure. A subsequent analysis of the finite-rate chemistry treatment included in the EDC was also carried out. The investigated Sandia flame D distinguishes itself from other flames (E, F) in the experimental series [99] through the inlet Reynolds number and, hence, the intensity of turbulence. Finally, the study of a lean-premixed oxyfuel flame operating with a $\text{CH}_4/\text{O}_2/\text{CO}_2$ mixture concludes this chapter. It constitutes preliminary work aiming to give an overview of the (modelling) challenges of oxyfuel combustion. A comparison with flow measurements and the lean premixed methane-air flame with the same adiabatic flame temperature as the oxyfuel flame is provided.

3.2 Cold flow unsteady RANS simulations ¹

The chosen case for the cold flow simulations is the non-reacting swirling jet N29S054 in the series of experiments carried out at the University of Sydney, documented in [98], and published for example in [76]. The burner, as sketched in Figure 6, is unconfined and located in a co-flow of ambient air with an axial velocity of $U_e = 20$ m/s and a turbulence intensity of $TI = 2\%$. The central jet of fuel with a diameter of $3.6 \cdot 10^{-3}$ m has a bulk velocity of $U_j = 66$ m/s. The bulk flow in the annulus is defined by an axial component $U_s = 29.74$ m/s and a tangential component W_s , defined by a swirl number of 0.54. The flow at the inlets is fully developed. Extensive first and second-moment velocity data are available from measurements of this benchmark case. The capability of two-equation

¹ Parts of this investigation were presented at the CLIMIT PhD and PostDoc Seminar 2019.

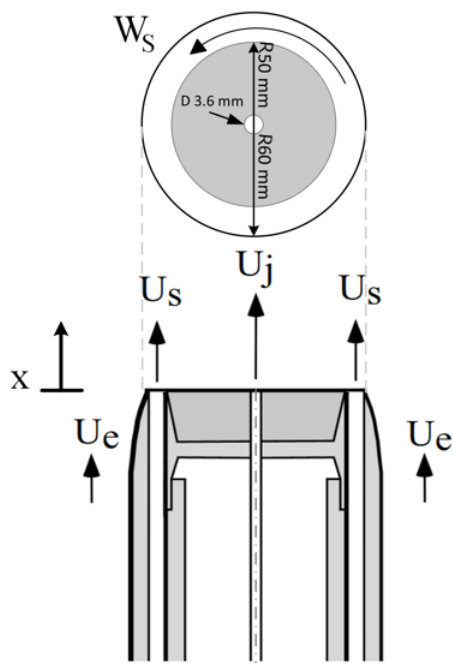


Fig. 6 Sketch of the inflow area with central jet, annular swirling jet and co-flow of the Sydney swirl burner, altered from [98].

RANS models to predict complex swirling flows is limited by the occurrence of transient, three-dimensional instabilities in these types of flows [100]. In an attempt to improve results under these conditions, an unsteady RANS approach was chosen in this study. The $k-\omega$ SST-SAS approach [90, 92] from Menter was used, which is implemented in OpenFOAM 5.0. Figure 7 shows the numerical grid used within this study. It consists of a rectangular main section of $0.13 \times 0.13 \times 0.2 \text{ m}^3$ and an inlet pipe for the central fuel jet. The number of cells of the structured, hexahedral mesh was 1.5 million. The inlet profiles for the axial and tangential velocity components of the central jet were simulated. The inlet profiles for the annulus were approximated at $x = 0$ and taken from [101]. The co-flow was assumed to be uniform at the inlet. The measurements closest to the inlet are available at a distance of $0.136D$ or $6.8 \cdot 10^{-3} \text{ m}$ downstream of the burner bluff body located at $x = 0$. Figure 8 presents the mean variations of the three velocity components (axial, radial, tangential) in the radial direction at $x/D = 0.136$, both for the simulations as well as experiments. Due to the short distance between the simulated inlet and axial measurement location, the inlet boundary conditions were important for the accuracy of the numerical results in this axial location. The mean velocity profiles show good agreement with experimental data, confirming the suitability of inlet conditions to

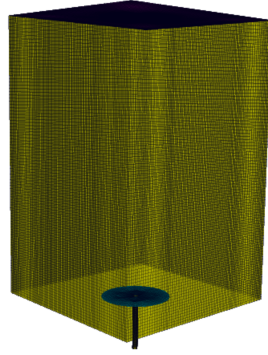


Fig. 7 Numerical grid for the cold flow simulations of the Sydney swirl burner.

capture the mean flow in this axial location. The RMS velocity variations shown in Figure 9 provide satisfactory results in this location, indicating that also the turbulence inflow conditions perform as expected.

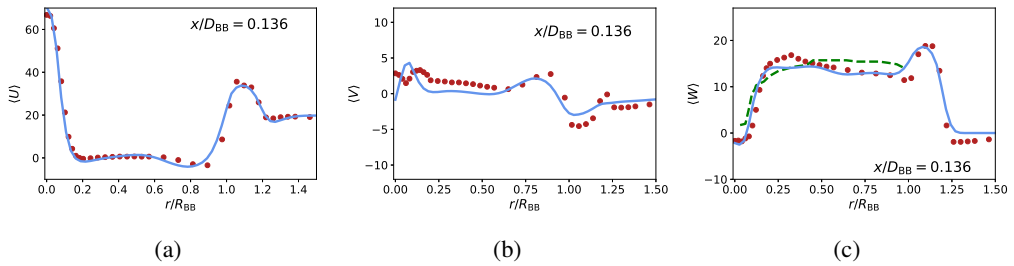


Fig. 8 Mean axial, radial, and tangential velocity variations at $x/D = 0.136$ or $6.8 \cdot 10^{-3}$ m from the inlet. Light blue, solid lines represent simulation results, green, dashed lines RANS data from Yang and Kær [102], red dots measurements available in [98].

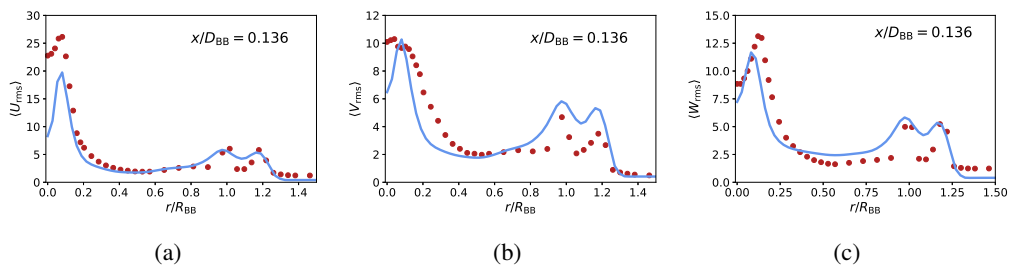


Fig. 9 RMS axial, radial, and tangential velocity variations at $x/D = 0.136$ or $6.8 \cdot 10^{-3}$ m from the inlet.

Figure 10 shows the cold flow field in the Sydney swirl burner predicted by the $k-\omega$ SST-SAS model. The measured flow field for case N29S054 is described in [103].

It is characterised by the formation of primary and secondary recirculation zones in the bluff body wake and along the geometry centreline. The recirculation zone in the bluff body wake was described to stagnate approximately 25 mm downstream of the burner inlet at $x = 0$ [103]. This agrees fairly well with the simulation results in Figure 10, even though slight asymmetries can be observed. Measurements captured a second recirculation zone located along the geometry centreline with stagnation points at $x = 5 \cdot 10^{-2}$ m and $x = 1.1 \cdot 10^{-1}$ m. The maximum negative velocity of 6 m/s was measured approximately halfway between the two axial positions. This region of reversed flow, confined by the two stagnation points, is connected to a bubble-type vortex breakdown acting as an obstacle in the flow, described in detail in [104]. The location of the onset of this recirculating vortex bubble is predicted reasonably well by the unsteady RANS simulation. However, the determined maximum negative velocity of 3m/s and the long, low-velocity tail reaching $x \approx 2 \cdot 10^{-1}$ m into the burner geometry for the simulations do not agree well with the experiments. A more detailed display of the agreement between experimental and numerical results is subsequently provided, plotting variations of the first and second moment of the three velocity components in axial, tangential, and radial directions. Results for the axial component, constituting the main flow direction, are provided in this section, radial, and tangential velocity profiles, complementing these data, are given in Appendix A.1. Unfortunately, the measurement region ends with the measured downstream stagnation point of the centre recirculation zone. The discrepancy downstream of this region cannot be closely evaluated. Generally of interest in the discussion of modelling performance is the comparison with other turbulence modelling approaches, which is why the numerical results of this study are shown together with RANS and LES results of the benchmark case N29S054 available in the literature [102, 105]. LES results from Stein et al. [105] are in subsequent figures shown as dash-dotted orange lines and were gathered using a dynamic Smagorinsky SGS closure for LES on a 3M mesh. Yang and Kær [102] used a $k - \epsilon$ RNG model on a mesh with 1M cells. Their results are shown as dashed green lines in subsequent figures where available.

The first and second-order moment velocity variations of the three different turbulence closures are shown in Figures 11 and 12 in this section and Appendix A.1. As these results stem from different sources with different numerical grids and inlet and boundary conditions, discrepancies between the cases may not solely be linked to the choice of turbulence modelling approach. However, their comparison reflects a common observation that increasingly sophisticated turbulence closures are required to capture complex flow fields and to reach good agreement with dependable measurements. LES results from [105] and the URANS approach perform both well, predicting the measured

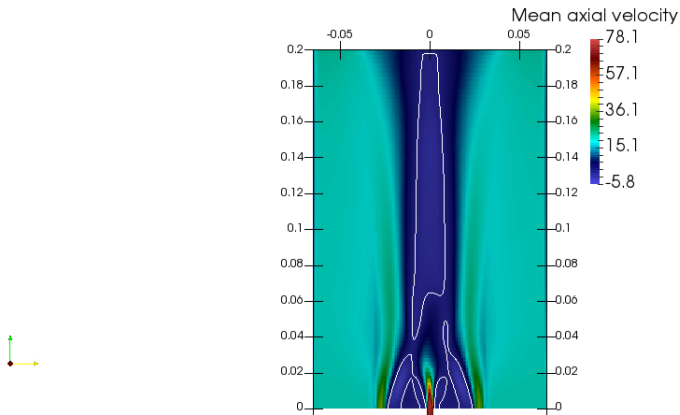


Fig. 10 URANS simulation of the cold benchmark case referred to as the Sydney swirl burner. White lines correspond to zero-axial velocity isolines.

mean velocity profiles qualitatively and quantitatively. There are only small differences observable between the two approaches. The actual performance indicator for the two approaches is the prediction of the turbulence field, which is captured by the RMS fluctuating velocity components given in Figure 12 and Appendix A.1. The weakness of the URANS approach to model the turbulence using the two turbulent quantities k and ω compared to LES resolving the large-scale motions, is expected to be partly responsible for the notable discrepancies in the plots. From the three studies compared, the LES study showed perceptibly best agreement with experimental data.

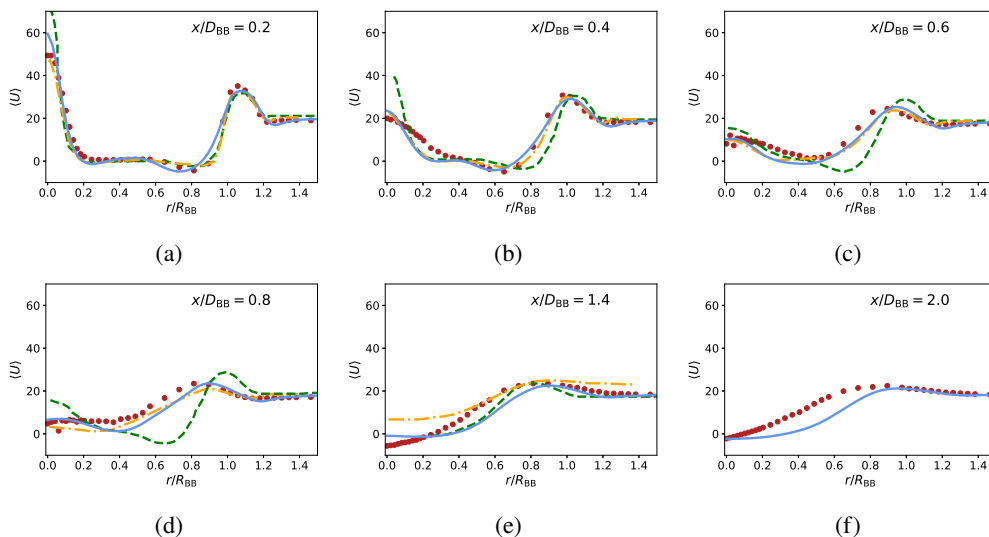


Fig. 11 Mean axial velocity variations. Red symbols \bullet denote measurement points from [98]. Blue, solid lines — give results of the investigated $k-\omega$ SST-SAS model. Orange, dash-dotted lines — represent LES results from Stein, Kempf and Janicka [105], green, dashed lines — RANS data from Yang and Kær [102].

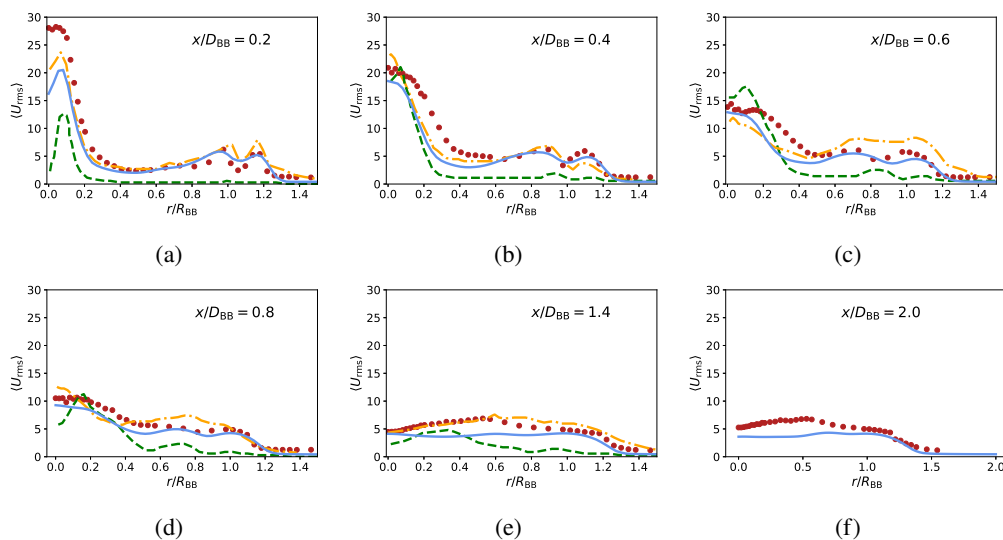


Fig. 12 RMS axial velocity variations, for the legend see Figure 11.

3.3 Reacting jet flame RANS-EDC simulations²

Within the subsequently presented study, a combined approach of CFD simulations and the a posteriori analysis of the on-the-fly finite-rate chemistry treatment was carried out

² Parts of this investigation were presented at the 9th European Combustion Meeting 2019.

for the Sandia flame D, a benchmark case of turbulent non-premixed combustion. The flame was thoroughly documented by Barlow and collaborators [80, 106] and has become a subject of high modelling interest in the wake of an international workshop [99] aiming to coordinate and facilitate the advancement of combustion modelling [15]. The Flame D distinguished itself from other flames in a series of experimental studies through the Reynolds number for both jet and pilot and, thus, the intensity of turbulence and the degree of local extinction. For the simulations, OpenFOAM 4.1 [75] was used together with the external edcSMOKE library developed by Cuoci and collaborators [78, 79], handling the combustion modelling through the implemented EDC. The edcPimpleSMOKE solver included in the edcSMOKE library solved the transient combustion problem. Chemical kinetics were included using both the implemented PFR and PSR model applying the GRI mechanism 3.0 [77]. The P1 model, described in [107], was used to include radiation. The reactor study investigating the EDC's finite-rate chemistry treatment was carried out using Cantera [108] for Matlab® and was based on actual parameter combinations determined from the simulations. For this reactor study, the two adiabatic constant-pressure reactors, PFR and PSR, commonly used in the context of the EDC finite-rate chemistry calculations, were compared. The input data for the study, such as the composition and temperature data, were collected from the flame zones in the OpenFOAM simulations. The turbulence data was used to define the reactor sizes and residence times of the considered reactors in Cantera. As a data source for the turbulence conditions, the EDC-Batch/PFR simulations were used. However, the choice was investigated to be insignificant, as both cases gave very similar results for turbulence quantities. The mesh

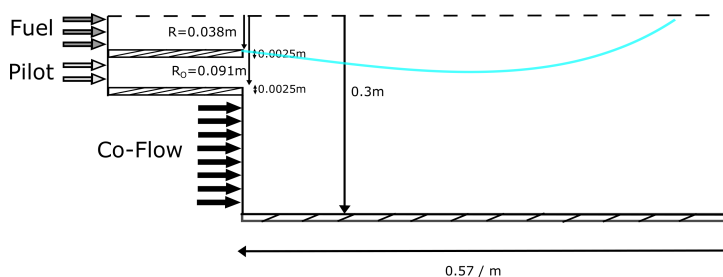


Fig. 13 Sketch of the burner geometry used for simulating Sandia flames D and E. The light blue line represents the position of the flame.

used for the Sandia flame simulations consisted of a narrow-angle wedge with 9000 cells. The outer dimensions of the investigated 2-d burner section are given in Figure 13. The radius of the central main jet $R = 0.0038$ m and the annular pilot with a slit width of 0.00525 m were each resolved by 5 cells in the radial direction. The wall between the two inlets had a thickness of $2.5 \cdot 10^{-4}$ m. The surrounding co-flowing air was separated from

the pilot through another wall of $2.5 \cdot 10^{-4}$ m thickness and was resolved by 60 cells in the radial direction. The combustion chamber was simulated along 75 diameters of the main jet $D = 7.6 \cdot 10^{-3}$ m in flow direction for the Sandia flame D. The resolution in the axial direction was 108 cells. The velocity was provided as bulk flow velocity. For Flame D, the central fuel jet was fed with a mixture of 25% CH₄ and 75% dry air by volume and entered the burner section with a bulk velocity of $U_B = 49.6$ m/s. The surrounding air flow had a constant bulk flow velocity of 0.9 m/s, which resulted in an equivalence ratio of $\phi = 0.77$ based on the mass streams. The pilot stream at the burner inlet was assumed to have completed reactions upstream of the burner entrance and was described by thermo-chemical data provided in [99] with a bulk flow velocity of 11.4 m/s. For the fuel nozzle and pilot, turbulence intensities were calculated based on an empirical relation with the Reynolds number. The inlet region was extended 15 diameters (main nozzle) upstream of the burner entrance to allow turbulent flow profiles to develop.

For comparison and evaluation, measurements for the main combustion educts (CH₄ and O₂), products (CO₂ and H₂O), and important minor species (CO, OH, H₂) are available [99]. The EDC was applied to this burner configuration before, both in RANS and LES framework, to investigate its ability to model this type of flame [48, 94]. The focus of this study was the impact of the reactor model on the prediction of the global flame structure under turbulence conditions evolving in the investigated Flame D. From the species profiles, which are presented in Figures 14 and 15 in this section and Appendix A.2, it was observable that the reactor choice did not have a qualitative impact on the prediction of the developing flame. The yellow, solid lines in these plots give the result for the plug flow reactor (constant velocity), the black, dashed lines results for the PSR, respectively. As the graphic displays a wide range of data, the lines are not distinguishable in the shown resolution. Therefore, the light blue, dotted lines provide the ratio between the respective mass fraction values at each point for the two used reactor models. Minor quantitative discrepancies between the species variations occurred, but as our results suggested, were not a relevant source of discrepancy between our simulation and experimental results in the investigated RANS context. For decreasing mass fractions, however, the difference between the two reactor models increased slightly but notably. The main combustion products CO₂ and H₂O showed little deviation over the whole burner region investigated in axial direction from $1D$ to $45D$.

As part of the reactor analysis within Cantera [108], we aimed to elucidate the role finite-rate chemistry effects play for the strength of deviations between the reactor models. The initial hypothesis was that for very fast reactions, hence for small chemical time scales, the results for both systems converge. This was based on order of magnitude considerations

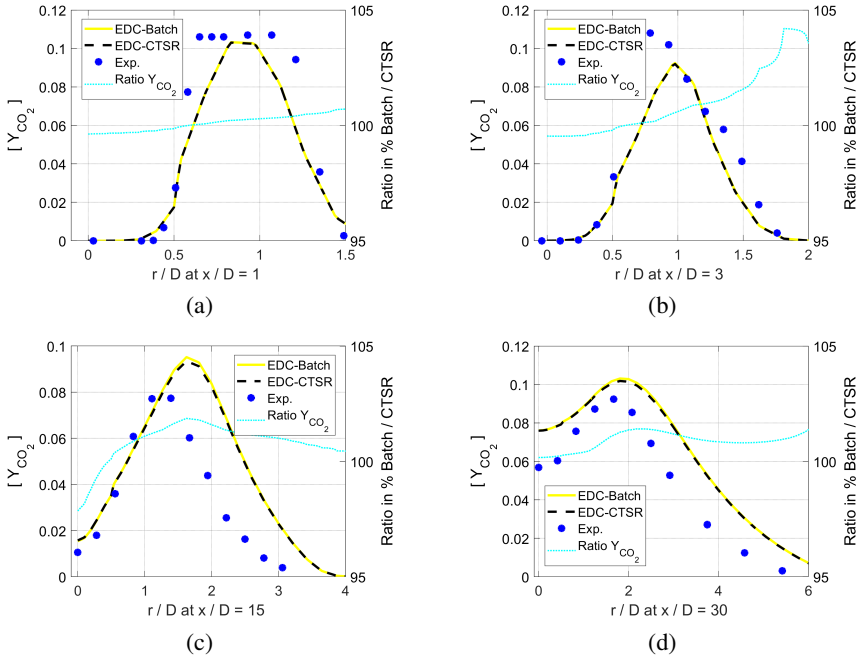


Fig. 14 Radial profiles of CO₂ mean mass fractions at varying axial positions in Flame D. Measurements are taken from [99].

of the terms in Equation 5, which involve two competing time scales related to the reactor through-flow \dot{m} and reaction kinetics \dot{m}''' , respectively. For $\tau_{res} \gg t_c$ chemical conversion is the dominant process in the system in which case Equation 5 is expected to approach approximately the form of Equation 6. To investigate this assumption, several 180 cells in the reaction zone were analysed at different positions of the flame, hence under varying turbulence and thermochemical conditions, for both reactor types. In Figure 16a, the mass fraction ratio for methane is shown as a function of the time scale ratio τ_{res}/t_c for the PSR. The chemical time scale was calculated from $t_c = \rho Y_k / \omega_k$ after the PSR has reached its steady state. The plot shows an S-shaped curve with good agreement between the reactor models for small time scale ratios and a steep increase of deviation between the results in the range of $\tau_{res} \approx 0.1$ to ≈ 10 . In contrast, in a second plot showing the ratio of methane reaction rates for the two reactor models, it is observable that for fast chemical kinetics and hence large time scale ratios, the PSR methane reaction rate approaches the behaviour in the PFR. The somewhat contradictory observations made in Figures 16a and 16b are sensible if one imagines that decreasing mass fractions become more sensitive to deviations. This behaviour could also be an explanation for the steep increase of differences that can be observed in the species mass fraction plots for fast-diminishing

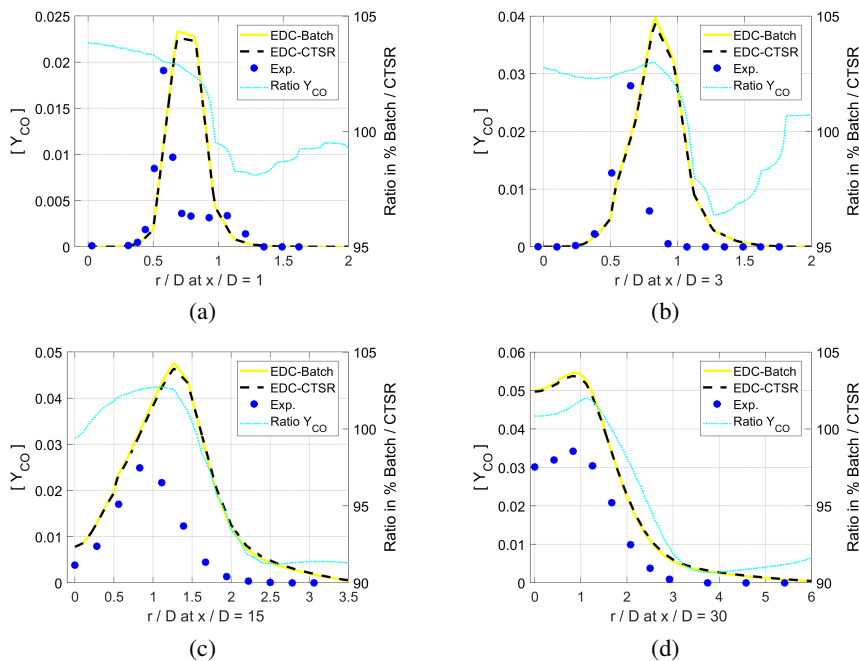


Fig. 15 Radial profiles of CO mean mass fractions at varying axial positions in Flame D. Measurements are taken from [99].

Y_i . Generally, this study reflected observations from previous studies [41, 94] that no considerable discrepancies were observable using the two reactor models.

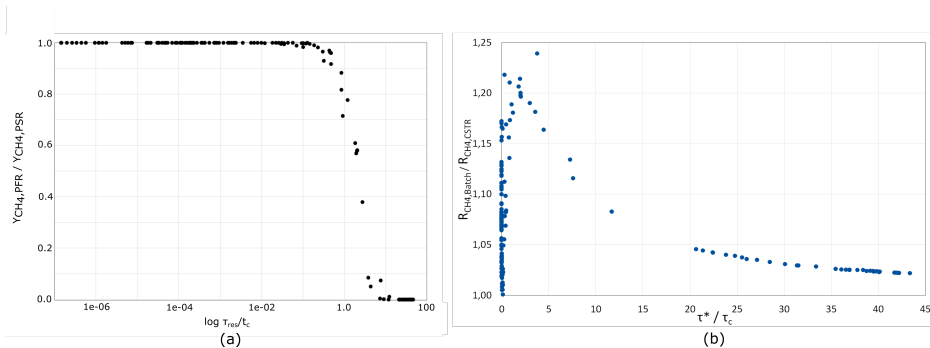


Fig. 16 Ratio of CH_4 mass fractions for PFR and PSR plotted over the PSR residence to chemical time scale ratio.

3.4 Transferring Paper III's numerical setup to an oxyfuel flame

This preliminary study constitutes an extension of the work done on the premixed swirl-stabilised flame in air. Through several publications on the swirl-stabilised turbulent premixed air-methane and oxy-methane flames [56, 63, 64], comprehensive data are available to compare these two operational modes. The numerical setup described in Paper III was used for additional simulations of the swirl-stabilised flame under oxyfuel conditions. For better comprehensibility, Paper III should be studied first, as it provides a detailed description of the simulation setup for this burner.

In this preliminary study, the aim was to get an overview of the challenges that have to be addressed transferring and applying the combustion closure presented in Papers II and III to a flame operated in a $\text{CH}_4/\text{O}_2/\text{CO}_2$ mixture. Based on the discussion of Chakroun [62], the different material properties of the $\text{CH}_4/\text{O}_2/\text{CO}_2$ mixture are expected to have a strong influence on the validity of modelling assumptions. A fundamental difference between the air-methane and oxy-methane case results from the considerably larger molar mass of CO_2 (44 kg/kmol) compared to N_2 (28 kg/kmol), leading to an increased density of the combustible mixture with carbon dioxide as diluent. To achieve similar inflow conditions and hence Reynolds numbers for both mixture compositions, the inflow velocity to the burner operated with a $\text{CH}_4/\text{CO}_2/\text{O}_2$ mixture was adjusted in [63] and accordingly also in this numerical study. The bulk inflow velocity of the oxyfuel mixture into the burner was 5.4 m/s, which corresponds to $Re \approx 20000$. The swirl number remained $S \approx 0.7$. The inflow setup (outer dimensions), the Reynolds number, and the swirl number were the same for experiments with both mixtures. Hence it was assumed that the same inflow profiles as applied in Paper III can be used for the oxyfuel case as well, changing solely the bulk flow velocity to 5.4 m/s. The inflow turbulence was provided by a synthetic inflow turbulence generator [109] assuming a turbulence intensity of 15%, and a large turbulence length scale of 10% of the step height $D/2 = 0.019$ m in agreement with the simulations presented in Paper III. A more comprehensive description of the applied inflow and boundary conditions can be found in Paper III. The same numerical grid and similar models as in Paper III were used for the oxyfuel flame in this first step. The oxyfuel flame was made comparable to the air-fuel Flame IV in Paper III by adjusting the amount of diluent CO_2 added [56]. This was to ensure the same equivalence ratio ($\phi = 0.65$) and adiabatic temperature $T_{\text{ad}} = 1753$ were achieved. The resulting mass fractions of the components CH_4 , CO_2 , and O_2 were $Y_{\text{CH}_4} = 0.0373$, $Y_{\text{CO}_2} = 0.836$ and $Y_{\text{O}_2} = 0.229$. Due to the higher heat capacity of CO_2 compared to N_2 , the fuel mass fraction for the oxyfuel case was higher than for combustion in air. The laminar flame properties for the given

compositions of the air-fuel and oxyfuel mixture differed considerably, despite having the same adiabatic temperature and equivalence ratio, which becomes clear from Table 2. The two most striking differences shown in Table 2 are the almost twice as large laminar flame speed for combustion in air and the below-unity Lewis number for methane in the O_2/CO_2 mixture, as was noted before by Chakroun [62]. Both these quantities and the current knowledge of their impact on flames are addressed in the literature review in Section 1.4.

Table 2 Reacting and transport properties for a methane mixture with air and O_2/CO_2 , the latter is abbreviated with oxy.

Parameter	τ	$S_{L,0}$	δ_{th}	α_{th}	Le
Related to	heat release		laminar flamelet		transport
Formula	$\tau = \frac{(T_{ad}-T_0)}{T_0}$	-	$\frac{(T_{ad}-T_0)}{\nabla T _{max}}$	-	$Le = \frac{\alpha_{th}}{D_{F,O}}$
Dimensions	[]	[m/s]	[m]	[m/s ²]	-
Air ($\phi = 0.65$)	4.88	0.15	0.0008	$2.25 \cdot 10^{-5}$	1.01
Oxy ($\phi = 0.65$)	4.86	0.079	0.001	$1.48 \cdot 10^{-5}$	0.81

As in Paper III, the numerical setup was tested in cold flow simulations before addressing the hot flow. In Figure 17, the mean axial velocity variations of the cold flow for the air-methane and oxy-methane cases are shown, normalised by the respective bulk flow velocities of $U_{Bulk} = 8.0$ and 5.4 m/s. Figure 17 underpins that the same Reynolds number and swirl number led to similar behaviour of the two investigated cold flows of different compositions and velocities, which becomes visible from the normalised velocity data. Also, the axial rms-velocity variations provided in Figure 18 suggest a good agreement between the two simulations and measurements. Additional velocity data in Appendix A.3 support these observations.

In [62], it was stated that the comparison of the oxyfuel and air cases resulted in differences between the flow fields. However, qualitatively, the measurements provided in [62] showed good agreement between the two experimental cases. Naturally, quantitative differences such as the peak velocities occurred due to different inflow velocities. This effect could be corrected through suitable normalisation, unfortunately not provided in [62]. The statistics of the cold flow presented herein show that, applying a suitable normalisation, a close similarity could be reached between the cold air-methane and oxy-methane simulations under the described conditions of constant outer dimensions, Reynolds and swirl number. This outcome is important for an eventual comparison of the

two reacting cases, as it relates discrepancies in the hot flow fields to a large degree to combustion activity.

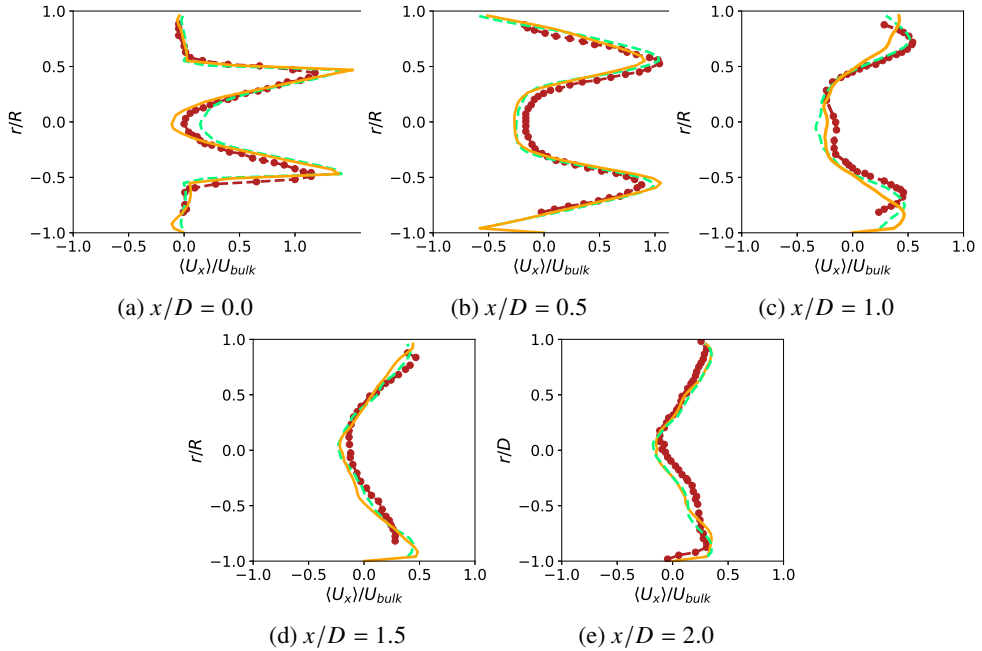


Fig. 17 Normalised mean axial velocity profiles in radial direction for the cold flow. Orange, solid lines — and light green, dashed lines --- denote the results for the cold flow with $\text{CH}_4/\text{O}_2/\text{CO}_2$ and CH_4/air composition. The dark red dots • connected by dashed lines are measurements from [61].

After investigating the cold flow, the turbulent oxy-methane flame with equivalence ratio $\phi = 0.65$ is addressed. As an initial step, the combustion closure described in Paper III was applied under the new conditions. Thermophysical and flame data shown in Table 2 were required by the code and provided for the oxyfuel flame as outlined in Section 3.5. The first observation from this study was that the flame transit time from the unstrained premixed laminar flamelet failed to represent the local flame time of the turbulent flame. This assumption was successfully used to capture the transition between two flame shapes in the air, relying on the correct prediction of the location of the flame within the shear layers. The flame transit time $t_c = D_r / (S_{u,0}^2)$ was used as a chemical time scale in Paper III due to its linking to the inner structure of the premixed laminar flame. In the air-fuel cases presented in Paper III, it was of a similar order of magnitude as the extinction time scale provided in [110]. However, the considerably decreased laminar flame speed and the resulting large flame time led to the unrealistic suppression of reactions in large regions of the shear layer for the oxyfuel conditions. In contrast to the major difference in flame

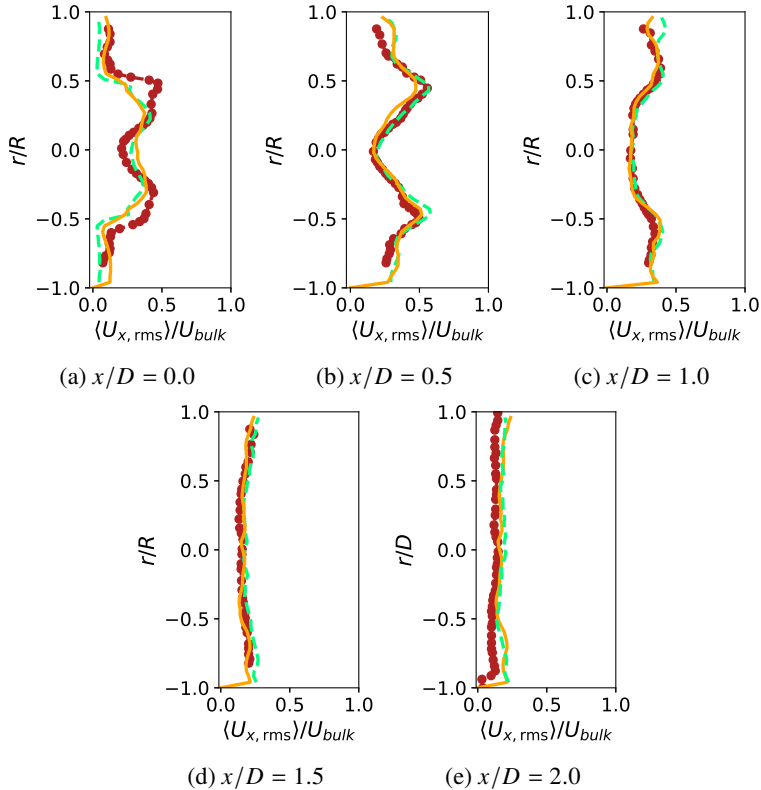


Fig. 18 Normalised rms axial velocity variations in radial direction, for the legend see Fig. 17.

transit time between oxyfuel ($t_{c,oxy} = 2.5 \cdot 10^{-3} \text{s}^{-1}$) and air ($t_{c,air} = 9.2 \cdot 10^{-4} \text{s}^{-1}$) observed here, Watanabe [56] reported similar extinction strain rates for these two flames, which were of the order of magnitude of $t_{c,air}$. From this perspective, a review of the inclusion of local extinction into the combustion closure for the oxyfuel conditions has to be done. To remove its problematic influence from the preliminary study of the oxy-methane flame, local extinction had to be excluded for the moment. In Paper III, it was observed that the notable impact of extinction was reduced in the transition from Flame III to Flame IV. However, it has yet to be investigated whether this is also true for oxyfuel conditions.

Detailed velocity data [62] were available to evaluate the reacting flow simulations under oxyfuel conditions. The results are given in Figures 19 and 20 (axial velocity) in this section as well as in Appendix A.3 (tangential velocity). The rms-velocity variations were determined in the same way as in Paper III by considering the resolved velocity component $\langle U^2 - \langle U \rangle^2 \rangle$ and the subgrid-scale component $\langle k_{SGS} \rangle = 3/2 \langle u'^2 \rangle$. The agreement with measurements for the oxyfuel flames was satisfactory for both mean and rms variations of velocity as trends and order of magnitude were in most regions captured. The agreement

of the air-fuel simulations with experiments was notably better for all mean and rms velocity profiles, which indicates that the transfer of the approach from Paper III to oxyfuel conditions is not straightforward. It is important to take a closer look at the differences resulting from using a O_2/CO_2 mixture as oxidiser instead of air. It should be noted that for the air-fuel case [111], axial and radial velocity data, and for the oxyfuel case [62], axial and tangential velocity data were available. Strictly, only the performance predicting the axial velocity variations can be directly compared between the two setups.

From the velocity profiles given in Figure 19 it becomes clear that the inner structure of the important centre vortex bubble with reversed flow was difficult to predict for the applied modelling approach. The major discrepancies were observed for the upstream stagnation point, which lay slightly downstream of the expansion plane for the experiments [62]. In the presented simulations, the vortex bubble was not fully separated from the wake downstream of the swirler hub and expanded into the upstream duct, which was not predicted by the experiments [62]. For the sake of completeness, it should be noted that this behaviour was also observable for Flame IV in Paper III, but the reverse flow was not as intense, which agreed better with the experiments [62]. Simulation results presented in [110] using a reduced mechanism for oxyfuel combustion from Frassoldati et al. [112] showed correct behaviour and positive velocities in this location. However, for another mechanism tested in [110], the upstream expansion of the inner recirculation zone into the swirler duct was also observed, which Chakroun connected to the varying extinction strain rates resulting from the mechanisms. To include a physically sound extinction model, more work is required to understand the interaction of chemical and small turbulence time scales under oxyfuel conditions.

The non-unity Lewis number is known to have a large influence on the reacting conditions in premixed flames. It has been observed to cause intense, fine flame wrinkling increasing the flame surface and thus reactions and alters the flame speed and the occurrence of transient phenomena such as extinction and ignition [74]. The implications of the non-unity Lewis number potentially require a thorough review of the modelling assumptions of the dissipation-based turbulence combustion model under these conditions. Previous studies on the inclusion of non-unity Lewis number effects in combustion modelling have already indicated the necessity of adjusted models under these conditions. Regele et al. [113] pointed out that single-variable approaches, as used in the current formulation of the model with a quantity such as progress variable, fail to accurately predict differential diffusion effects in non-unity Lewis number combustion. High-fidelity studies applying DNS analysis for non-unity Lewis number conditions [114, 115] also raised the point that unclosed terms in the reactive scalar transport equations require modifications

under these conditions. Gao et al. [115], for example, suggested a correction for the modelling expression of the scalar dissipation rate.

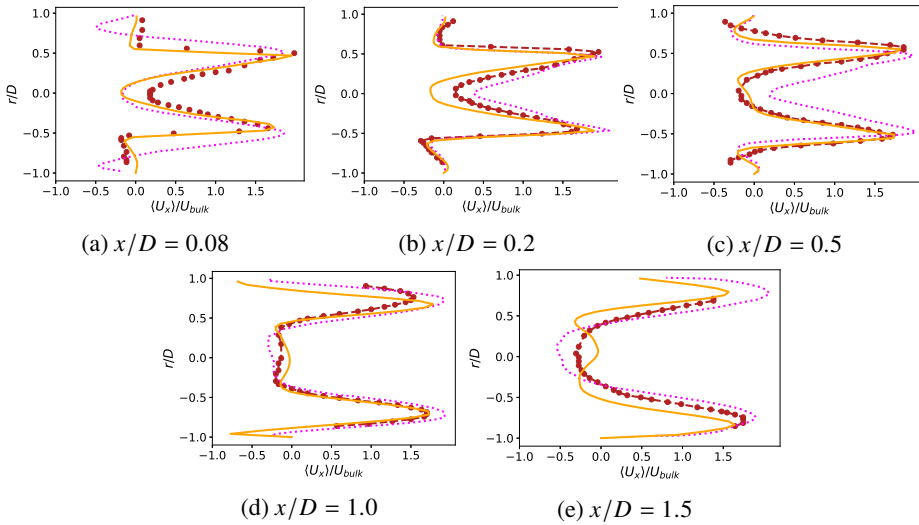


Fig. 19 Normalised mean axial velocity profiles in radial direction for the hot flow with oxy-methane combustion at equivalence ratio $\phi = 0.65$. Orange, solid lines represent simulation results of this study. The magenta dotted lines denote simulation results in [62] and the dark red dots connected by dashed lines are respective measurements from [62].

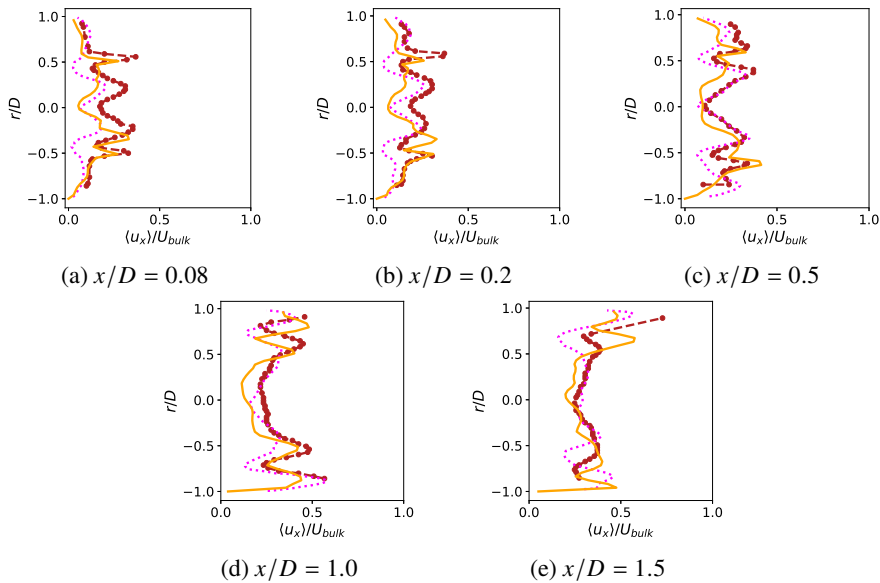


Fig. 20 Normalised rms axial velocity profiles in radial direction for the hot flow with oxy-methane combustion at equivalence ratio $\phi = 0.65$. For the legend see Figure 19.

3.5 Insights from the preliminary studies

The preliminary studies were important steps preceding the research output with the objective to familiarise with the theory, modelling methods, software etc. Their scope did for one or the other reason not provide enough material to pursue publication. Nevertheless, the studies were well suited to provide a first assessment of the quality of results to be expected and elucidate potential room for development. In the first preliminary study, URANS was used to model a cold swirling flow characterised by a moderate swirl number, a bluff body (wake) and multiple shear layers located between the central and annular jet and the co-flow. The described flow field showed complex flow structures caused by instabilities, such as the central recirculation bubble induced by vortex breakdown. These structures were also relevant for the swirl-stabilised flame studied in Paper III. Among the investigated inflow conditions for the preliminary swirling flow study was an implementation of a fixed velocity profile boundary condition, which could be used to approximate the swirling inflow from measurements. This boundary condition was applied as the swirling inflow condition for the simulations presented in Paper III. The experience with two-equations RANS and subsequently two-equation URANS models gave also a good indication on the accuracy to be expected using RANS in complex flows. For high-fidelity modelling of complex modern burner systems the application of LES appeared preferential from this viewpoint. This approach was chosen for all three papers that are included in the research output.

In the preliminary study of the Sandia flames D, summarised in this thesis, and E, experience was gathered in the usage of the EDC in the RANS framework in general and specifically of the edcSMOKE library from [78, 79], which is a C++-based code to be linked into OpenFOAM for numerical modelling of reacting flows. The edcSMOKE library has different versions of the EDC implemented and was used for reacting flow simulations in the LES framework presented in Paper I. For a theoretical discussion of the different versions of the EDC developed over the years, the reader is referred to Ertesvåg [53, 116]. The post-simulation analysis of thermochemical data of Sandia flames D and E using the software toolkit Cantera [108] was used to gain experience in this software and provided the basis for later studies with this full-featured open-source code for chemical, thermodynamic and transport problems. The software was used for laminar premixed flame calculations and Probability density function (Pdf) generation for the simulations presented in Papers II and III.

The study of the oxyfuel combustor as an extension to the work done in Paper III is yet at a preliminary stage. It has so far been aimed at identifying necessary modelling

adjustments to apply the approach used in Paper III to oxyfuel combustion. The application of the new dissipation-based model is highly relevant to gain a good understanding of its capabilities and incapacities under a broad spectrum of conditions. No solid conclusions can yet be drawn from the presented preliminary study, but first indications exist where further work should have its focus. While the consideration of local extinction through a Damköhler number criterion based on laminar flame properties performed well under air-fuel conditions, it turned out to be unsuitable for oxyfuel conditions. With no extinction model applied, better results were achieved but the competitiveness of the approach when compared with other LES studies showed a poorer outcome for the oxy-methane flame. A crucial aspect of the successful application of the newly introduced approach under oxyfuel conditions is a physically-sound consideration of non-unity Lewis number effects. This requires the development of dependable (sub-)models to capture the multifaceted and non-linear influence on flame characteristics. Also the chemical activity of CO_2 , radiation, and other phenomena require thorough investigation in the future.

4 Contributions to the research output

4.1 Overview

The research output as the core of this thesis is composed of three manuscripts, which were published/ prepared for submission to peer-reviewed specialist journals in the fields of combustion and modelling. The common thread within the manuscripts is the usage of dissipation-based finite-rate chemistry combustion models for turbulent reacting flow simulations in the LES framework. Paper I was the result of collaborative work during my research stay at the University of Cambridge. The paper was submitted to the 38th International Symposium on Combustion and was published in the Proceedings of the Combustion Institute. The research stay at the University of Cambridge under the supervision of Professor Swaminathan provided also an incentive for the work on a new dissipation-based combustion model to be applied under premixed conditions, which resulted in Paper II and was published in Combustion Theory and Modelling. Paper III is built upon the work presented in Paper II and applied the combustion model in a different premixed reacting flow setting and is to be submitted to a journal.

4.2 List of papers

Paper I

Study of MILD combustion using LES and advanced analysis tools

Zhiyi Li; Stefanie Tomasch; Zhi X. Chen; Alessandro Parente; Ivar S. Ertesvåg; Nedunchezhian Swaminathan

The PhD candidate's contribution to the paper: Jointly with the first author Zhiyi Li, I worked on the used CFD simulation setup. This included a literature study on the case, setting initial and boundary conditions, both for the cold and hot flow simulations, and carrying out grid quality checks. I ran the simulations using the EDC and assisted the first author in the post-processing and writing process. For the discussion of results, I contributed calculations to assess the dependability of available experimental measurements based on energy balance considerations, which are included in the supplemental material of the published paper. I made no contributions to the analysis of reaction zones.

Paper II

Development of a turbulence dissipation-based reaction rate model for progress variable in turbulent premixed flames.

Stefanie Tomasch; Nedunchezhian Swaminathan; Christoph Spijker; Ivar S. Ertesvåg

The PhD candidate's contribution to the paper: I conceptualised and implemented the final version of the model presented in the paper, which was inspired by discussions with Prof. Swaminathan at the University of Cambridge, who contributed with valuable insights into premixed combustion modelling. I ran the simulations presented in the paper and evaluated results as well as wrote and revised the paper as first author. The co-authors contributed with discussions, suggestions, critical review as well as contributed to the revision process.

Paper III

A numerical study of flow structures and flame shape transition in swirl-stabilised turbulent premixed flames subject to local extinction.

Stefanie Tomasch; Nedunchezhian Swaminathan; Christoph Spijker; Ivar S. Ertesvåg

The PhD candidate's contribution to the paper: I ran the simulations presented in the paper and evaluated results as well as wrote the paper as first author. The co-authors contributed with valuable discussions, suggestions and critical review.

5 Conclusion and outlook

The papers contained in the research section include separate conclusions for each corresponding study, but a short general summary of the findings of this thesis will be given herein. Within this thesis dissipation-based combustion modelling was applied and developed primarily for LES, as a review of literature and also experience with RANS and LES studies indicated the necessity of high-fidelity turbulence modelling for a sophisticated description of complex modern burner systems. The combustion models were applied in a wide range of settings in this thesis, with studied flames being in non-premixed, premixed (oxyfuel and air-fuel) and MILD combustion mode. Advantages and disadvantages of the models emerged from these studies. As the EDC tracks the complete thermochemical state on-the-fly, composition and reactions are able to adapt quickly to outer flow and thermal conditions. This flexibility is also a key argument for the application of the EDC in a wide range of combustion settings, including MILD, and makes the inclusion of wall heat losses and radiation relatively straight-forward. At the same time, the computational expenses related to keeping track of the complete thermochemical state are a limiting factor for the feasibility of simulations and the choice of chemical mechanism. In contrast, the newly introduced algebraic finite-rate dissipation-based combustion model turned out computationally highly-efficient and feasible also for high-fidelity simulations. Furthermore, the tabulation of thermochemical data allowed for the usage of sophisticated chemical mechanisms such as the GRI 3.0. However, this simplicity came at the price of reduced flexibility of the combustion model to consider the outer thermal conditions and the necessity to apply predefined PDFs to recover thermochemical data from the CFD simulations. In addition, the algebraic model was conceptualised and has so far only been tested with lean premixed combustion. Other application possibilities have yet to be evaluated in detail.

This leads to the outlook for this thesis, where the author would like to stress specifically the development possibilities for the newly introduced algebraic dissipation-based combustion model. Many aspects of this model deserve a closer investigation. An evaluation of the model expression based on DNS data was proposed by a reviewer of Paper II to better understand its capability to describe the underlying combustion physics. Its application to a non-unity Lewis number oxy-methane flame, as described in Section 3.4 revealed the need for a review of the modelling assumptions under these conditions. So far, the model has proven to cope well with flame thickening and extinction phenomena for lean premixed air-methane combustion. The introduction of an additional degree of freedom into the tables of thermochemical data to consider heat loss would also extend the sophistication of the model and its ability to model realistic non-adiabatic combustion processes. Subsequently, studies on its application to partially-premixed and MILD combustion could provide valuable information on the flexibility of the model to cope with varying flame and flow conditions. The direct comparison with results of the EDC or PaSR model would also provide valuable insights concerning the competitiveness of the new model with existing approaches in the sub-category of dissipation-based combustion models. However, a suitable case for comparison between the models has to be a compromise in terms of complexity of the flow and chemical mechanism chosen. Considerable differences in computational expenses exist between the approaches, as both the EDC and PaSR involve computationally demanding on-the-fly chemistry calculation.

References

- [1] S.J. Pyne, *Fire: a brief history*, University of Washington Press, Seattle & London, 2019.
- [2] N. Oreskes, *The scientific consensus on climate change*, *Science* 306 (2004), pp. 1686–1686. DOI: 10.1126/science.1103618.
- [3] Core Writing Team, R.K. Pachauri, and L.A. Meyer (eds.), *Climate change 2014: Synthesis report. contribution of working groups I II and III to the fifth assessment report of the intergovernmental panel on climate change*, Report, Intergovernmental Panel on Climate Change, 2014, Available at <https://www.ipcc.ch/report/ar5/syr/>.
- [4] *Paris agreement*, United Nations (2015). Available at https://unfccc.int/sites/default/files/english_paris_agreement.pdf.
- [5] IEA, *World Energy Outlook 2020*, International Energy Agency, 2020. DOI: doi.org/10.1787/557a761b-en.
- [6] N. Swaminathan, *Physical insights on MILD combustion from DNS*, *Frontiers in Mechanical Engineering* 5 (2019). DOI: 10.3389/fmech.2019.00059.
- [7] IEA, *World Energy Outlook 2019*, International Energy Agency, 2019. DOI: [doi:10.1787/caf32f3b-en](https://doi.org/10.1787/caf32f3b-en).
- [8] M.A. Nemitallah, S.S. Rashwan, I.B. Mansir, A.A. Abdelhafez, and M.A. Habib, *Review of novel combustion techniques for clean power production in gas turbines*, *Energy & Fuels* 32 (2018), pp. 979–1004. DOI: 10.1021/acs.energyfuels.7b03607.
- [9] A. Cavaliere and M. de Joannon, *MILD combustion*, *Progress in Energy and Combustion Science* 30 (2004), pp. 329–366. DOI: 10.1016/j.pecs.2004.02.003.
- [10] J. Kariuki, J.R. Dawson, and E. Mastorakos, *Measurements in turbulent premixed bluff body flames close to blow-off*, *Combustion and Flame* 159 (2012), pp. 2589–2607. DOI: 10.1016/j.combustflame.2012.01.005.
- [11] J.R. Dawson, R.L. Gordon, J. Kariuki, E. Mastorakos, A.R. Masri, and M. Juddoo, *Visualization of blow-off events in bluff-body stabilized turbulent premixed flames*, *Proceedings of the Combustion Institute* 33 (2011), pp. 1559–1566. DOI: 10.1016/j.proci.2010.05.044.

- [12] F. Liu, H. Guo, G.J. Smallwood, and O.L. Gülder, *The chemical effects of carbon dioxide as an additive in an ethylene diffusion flame: implications for soot and nox formation*, *Combustion and Flame* 125 (2001), pp. 778–787. DOI: 10.1016/S0010-2180(00)00241-8.
- [13] A.N. Mazas, B. Fiorina, D.A. Lacoste, and T. Schuller, *Effects of water vapor addition on the laminar burning velocity of oxygen-enriched methane flames*, *Combustion and Flame* 158 (2011), pp. 2428–2440. DOI: 10.1016/j.combustflame.2011.05.014.
- [14] K. Kohse-Höinghaus, *Clean combustion: Chemistry and diagnostics for a systems approach in transportation and energy conversion*, *Progress in Energy and Combustion Science* 65 (2018), pp. 1–5. DOI: 10.1016/j.peccs.2017.10.001.
- [15] A. Giusti and E. Mastorakos, *Turbulent combustion modelling and experiments: Recent trends and developments*, *Flow, Turbulence and Combustion* 103 (2019), pp. 847–869. DOI: 10.1007/s10494-019-00072-6.
- [16] T. Echekki and E. Mastorakos, *Turbulent combustion modeling: Advances, new trends and perspectives*, Vol. 95, Springer Science & Business Media, Heidelberg, 2010. DOI: 10.1007/978-94-007-0412-1.
- [17] N. Swaminathan, X.S. Bai, N.E.L. Haugen, C. Fureby, and G. Brethouwer, *Advanced Turbulent Combustion Physics and Applications*, Cambridge University Press, Cambridge, UK, 2021. DOI: 10.1017/9781108671422.
- [18] D. Veynante and L. Vervisch, *Turbulent combustion modeling*, *Progress in Energy and Combustion Science* 28 (2002), pp. 193–266. DOI: 10.1016/S0360-1285(01)00017-X.
- [19] N. Peters, *Laminar flamelet concepts in turbulent combustion*, *Symposium (International) on Combustion* 21 (1988), pp. 1231–1250. DOI: 10.1016/S0082-0784(88)80355-2.
- [20] J.H. Frank and R.S. Barlow, *Non-premixed turbulent combustion.*, Tech. Rep. SAND2007-6197P 520577, Sandia National Laboratories, Livermore, CA, 2007, Available at <https://www.osti.gov/biblio/1714512>.
- [21] J.F. Driscoll, *Turbulent premixed combustion: Flamelet structure and its effect on turbulent burning velocities*, *Progress in Energy and Combustion Science* 34 (2008), pp. 91–134. DOI: 10.1016/j.peccs.2007.04.002.
- [22] A. Ratner, J. Driscoll, J. Donbar, C. Carter, and J. Mullin, *Reaction zone structure of non-premixed turbulent flames in the "intensely wrinkled" regime*, *Proceedings of The Combustion Institute* 28 (2000), pp. 245–252. DOI: 10.1016/S0082-0784(00)80217-9.
- [23] C. Meneveau and T. Poinso, *Stretching and quenching of flamelets in premixed turbulent combustion*, *Combustion and Flame* 86 (1991), pp. 311–332. DOI: 10.1016/0010-2180(91)90126-V.
- [24] M.M. Kamal, R.S. Barlow, and S. Hochgreb, *Conditional analysis of turbulent premixed and stratified flames on local equivalence ratio and progress of reaction*, *Combustion and Flame* 162 (2015), pp. 3896–3913. DOI: 10.1016/j.combustflame.2015.07.026.

- [25] F. Proch, P. Domingo, L. Vervisch, and A.M. Kempf, *Flame resolved simulation of a turbulent premixed bluff-body burner experiment. Part I: Analysis of the reaction zone dynamics with tabulated chemistry*, *Combustion and Flame* 180 (2017), pp. 321–339. DOI: 10.1016/j.combustflame.2017.02.011.
- [26] K. Kohse-Höinghaus, *Combustion in the future: The importance of chemistry*, *Proceedings of the Combustion Institute* 38 (2021), pp. 1–56. DOI: 10.1016/j.proci.2020.06.375.
- [27] P. Wang, F. Zieker, R. Schießl, N. Platova, J. Fröhlich, and U. Maas, *Large eddy simulations and experimental studies of turbulent premixed combustion near extinction*, *Proceedings of the Combustion Institute* 34 (2013), pp. 1269–1280. DOI: 10.1016/j.proci.2012.06.149.
- [28] A.A.V. Perpignan, A. Gangoli Rao, and D.J.E.M. Roekaerts, *Flameless combustion and its potential towards gas turbines*, *Progress in Energy and Combustion Science* 69 (2018), pp. 28–62. DOI: 10.1016/j.pecs.2018.06.002.
- [29] A. Cavigiolo, M.A. Galbiati, A. Effuggi, D. Gelosa, and R. Rota, *MILD combustion in a laboratory-scale apparatus*, *Combustion Science and Technology* 175 (2003), pp. 1347–1367. DOI: 10.1080/00102200302356.
- [30] X. Huang, M.J. Tummers, and D.J.E.M. Roekaerts, *Experimental and numerical study of MILD combustion in a lab-scale furnace*, *Energy Procedia* 120 (2017), pp. 395–402. DOI: 10.1016/j.egypro.2017.07.231.
- [31] G. Sorrentino, P. Sabia, M. de Joannon, A. Cavaliere, and R. Ragucci, *Design and development of a lab-scale burner for MILD/flameless combustion*, *Chemical Engineering Transactions* 43 (2015), pp. 883–888. DOI: 10.3303/CET1543148.
- [32] M. Ihme and Y.C. See, *LES flamelet modeling of a three-stream MILD combustor: Analysis of flame sensitivity to scalar inflow conditions*, *Proceedings of the Combustion Institute* 33 (2011), pp. 1309–1317. DOI: 10.1016/j.proci.2010.05.019.
- [33] Z. Chen, V.M. Reddy, S. Ruan, N.A.K. Doan, W.L. Roberts, and N. Swaminathan, *Simulation of MILD combustion using perfectly stirred reactor model*, *Proceedings of the Combustion Institute* 36 (2017), pp. 4279–4286. DOI: 10.1016/j.proci.2016.06.007.
- [34] Z. Li, A. Cuoci, and A. Parente, *Large eddy simulation of MILD combustion using finite rate chemistry: Effect of combustion sub-grid closure*, *Proceedings of the Combustion Institute* 37 (2019), pp. 4519–4529. DOI: 10.1016/j.proci.2018.09.033.
- [35] F.C. Christo and B.B. Dally, *Modeling turbulent reacting jets issuing into a hot and diluted coflow*, *Combustion and Flame* 142 (2005), pp. 117–129. DOI: 10.1016/j.combustflame.2005.03.002.
- [36] B.F. Magnussen and B.H. Hjertager, *On mathematical modeling of turbulent combustion with special emphasis on soot formation and combustion*, *Symposium (International) on Combustion* 16 (1977), pp. 719–729. DOI: 10.1016/S0082-0784(77)80366-4.
- [37] I.R. Gran and B.F. Magnussen, *A numerical study of a bluff-body stabilized diffusion flame. Part 2. influence of combustion modeling and finite-rate chem-*

- istry, *Combustion Science and Technology* 119 (1996), pp. 191–217. DOI: 10.1080/00102209608951999.
- [38] B.F. Magnussen, *On the structure of turbulence and a generalized Eddy dissipation concept for chemical reaction in turbulent flow*, in *19th Aerospace Sciences Meeting*, January 12-15, St. Louis, MO. 1981. DOI: 10.2514/6.1981-42.
- [39] I.S. Ertesvåg and B.F. Magnussen, *The Eddy dissipation turbulence energy cascade model*, *Combustion Science and Technology* 159 (2000), pp. 213–235. DOI: 10.1080/00102200008935784.
- [40] A. De, E. Oldenhof, P. Sathiah, and D. Roekaerts, *Numerical simulation of delft-jet-in-hot-coflow (djhc) flames using the Eddy dissipation concept model for turbulence-chemistry interaction*, *Flow Turbulence and Combustion* 87 (2011), pp. 537–567. DOI: 10.1007/s10494-011-9337-0.
- [41] Z. Li, A. Cuoci, A. Sadiki, and A. Parente, *Comprehensive numerical study of the adelaide jet in hot-coflow burner by means of rans and detailed chemistry*, *Energy* 139 (2017), pp. 555–570. DOI: 10.1016/j.energy.2017.07.132.
- [42] Z. Li, A. Cuoci, A. Sadiki, and A. Parente, *Finite-rate chemistry modelling of non-conventional combustion regimes*, *Energy Procedia* 142 (2017), pp. 1570–1576. DOI: 10.1016/j.egypro.2017.12.608.
- [43] B. Lakshminarayana, *Turbulence modeling for complex shear flows*, *AIAA Journal* 24 (1986), pp. 1900–1917. DOI: 10.2514/3.9547.
- [44] C.H. Cheng and S. Farokhi, *The effects of streamline curvature and swirl on turbulent flows in curved ducts*, Report, Kansas Univ. Center for Research, Inc. Lawrence, KS, United States, 1990, Available at <https://ntrs.nasa.gov/citations/19910006193>.
- [45] B.E. Launder, *Second-moment closure: present... and future?*, *International Journal of Heat and Fluid Flow* 10 (1989), pp. 282–300. DOI: 10.1016/0142-727X(89)90017-9.
- [46] G.M. Ottino, A. Fancello, M. Falcone, R.J.M. Bastiaans, and L.P.H. de Goeij, *Combustion modeling including heat loss using flamelet generated manifolds: A validation study in OpenFOAM*, *Flow, Turbulence and Combustion* 96 (2016), pp. 773–800. DOI: 10.1007/s10494-015-9666-5.
- [47] S.E. Jella, J.M. Bergthorson, P.Q. Gauthier, and G. Bourque, *CFD Modeling of Equivalence Ratio Effects on a Pressurized Turbulent Premixed Flame*, in *ASME Turbo Expo 2016: Turbomachinery Technical Conference and Exposition*, Vol. 4B: Combustion, Fuels and Emissions, June 13-17, Seoul, South Korea. 2016. DOI: 10.1115/gt2016-58074.
- [48] D.A. Lysenko, I.S. Ertesvåg, and K.E. Rian, *Numerical simulations of the sandia flame d using the Eddy dissipation concept*, *Flow Turbulence and Combustion* 93 (2014), pp. 665–687. DOI: 10.1007/s10494-014-9561-5.
- [49] E. Fedina and C. Fureby, *A comparative study of flamelet and finite rate chemistry LES for an axisymmetric dump combustor*, *Journal of Turbulence* 12 (2011), pp. 1–20. DOI: 10.1080/14685248.2011.582586.
- [50] B. Panjwani, I.S. Ertesvåg, A. Gruber, and K. Rian, *Turbulence combustion closure model based on the Eddy dissipation concept for Large eddy simulation*, *Advances*

in Fluid Mechanics VIII 69 (2010), p. 27.

- [51] Z.B. Chen, J. Wen, B.P. Xu, and S. Dembele, *Extension of the Eddy dissipation concept and smoke point soot model to the LES frame for fire simulations*, Fire Safety Journal 64 (2014), pp. 12–26. DOI: 10.1016/j.firesaf.2014.01.001.
- [52] S. Jella, P. Gauthier, G. Bourque, J. Bergthorson, G. Bulat, J. Rogerson, and S. Sadasivuni, *Large eddy simulation of a pressurized, partially premixed swirling flame with finite-rate chemistry*, Journal of Engineering for Gas Turbines and Power 140 (2018). DOI: 10.1115/1.4040007.
- [53] I.S. Ertesvåg, *Analysis of some recently proposed modifications to the Eddy dissipation concept (EDC)*, Combustion Science and Technology (2019), pp. 1–29. DOI: 10.1080/00102202.2019.1611565.
- [54] J.R. Hertzberg, I.G. Shepherd, and L. Talbot, *Vortex shedding behind rod stabilized flames*, Combustion and Flame 86 (1991), pp. 1–11. DOI: 10.1016/0010-2180(91)90051-C.
- [55] J.C. Pan, M.D. Vangsness, S.P. Heneghan, and D.R. Ballal, *Scalar Measurements in Bluff Body Stabilized Flames Using Cars Diagnostics*, in ASME 1991 International Gas Turbine and Aeroengine Congress and Exposition, Vol. 3: Coal, Biomass and Alternative Fuels; Combustion and Fuels; Oil and Gas Applications; Cycle Innovations, June 3-6, Orlando, FL. 1991. DOI: 10.1115/91-gt-302.
- [56] H. Watanabe, S.J. Shanbhogue, S. Taamallah, N.W. Chakroun, and A.F. Ghoniem, *The structure of swirl-stabilized turbulent premixed CH₄/air and CH₄/O₂/CO₂ flames and mechanisms of intense burning of oxy-flames*, Combustion and Flame 174 (2016), pp. 111–119. DOI: 10.1016/j.combustflame.2016.09.015.
- [57] T.D. Dunstan, Y. Minamoto, N. Chakraborty, and N. Swaminathan, *Scalar dissipation rate modelling for Large eddy simulation of turbulent premixed flames*, Proceedings of the Combustion Institute 34 (2013), pp. 1193–1201. DOI: 10.1016/j.proci.2012.06.143.
- [58] I. Langella, N. Swaminathan, and R.W. Pitz, *Application of unstrained flamelet SGS closure for multi-regime premixed combustion*, Combustion and Flame 173 (2016), pp. 161–178. DOI: 10.1016/j.combustflame.2016.08.025.
- [59] J.C. Massey, I. Langella, and N. Swaminathan, *A scaling law for the recirculation zone length behind a bluff body in reacting flows*, Journal of Fluid Mechanics 875 (2019), pp. 699–724. DOI: 10.1017/jfm.2019.475.
- [60] Z.X. Chen, I. Langella, R.S. Barlow, and N. Swaminathan, *Prediction of local extinctions in piloted jet flames with inhomogeneous inlets using unstrained flamelets*, Combustion and Flame 212 (2020), pp. 415–432. DOI: 10.1016/j.combustflame.2019.11.007.
- [61] S. Taamallah, Y. Dagan, N. Chakroun, S.J. Shanbhogue, K. Vogiatzaki, and A.F. Ghoniem, *Helical vortex core dynamics and flame interaction in turbulent premixed swirl combustion: A combined experimental and Large eddy simulation investigation*, Physics of Fluids 31 (2019). DOI: 10.1063/1.5065508.
- [62] N.W. Chakroun, *Dynamics, stability and scaling of turbulent methane oxy-combustion*, Doctoral thesis, Massachusetts Institute of Technology, Cambridge,

MA, 2018, Available at <https://dspace.mit.edu/handle/1721.1/115722>.

- [63] S. Taamallah, N.W. Chakroun, H. Watanabe, S.J. Shanbhogue, and A.F. Ghoniem, *On the characteristic flow and flame times for scaling oxy and air flame stabilization modes in premixed swirl combustion*, Proceedings of the Combustion Institute 36 (2017), pp. 3799–3807. DOI: 10.1016/j.proci.2016.07.022.
- [64] N.W. Chakroun, S.J. Shanbhogue, Y. Dagan, and A.F. Ghoniem, *Flamelet structure in turbulent premixed swirling oxy-combustion of methane*, Proceedings of the Combustion Institute 37 (2019), pp. 4579–4586. DOI: 10.1016/j.proci.2018.06.181.
- [65] P. Glarborg and L.L.B. Bentzen, *Chemical effects of a high CO₂ concentration in oxy-fuel combustion of methane*, Energy & Fuels 22 (2008), pp. 291–296. DOI: 10.1021/ef7005854.
- [66] A. Sevault, M. Dunn, R.S. Barlow, and M. Ditaranto, *On the structure of the near field of oxy-fuel jet flames using raman/rayleigh laser diagnostics*, Combustion and Flame 159 (2012), pp. 3342–3352. DOI: 10.1016/j.combustflame.2012.06.017.
- [67] R. Marsh, J. Runyon, A. Giles, S. Morris, D. Pugh, A. Valera-Medina, and P. Bowen, *Premixed methane oxycombustion in nitrogen and carbon dioxide atmospheres: measurement of operating limits, flame location and emissions.*, Proceedings of the Combustion Institute 36 (2017), pp. 3949–3958. DOI: 10.1016/j.proci.2016.06.057.
- [68] P. Kutne, B.K. Kapadia, W. Meier, and M. Aigner, *Experimental analysis of the combustion behaviour of oxyfuel flames in a gas turbine model combustor*, Proceedings of the Combustion Institute 33 (2011), pp. 3383–3390. DOI: 10.1016/j.proci.2010.07.008.
- [69] N.A.K. Doan and N. Swaminathan, *Role of radicals on MILD combustion inception*, Proceedings of the Combustion Institute 37 (2019), pp. 4539–4546. DOI: 10.1016/j.proci.2018.07.038.
- [70] S.G. Sundkvist, A. Dahlquist, J. Janczewski, M. Sjödin, M. Bysveen, M. Ditaranto, Ø. Langørgen, M. Seljeskog, and M. Siljan, *Concept for a combustion system in oxyfuel gas turbine combined cycles*, Journal of Engineering for Gas Turbines and Power 136 (2014). DOI: 10.1115/1.4027296.
- [71] A.J. Aspden, M.S. Day, and J.B. Bell, *Characterization of low Lewis number flames*, Proceedings of the Combustion Institute 33 (2011), pp. 1463–1471. DOI: 10.1016/j.proci.2010.05.090.
- [72] A. Potnis, V.R. Unni, H.G. Im, and A. Saha, *Extinction of non-equidiffusive premixed flames with oscillating strain rates*, Combustion and Flame 234 (2021), p. 111617. DOI: 10.1016/j.combustflame.2021.111617.
- [73] T.H. Kim, J.W. Park, H.Y. Park, J. Park, J.H. Park, and I.G. Lim, *Chemical and radiation effects on flame extinction and NO_x formation in oxy-methane combustion diluted with CO₂*, Fuel 177 (2016), pp. 235–243. DOI: 10.1016/j.fuel.2016.03.012.
- [74] S.R. Lee and J.S. Kim, *The asymptotic structure of strained chain-branching premixed flames with nonunity Lewis numbers and their extinction*, Combustion Science and Technology (2022), pp. 1–30. DOI: 10.1080/00102202.2022.2114798.

- [75] *OpenFOAM (field operation and manipulation)*. Available at www.openfoam.org, last visited 2022-11-16.
- [76] Y.M. Al-Abdeli and A.R. Masri, *Recirculation and flowfield regimes of unconfined non-reacting swirling flows*, *Experimental Thermal and Fluid Science* 27 (2003), pp. 655–665. DOI: 10.1016/S0894-1777(02)00280-7.
- [77] G.P. Smith, M. Golden D. M. and Frenklach, B. Moriarty N. W. and Eiteneer, M. Goldenberg, C.T. Bowman, R.K. Hanson, S. Song, W.C. Gardiner Jr., V.V. Lissianski, and Z. Qin, *Gri-mech 3.0*. Available at <http://combustion.berkeley.edu/gri-mech/version30/text30.html>, last visited 2022-09-14.
- [78] A. Parente, M.R. Malik, F. Contino, A. Cuoci, and B.B. Dally, *Extension of the Eddy dissipation concept for turbulence/chemistry interactions to MILD combustion*, *Fuel* 163 (2016), pp. 98–111. DOI: 10.1016/j.fuel.2015.09.020.
- [79] A. Cuoci, A. Frassoldati, T. Faravelli, and E. Ranzi, *Opensmoke++: An object-oriented framework for the numerical modeling of reactive systems with detailed kinetic mechanisms*, *Computer Physics Communications* 192 (2015), pp. 237–264. DOI: 10.1016/j.cpc.2015.02.014.
- [80] R.S. Barlow and J.H. Frank, *Effects of turbulence on species mass fractions in methane/air jet flames*, *Symposium (International) on Combustion* 27 (1998), pp. 1087–1095. DOI: /10.1016/S0082-0784(98)80510-9.
- [81] C. Schneider, A. Dreizler, J. Janicka, and E.P. Hassel, *Flow field measurements of stable and locally extinguishing hydrocarbon-fuelled jet flames*, *Combustion and Flame* 135 (2003), pp. 185–190. DOI: 10.1016/S0010-2180(03)00150-0.
- [82] A.S. Veríssimo, A.M.A. Rocha, and M. Costa, *Operational, combustion, and emission characteristics of a small-scale combustor*, *Energy & Fuels* 25 (2011), pp. 2469–2480. DOI: 10.1021/ef200258t.
- [83] R.W. Bilger, S.H. Stårner, and R.J. Kee, *On reduced mechanisms for methane-air combustion in nonpremixed flames*, *Combustion and Flame* 80 (1990), pp. 135–149. DOI: 10.1016/0010-2180(90)90122-8.
- [84] S. Nandula, R. Pitz, R. Barlow, and G. Fiechtner, *Rayleigh/Raman/LIF measurements in a turbulent lean premixed combustor*, in *34th Aerospace Sciences Meeting and Exhibit*, January 15–18, Reno, NV. AIAA, 1996. DOI: 10.2514/6.1996-937.
- [85] S. Taamallah, *Impact of fuel and oxidizer composition on premixed flame stabilization in turbulent swirling flows : dynamics and scaling*, Doctoral thesis, Massachusetts Institute of Technology, Cambridge, MA, 2016, Available at <https://dspace.mit.edu/handle/1721.1/103437>.
- [86] G. Kewlani, *Large eddy simulations of premixed turbulent flame dynamics : combustion modeling, validation and analysis*, Doctoral thesis, Massachusetts Institute of Technology, Cambridge, MA, 2014, Available at <https://dspace.mit.edu/handle/1721.1/93863>.
- [87] G. Kewlani, S. Shanbhogue, and A. Ghoniem, *Investigations into the impact of the equivalence ratio on turbulent premixed combustion using particle image velocimetry and Large eddy simulation techniques: “V” and “M” flame configurations in a swirl combustor*, *Energy & Fuels* 30 (2016), pp. 3451–3462. DOI:

- 10.1021/acs.energyfuels.5b02921.
- [88] O. Reynolds, *On the dynamical theory of incompressible viscous fluids and the determination of the criterion*, Philosophical Transactions of the Royal Society of London. (A.) 186 (1895), pp. 123–164. DOI: doi:10.1098/rsta.1895.0004.
- [89] J. Boussinesq, *Essai sur la théorie des eaux courantes*, Mémoires présentés par divers savants à l'Académie de Sciences de l'Institut National de France Vol. 23, Imprimerie nationale, Paris, FR, 1877.
- [90] F.R. Menter and Y. Egorov, *The scale-adaptive simulation method for unsteady turbulent flow predictions. part 1: Theory and model description*, Flow, Turbulence and Combustion 85 (2010), pp. 113–138. DOI: 10.1007/s10494-010-9264-5.
- [91] D.C. Wilcox, *Turbulence modeling for CFD*, 3rd ed., DCW Industries, La Cănada, Calif., 2006.
- [92] Y. Egorov and F. Menter, *Development and Application of SST-SAS Turbulence Model in the DESIDER Project*, in *Advances in Hybrid RANS-LES Modelling*. Springer Berlin Heidelberg, Notes on Numerical Fluid Mechanics and Multidisciplinary Design, 2008, pp. 261–270.
- [93] M.T. Lewandowski and I.S. Ertesvåg, *Analysis of the Eddy dissipation concept formulation for MILD combustion modelling*, Fuel 224 (2018), pp. 687–700. DOI: 10.1016/j.fuel.2018.03.110.
- [94] M. Bösenhofer, E.M. Wartha, C. Jordan, and M. Harasek, *The Eddy dissipation concept-analysis of different fine structure treatments for classical combustion*, Energies 11 (2018). DOI: 10.3390/en11071902.
- [95] M. Lesieur, O. Métais, and P. Comte, *Large-Eddy Simulations of Turbulence*, Cambridge University Press, Cambridge, UK, 2005. DOI: 10.1017/CBO9780511755507.
- [96] C. Dopazo, N. Swaminathan, L. Cifuentes, and X.S. Bai, *Premixed Combustion Modeling*, in *Advanced Turbulent Combustion Physics and Applications*, C. Fureby, G. Brethouwer, N. Swaminathan, N.E.L. Haugen, and X.S. Bai, eds., book section 3, Cambridge University Press, Cambridge (2022), pp. 100–161. DOI: 10.1017/9781108671422.004.
- [97] C. Greenshields, *OpenFOAM v6 User Guide*, The OpenFOAM Foundation, London, UK, 2018. Available at <https://doc.cfd.direct/openfoam/user-guide-v6>, last visited 2022-09-14.
- [98] P. Kalt, Y. Al-Abdeli, A. Masri, and R. Barlow, *Swirl flows and flames dataset*. Available at <https://web.aeromech.usyd.edu.au/thermofluids/swirl.php>, last visited 2022-09-14.
- [99] *Sandia/TUD piloted CH4/air jet flames* (2003). International Workshop on Measurement and Computation of Turbulent Flames, Available at <https://tnfworkshop.org/data-archives/pilotedjet/ch4-air/>, last visited 2022-09-14.
- [100] B. Wegner, A. Maltsev, C. Schneider, A. Sadiki, A. Dreizler, and J. Janicka, *Assessment of unsteady rans in predicting swirl flow instability based on LES and experiments*, International Journal of Heat and Fluid Flow 25 (2004), pp. 528–536. DOI: 10.1016/j.ijheatfluidflow.2004.02.019.

- [101] A.R. Masri, S.B. Pope, and B.B. Dally, *Probability density function computations of a strongly swirling nonpremixed flame stabilized on a new burner*, Proceedings of the Combustion Institute 28 (2000), pp. 123–131. DOI: 10.1016/S0082-0784(00)80203-9.
- [102] A. Kempf, W. Malalasekera, K.K.J. Ranga-Dinesh, and O. Stein, *Large eddy simulations of swirling non-premixed flames with flamelet models: A comparison of numerical methods*, Flow, Turbulence and Combustion 81 (2008), pp. 523–561. DOI: 10.1007/s10494-008-9147-1.
- [103] Y.M. Al-Abdeli and A.R. Masri, *Recirculation and flowfield regimes of unconfined non-reacting swirling flows*, Experimental Thermal and Fluid Science 27 (2003), pp. 655–665. DOI: 10.1016/S0894-1777(02)00280-7.
- [104] T.C. Lieuwen, *Unsteady Combustor Physics*, Cambridge University Press, Cambridge, 2012. DOI: doi: 10.1017/CBO9781139059961.
- [105] O. Stein, A.M. Kempf, and J. Janicka, *LES of the sydney swirl flame series: An initial investigation of the fluid dynamics*, Combustion Science and Technology 179 (2007), pp. 173–189. DOI: 10.1080/00102200600808581.
- [106] R.S. Barlow, J.H. Frank, A.N. Karpetis, and J.Y. Chen, *Piloted methane/air jet flames: Transport effects and aspects of scalar structure*, Combustion and Flame 143 (2005), pp. 433–449. DOI: 10.1016/j.combustflame.2005.08.017.
- [107] M. Modest and D. Haworth, *Radiative Heat Transfer in Turbulent Combustion Systems: Theory and Applications*, Springer International Publishing, 2016.
- [108] D.K. Goodwin G.and Moffat, H.S. Speth, and Raymond, *Cantera: An object-oriented software toolkit for chemical kinetics, thermodynamics, and transport processes.*, <https://www.cantera.org> (2015). Version 2.4.0.
- [109] N.V. Kornev and E. Hassel, *Method of random spots for generation of synthetic turbulent fields with prescribed autocorrelation functions*, Communications in Numerical Methods in Engineering 23 (2006), pp. 35–43. DOI: 10.1002/cnm.880.
- [110] S.J. Shanbhogue, Y.S. Sanusi, S. Taamallah, M.A. Habib, E.M.A. Mokheimer, and A.F. Ghoniem, *Flame macrostructures, combustion instability and extinction strain scaling in swirl-stabilized premixed CH₄/H₂ combustion*, Combustion and Flame 163 (2016), pp. 494–507. DOI: 10.1016/j.combustflame.2015.10.026.
- [111] G. Kewlani, S. Shanbhogue, and A. Ghoniem, *Investigations into the impact of the equivalence ratio on turbulent premixed combustion using particle image velocimetry and Large eddy simulation techniques: “V” and “M” flame configurations in a swirl combustor*, Energy & Fuels 30 (2016), pp. 3451–3462. DOI: 10.1021/acs.energyfuels.5b02921.
- [112] A. Frassoldati, A. Cuoci, T. Faravelli, E. Ranzi, C. Candusso, and D. Tolazzi, *Simplified kinetic schemes for oxy-fuel combustion*, in *1st international conference on sustainable fossil fuels for future energy*, July 6-10, Rome, Italy. 2009, pp. 6–10.
- [113] J.D. Regele, E. Knudsen, H. Pitsch, and G. Blanquart, *A two-equation model for non-unity Lewis number differential diffusion in lean premixed laminar flames*, Combustion and Flame 160 (2013), pp. 240–250. DOI: 10.1016/j.combustflame.2012.10.004.

- [114] N. Chakraborty and N. Swaminathan, *Effects of Lewis number on scalar variance transport in premixed flames*, *Flow, Turbulence and Combustion* 87 (2011), pp. 261–292. DOI: 10.1007/s10494-010-9305-0.
- [115] Y. Gao, N. Chakraborty, and N. Swaminathan, *Scalar dissipation rate transport in the context of Large eddy simulations for turbulent premixed flames with non-unity Lewis number*, *Flow, Turbulence and Combustion* 93 (2014), pp. 461–486. DOI: 10.1007/s10494-014-9553-5.
- [116] I.S. Ertesvåg, *Scrutinizing proposed extensions to the Eddy dissipation concept (EDC) at low turbulence Reynolds numbers and low Damköhler numbers*, *Fuel* 309 (2022), p. 122032. DOI: 10.1016/j.fuel.2021.122032.

Part II
Research Output

Paper I

Study of MILD combustion using LES and advanced analysis tools

Zhiyi Li; Stefanie Tomasch; Zhi X. Chen; Alessandro Parente; Ivar S. Ertesvåg; Nedunchezhian Swaminathan

Proceedings of the Combustion Institute
DOI: 10.1016/j.proci.2020.06.298

Study of MILD combustion using LES and advanced analysis tools

Zhiyi Li^{a,*}, Stefanie Tomasch^{a,b}, Zhi X. Chen^{a,*}, Alessandro Parente^{c,d},
Ivar S. Ertesvåg^b, Nedunchezhian Swaminathan^a

^a Cambridge University, Engineering Department, Hopkinson Lab, Trumpington Street, Cambridge CB2 1PZ, UK

^b Norwegian University of Science and Technology, Department of Energy and Process Engineering,
Trondheim NO-7491, Norway

^c Université Libre de Bruxelles, Ecole polytechnique de Bruxelles, Aero-Thermo-Mechanics Laboratory,
Brussels 1050, Belgium

^d Université Libre de Bruxelles and Vrije Universiteit Brussel, Combustion and Robust Optimization Group (BURN),
Brussels 1050, Belgium

Received 7 November 2019; accepted 22 June 2020

Available online 20 September 2020

Abstract

A cylindrical confined combustor operating under MILD condition is investigated using LES. The combustion and its interaction with turbulence are modeled using two reactor based models, PaSR and EDC. Results show that the Partially Stirred Reactor (PaSR) model yields improved estimation for mean temperature and species mole fractions compared to Eddy Dissipation Concept (EDC). LES data are analysed using advanced post-processing methods such as the chemical Tangential Stretching Rate (TSR), balance analysis and local Principle Component (PCA) analysis. TSR can identify chemical explosive (ignition-like) and contractive (burnt) regions. With the balance analysis of the convective, diffusive and reactive terms in temperature equation, regions with substantial heat release coming from ignition or flame are identified. The local PCA analysis classifies the whole domain into clusters (regions with specific features) and provides the leading species in each cluster. The three analyses correlate well with one another and it is observed that the most chemically active region locates upstream (in the near-field). Also, both autoignition and flame-like structures play equally important roles in MILD combustion.

© 2020 The Combustion Institute. Published by Elsevier Inc. All rights reserved.

Keywords: MILD combustion; LES; Reactor-based models; CSP analysis; local PCA

1. Introduction

More than 90% of the world total primary energy supply comes from combustion in one form or another. There are challenges to meet future energy requirement because of the limited fossil

* Corresponding authors.

E-mail addresses: zl443@cam.ac.uk (Z. Li),
zc252@cam.ac.uk (Z.X. Chen).

fuel resources. Also, the impact of combustion on the environment through emissions of green house gases, CO₂, and pollutants such as NO_x and soot is well-known. Hence, developing efficient combustion technologies with low emissions and fuel flexibility has become imperative. Moderate or Intense Low oxygen Dilution (MILD) combustion is a very promising technology and requires a massive recirculation of exhaust gases within the reaction region [1,2]. The hot exhaust gas preheating reactants helps to stabilize combustion and minimise hotspots, which yields a uniform temperature field and suppresses combustion noise [1]. Also, the temperature rise across the combustion zone is only few tens of Kelvin above the background hot gas temperature, typically below 1800 K, inhibiting production of thermal NO_x, CO and soot [1,2].

Various lab-scale burners have been used in experimental studies, including the Jet in Hot Coflow (JHC) burner [3,4], reversed-flow arrangement having the inlet and outlet on the same side [5] and cylindrical combustor with a converging duct towards the outlet [6]. The effect of hot gas recirculation is included in JHC configuration by using combustion products of an upstream burner. However, this configuration does not account for the effect of internal recirculation as it happens in realistic industrial systems. It is therefore not considered in the current study. The geometry of the other two configurations inherently include the recirculation of hot gases. More spatially uniform temperature field was observed in these configurations compared to JHC case. Also, the combustor in reversed-flow case was well-insulated, but the case in [6] allows heat loss through the wall, which could influence the combustion stability. Hence, conditions achieved in [6] are expected to be representative of practical MILD combustion conditions and thus, this burner is of interest here.

Large Eddy Simulation (LES) using a three-stream Flamelet Progress Variable (FPV) formulation was used in [7] to model the JHC flame. This burner was also studied using Partially Stirred Reactor (PaSR) [8] and laminar chemistry (without turbulence-chemistry interaction effects) [8] in the context of LES. All of these studies showed good agreement with measurements. The other two enclosed cases have also been investigated in past studies using tabulated chemistry approaches. The FPV involving counter-flow diffusion flames was extended to include the dilution effects in [9] and a diluted homogeneous reactor was used in [10]. Both of these approaches use tabulated chemistry and provided results in good agreement with the experimental data. These approaches involve a multi-dimensional lookup table, whose generation is quite tedious and time consuming. Reactor-based models such as PaSR and EDC do not require to consider dilution explicitly since the chemical species of interest (involved in the kinetic

mechanism used) are transported. Depending on the size of the chemical mechanism, these methods can be more computationally expensive, compared to tabulated chemistry.

The objectives of the present study are (i) to conduct LES of MILD combustion in experiment [6] using the PaSR and EDC models for subgrid scale (SGS) combustion, (ii) to analyse the LES data using Computational Singular Perturbation (CSP) [11] and balance [12,13] analyses to identify autoignition and flame regions, and (iii) to apply local Principal Component Analysis (PCA) [14] to extract potential chemical markers for these regions. We believe that this is the first direct comparison of PaSR and EDC models for MILD combustion in a combustor with strong internal recirculation zones simulated using LES paradigm. Most importantly, the advanced data analysis tools reveal intriguing features of MILD combustion, providing impetus to further numerical and experimental investigations.

This paper is organised as follows. The test case and its numerical modelling are described in Sections 2 and 3 respectively. The SGS combustion models are described briefly in Section 4 and the results are discussed in Section 5. The analyses to identify autoignition and flame regions are discussed in Section 6 and conclusions are summarised in the final section.

2. Experimental configuration

A 10 kW lab-scale MILD combustor investigated in [6] is chosen as the test case for this study. This cylindrical combustor operating at atmospheric pressure has air at 673.15 K entering through a central jet of diameter $d_a = 10$ mm with a bulk-mean velocity of $U_a = 113.2$ m/s, giving a Reynolds number of 17526. Methane at 298.15 K is injected into the combustor through 16 jets with $d_f = 2$ mm and $U_f = 6.2$ m/s. The cylindrical combustor has a diameter of 100 mm for a length of 340 mm and then it converges at 15°, as shown in Fig. 1. A strong recirculation region with hot flue gases is achieved aerodynamically because of the converging section.

Several experiments were conducted in [6] with an excess air ratio in the range of $1.1 \leq \lambda \leq 2.2$. Among these various experimental cases, the case labelled RUN2 with $\lambda = 1.3$ is under MILD condition and it is selected for this study. Detailed measurements of mean temperature, dry mole fractions of O₂, CO₂, HC, NO_x and CO are reported in [6]. The mole fractions are measured using stainless steel water-cooled sampling probes (average repeatability of data within 10%) and local mean temperature measurements were obtained using 13% rhodium (type R) thermocouples with uncertainty less than 5% [6]. The radial variations of

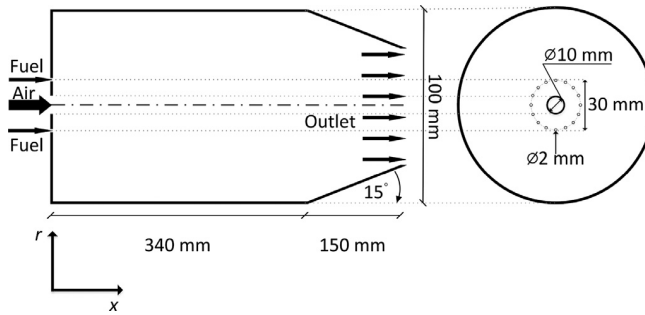


Fig. 1. Schematic view of the combustor geometry [6].

these quantities are reported in [6] for several axial locations in the non-converging section of the combustor.

3. Numerical set-up

The schematic shown in Fig. 1 forms the cylindrical computational domain and it is discretised using O-grid. Three different grids having 2, 4, and 8M cells are considered. The flow rates at the inlet are specified to match the conditions of the fuel and air streams. Since the fuel jet Reynolds number is small, no turbulence is specified but the air stream turbulence is specified using a synthetic turbulence [15] based inflow generator. The RMS velocity for air stream is $u_{rms} = 20$ m/s, following an earlier study [10] and the length scale specified for the inflow generator is 5.5 mm, 55% of jet diameter. Mean top-hat profiles without fluctuation are used for inlet scalar boundary conditions. The no-slip walls are specified to be at 1000 K based on previous studies [9,10]. The boundary layers are unresolved and represented with wall functions. All the scalar and velocity gradients in the direction normal to the outlet plane are specified to be zero. The simulations are run for $21\tau_{flow}$, where τ_{flow} is the flow through time for the entire combustor length based on U_a . The statistics are collected over the last $8\tau_{flow}$ after allowing the initial transients to leave the combustor. First, a non-reacting flow is simulated using OpenFOAM-2.3.0 [16] software and the above three grids. This code solves Favre-filtered mass, momentum, and energy conservation equations along with filtered transport equations for scalars required in combustion modelling. The sub-grid stresses are modelled using one equation (for SGS kinetic energy, \mathcal{K}) model with constant coefficient. Simulation results from the three grids are included in the supplementary material. Detailed analysis of the non-reacting flow results showed that more than 80% (indeed 90% in regions of scalar mixing and combustion) of the turbulent kinetic energy is resolved using the mesh with 2M cells. Moreover, past DNS studies [12] of MILD combustion showed that the reactive struc-

tures are broader than Kolmogorov scales and using grid spacing of 3–5 times the laminar thermal thickness is sufficient for a good LES. In the current case, the estimated laminar thermal thickness [12] is 0.36 mm. The cell size of the 2 M grid ranges from 0.27 to 1.8 mm. Thus, this mesh is appropriate for the current MILD combustion simulation. The edcSMOKE [17] finite rate chemistry solver is used for the PaSR and EDC sub-grid (SGS) combustion models, briefly described in the following.

4. Combustion models

Methane-air combustion chemistry is modelled using a skeletal mechanism [18], which was shown to be adequate for MILD conditions in [13] and in [8,19]. For the finite-rate based LES of a combustion with the current geometry, such mechanism is considered to be the best to balance between CPU hour requirement and accuracy. Both PaSR and EDC assume that each computational cell consists of a reactive structure and a surrounding fluid. Combustion occurs in the reactive structure while surrounding fluid accounts for scalar mixing processes. These mixing processes can be imperfect in turbulent combustion and thus the filtered reaction rate, $\bar{\omega}_k$ required for the scalar transport equation is specified using $\bar{\omega}_k = F \cdot \dot{\omega}_k^*(\tilde{Y}, \tilde{T})$, where $\dot{\omega}_k^*(\tilde{Y}, \tilde{T})$ represents the reaction rate of species k in the reactive structure. The reactive structure reaction rates are estimated by solving a canonical reactor, typically a perfectly stirred reactor (PSR) or a plug flow reactor (PFR). The residence time in the canonical reactor for this study is set to be CFD time step [8]. The term F in the above equation represents the fraction of the reactive structure in a numerical cell and its detail depends on the modelling approach used.

4.1. Partially Stirred Reactor model

The reactive fraction F for the PaSR model, typically denoted using κ [20], is calculated as

$$F \equiv \kappa = \frac{\tau_c}{\tau_c + \tau_{mix}}, \quad (1)$$

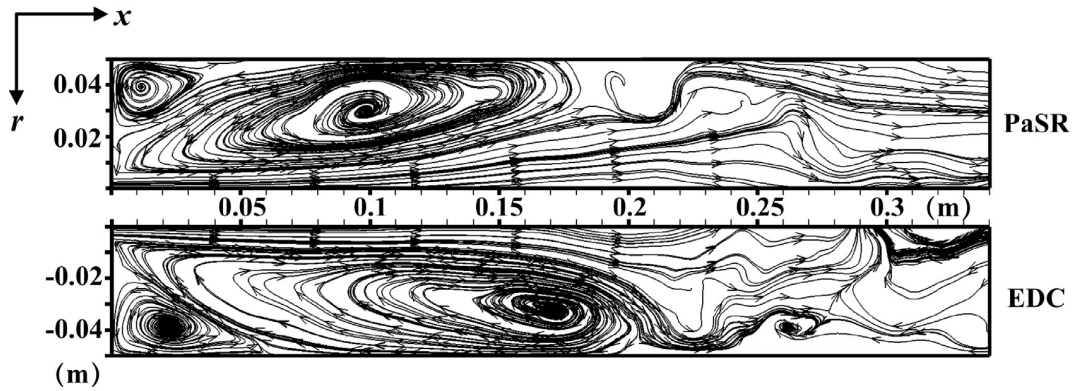


Fig. 2. Streamline profiles from PaSR and EDC combustion models.

where τ_c and τ_{mix} are the characteristic chemical and mixing time scales respectively in a cell. Here, the chemical time scale for species k is estimated as $\tau_{c,k} = Y_k^* / (dY_k^* / dt)$, which is obtained from a PFR solution. The symbol t denotes the time. The maximum value of $\tau_{c,k}$ (removing the dormant species) is chosen as τ_c [21]. The mixing time scale is defined as $\tau_{mix} = \sqrt{\tau_\Delta \tau_\eta}$, where $\tau_\Delta \simeq \Delta / \sqrt{\mathcal{K}}$ is the SGS flow time scale and $\tau_\eta \simeq \sqrt{\nu / \epsilon_{sgs}}$ is the SGS viscous time scale [8]. The symbols Δ and ϵ_{sgs} denote the LES filter width and SGS dissipation rate of \mathcal{K} .

4.2. Eddy Dissipation Concept model

EDC is based on turbulent kinetic energy cascade [22]. This provides the fraction of the reactive structures F in the flow [22], as:

$$F = \frac{\gamma_\lambda^2}{1 - \gamma_\lambda^2}, \tag{2}$$

with γ_λ estimated as a function of the flow characteristic scales:

$$\gamma_\lambda = C_\gamma \left(\frac{\nu \epsilon_{sgs}}{\mathcal{K}^2} \right)^{1/4}. \tag{3}$$

The model constant $C_\gamma = 2.1377$ is taken from a RANS study [22] as a first approximation.

Compared to PaSR model, EDC utilises only fluid mechanical time scales, more precisely it involves a ratio of molecular to SGS eddy viscosities, without involving a chemical time scale to evaluate F .

5. Results and discussion

5.1. Streamline profiles

The time-averaged streamline profiles on the mid-plane for the two models are shown in Fig. 2,

marking the recirculation zones. There are mainly two recirculation zones. The smaller one is located at the side corner ($|r| \geq 0.02$ m, $x \leq 0.05$ m) and the larger one, which brings the hot flue gases upstream and heats up the fresh air and fuel mixture, is established in the middle of the domain. Compared to PaSR model, the centre of the large recirculation zone from the EDC is situated more downstream, at around $x = 0.17$ m, while it is at about $x = 0.1$ m for PaSR. Since the same boundary conditions are used for both models, the differences in the streamlines come from combustion effects, showing that the most reactive region for EDC is probably located further downstream than that for PaSR.

5.2. Comparisons with measurements

Figure 3 shows the time-averaged temperature fields obtained from the LES using the PaSR and EDC models along with experimental results taken from [6]. The symbols in the experimental frame show scalar probe measurement locations. Overall, a reasonable agreement with experimental profile is observed for the PaSR model. However, the penetration of the air jet is over estimated (0.1 m compared to 0.079 m in the experiment) which could be related to the turbulence conditions specified at the air stream inlet. The incoming turbulence and boundary layer at the lip will influence the jet spreading angle and these affect the near-field behaviour, which is also apparent in the results. The high temperature region predicted by the PaSR model spans between $x = 0.1$ m and 0.25 m, while this region extends up to $x = 0.3$ m in the experiment. Hence under-prediction of temperature is anticipated after $x = 0.25$ m. The general pattern of the temperature variation predicted using the EDC is similar to that obtained using the PaSR model but the temperature values are under-predicted by the model as seen in Fig. 3. At $x = 0.11$ m, the PaSR model shows a large temperature gradient while, for EDC, the temperature

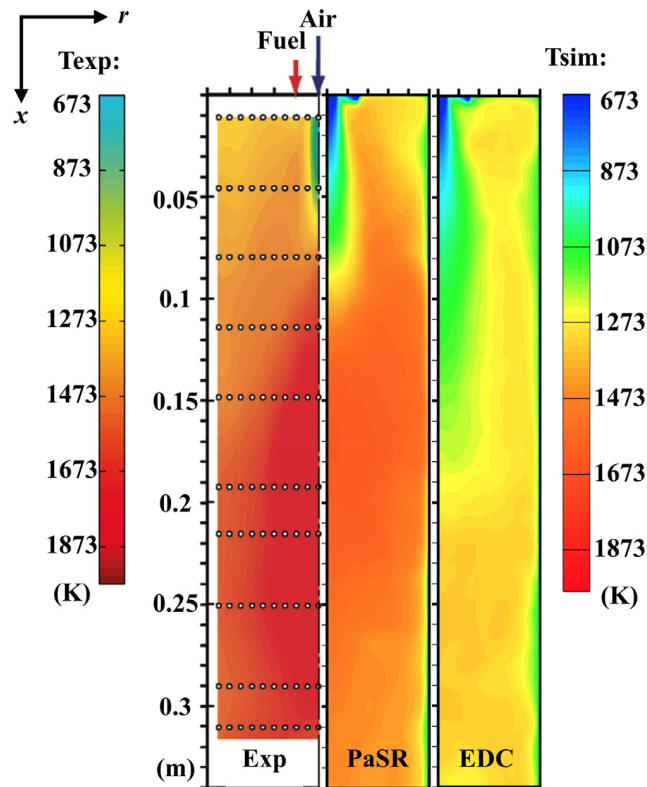


Fig. 3. Averaged temperature fields in the mid plane for PaSR and EDC models and measurements.

increase is located at around $x = 0.185$ m. These locations correlate with the centre of the large streamlines accounting for flue gas recirculation in Fig. 2.

The measured temperature field shows a strong radial gradient for $x \leq 0.15$ m which is also represented in the computational results. For further evaluations, the axial locations of $x = 11/45/79/113/147/310$ mm are considered.

The radial variations of mean temperature computed using the PaSR and EDC models are compared to the experimental data in Fig. 4. The results are shown for six axial locations. The EDC underpredicts temperature in general as observed in the previous figure. The values computed using the PaSR model compares quite well with the measurements and this comparison is similar to those obtained in [9,10]. However, the average temperatures at $x = 310$ mm is underestimated by about 200 K. On the other hand, earlier studies [9,10] showed an overestimation by about 150–200 K.

The species mole fraction for O_2 and CO_2 are shown in Figs. 5 and 6. The computed values of these species mole fractions compare quite well with experimental data for the location $x = 11$ mm and the difference between the PaSR and EDC models is small. The difference between the models'

prediction increases as one moves downstream with almost no difference for $x = 310$ mm, where the equilibrium values are expected. A closer scrutiny of the results in these two figures show a substantial difference between the computed and measured mole fractions for the first three experimental data points of $r \leq 10$ mm at $x = 45, 79, 113$ and 147 mm, which is also consistent with earlier studies using different combustion models [9,10]. For the incoming air and fuel stream temperatures, one would expect relatively higher CO_2 values and O_2 mole fractions substantially lower than 0.2 in the regions with temperature larger than about 1100 K. The experimental data seem to contradict this and a simple energy balance analysis discussed in the supplementary material suggests that there might be some issues in the measurements of CO_2 and O_2 mole fractions in the regions noted above. For these reasons, these specific experimental data points are excluded while evaluating the overall model performance. To conclude, the species mole fraction are well predicted for $x = 11$ mm by both PaSR and EDC models. After $x = 45$ mm, EDC under and over predicts CO_2 and O_2 respectively. The PaSR model works well across the whole domain if one excludes the specific data points noted above.

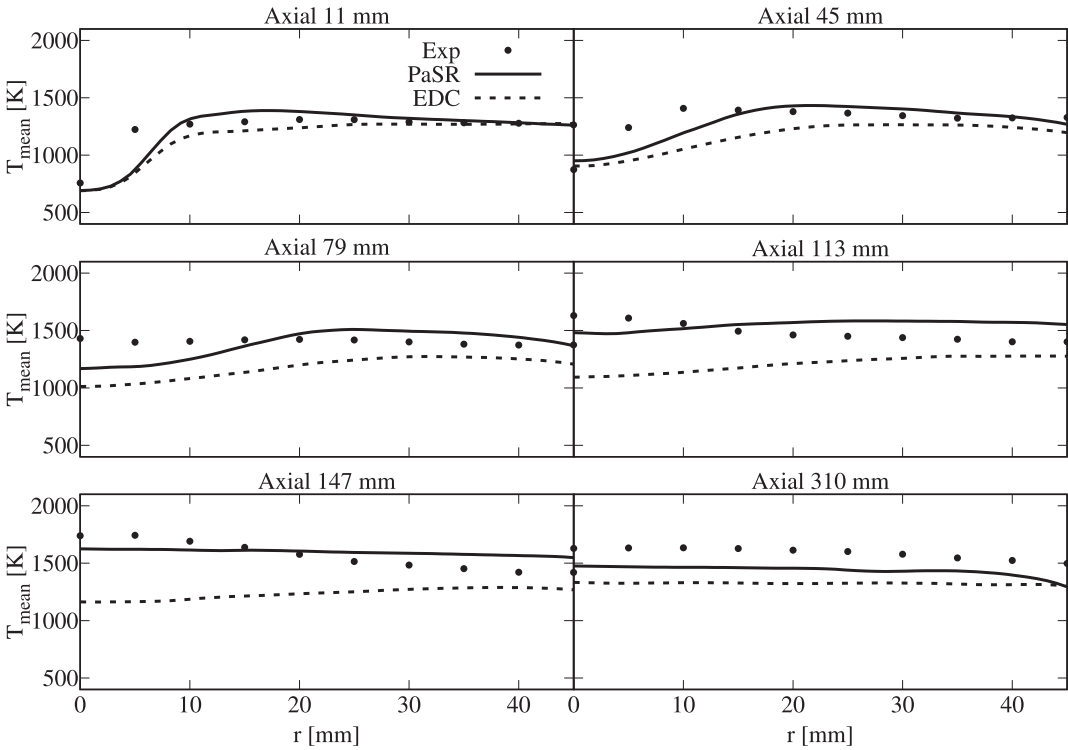


Fig. 4. Comparison of computed and measured radial variation of mean temperature at six axial locations.

6. Analysis of reaction zones

6.1. Analysis methods

Three methods, CSP, a balance analysis and local PCA, are used to extract information required to identify ignition- and flame-like regions in MILD combustion. These methods are explained briefly below before presenting the results.

6.1.1. TSR obtained from CSP analysis

The general form of species and energy equations in a homogeneous reactive system can be expressed with $\partial \mathbf{z} / \partial t = \mathbf{g}(\mathbf{z})$, where $\mathbf{g}(\mathbf{z})$ is the chemical source vector and \mathbf{z} is N dimensional state vector including N_s , the species mass fractions and temperature: $N = N_s + 1$. The chemical source vector can also be written using a new set of basis vectors $\mathbf{a}_i(\mathbf{z})$, with $\mathbf{g}(\mathbf{z}) = \sum_{i=1}^N \mathbf{a}_i(\mathbf{z}) f^i(\mathbf{z})$, where $f^i(\mathbf{z})$ is the amplitude of the i th mode. The term $f^i(\mathbf{z})$ can be further expressed as $f^i(\mathbf{z}) = f^i(\mathbf{g}(\mathbf{z})) := \mathbf{b}^i \cdot \mathbf{g}(\mathbf{z})$ and \mathbf{b}^i denotes the dual basis vector. The bi-orthonormality condition allows to recover the original representation of $\mathbf{g}(\mathbf{z})$. Based on CSP, the basis vectors \mathbf{a}_i and covectors \mathbf{b}^i can be approximated to leading order, by the right and left eigenvectors of the Jacobian \mathbf{J}_g of $\mathbf{g}(\mathbf{z})$, respectively. This set of basis vectors is traditionally employed

in CSP [11] to decouple local time scales $\tau^i = 1/\lambda_i$, where λ_i are the eigenvalues of Jacobian $\mathbf{J}_g = |\partial \mathbf{g} / \partial \mathbf{z}|$.

The tangential stretching rate (TSR) [23] denotes the level of stretching or contraction of the dynamics of interest along the direction of a vector field and is used here to characterize the most *energy-containing* time scales developing in the chemically reactive system of interest here [24,25]. This method was used for turbulent premixed flames [26] and MILD flames [19] in previous studies. The stretching rate of the reactor dynamics in the direction tangential to the vector field $\mathbf{g}(\mathbf{z})$ is $\omega_{\bar{z}}(\mathbf{g}) := \sum_{i=1}^N W_i(\mathbf{g}) \lambda_i$, with λ_i as the eigenvalue of i th mode. The weight, W_i , is

$$W_i(\mathbf{g}) := \frac{h^i(\mathbf{g})}{|\mathbf{g}|} \sum_{k=1}^N \frac{h^k(\mathbf{g})}{|\mathbf{g}|} (\mathbf{a}_k \cdot \mathbf{a}_i). \tag{4}$$

It follows that $\omega_{\bar{z}}$ is essentially a time scale obtained as a weighted average of all *energy-containing* time scales with the weight depending on the mode amplitude associated with that scale. The magnitude of the TSR represents the reciprocal of the most energy containing time scale of the system, while the positive and negative sign of TSR, $\omega_{\bar{z}}$, indicates an explosive (tendency to react) or non-explosive/dissipative nature of the dynamics respectively.

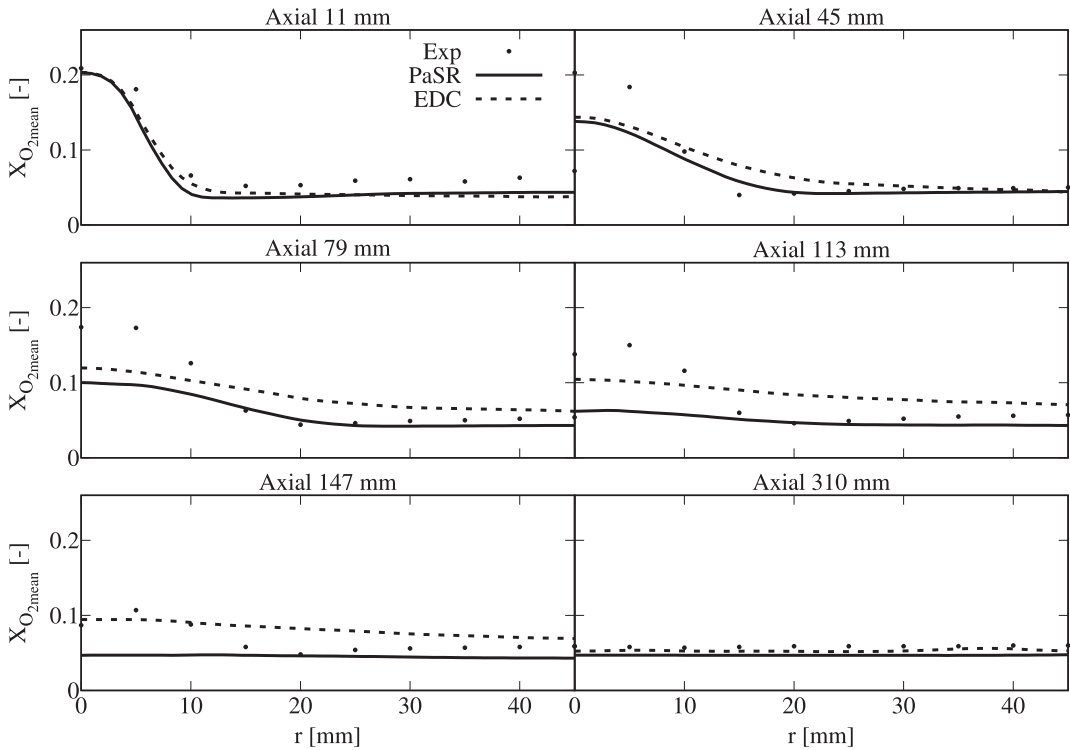


Fig. 5. Comparison of computed and measured mean O_2 mole fraction for six axial locations.

6.1.2. Balance analysis

The balance analysis considers $B = |C - D| - |R|$, where C , D and R are the convective, diffusive and reactive terms in a species or temperature transport equation [12,13]. This quantity varies spatially and $B < 0$ signifies reaction dominated (ignition-like) regions, $B = 0$ represents flame-like region because of convective-diffusive-reactive balance and $B > 0$ identifies unburnt or burnt (convective-diffusive) regions. This analysis was developed and used in past studies of MILD combustion [12,13] and it is used here along with TSR analysis to gain further insights.

6.1.3. local PCA

Principal Component Analysis (PCA) [27] is a statistical technique often used for size reduction. It detects the directions which are most active in a multi-dimensional data set, providing a mathematical formulation to select optimal parameters representing the local thermochemical state.

For a data set, \mathbf{X} , consisting of n observations of p variables, the Principal Components (PCs), \mathbf{Z} , are defined by the projection of the original data onto the eigenvectors, \mathbf{A} , of the covariance matrix, \mathbf{S} , $\mathbf{Z} = \mathbf{XA}$. The eigenvalue matrix, \mathbf{L} associated to \mathbf{S} quantifies the relative importance of the PCs. Thus a reduced subset of PCs with size q is defined: $\mathbf{Z}_q = \mathbf{XA}_q$. Such approach minimizes the amount of

information loss in the dimension reduction. Each PC is a linear combination of the variables, with weights defined by the covariance matrix eigenvectors. The global PCA analysis cannot handle highly non-linear systems, like turbulent reacting systems. Such realization has prompted the development of a local PCA approach, which employs a partition of the data set into clusters (regions), followed by the local application of PCA in each cluster [14]. Details about the application of local PCA are presented in [14].

6.2. Insights gathered

The above tools are used on the data from the PaSR model, since both instantaneous and time-averaged values of κ in Eq. (1) approach almost 1 in regions of high heat release across the whole domain. The TSR values are obtained using CSPTk software toolkit and the values of B are normalised using $(\Delta T \rho_r S_L / \delta_{th})$ for stoichiometric methane-air flame with reactants conditions used in the experiment. Fig. 7 shows typical variation of $\psi_{\vec{r}} = (|\omega_{\vec{r}}| / \omega_{\vec{r}}) \log |\omega_{\vec{r}}|$ in the mid-plane at an arbitrarily chosen time as a color map. Two more time moments are analysed and results show similar distributions. The snap shots are included in the supplementary material. The regions with high heat release rate, \tilde{Q} , are marked using two con-

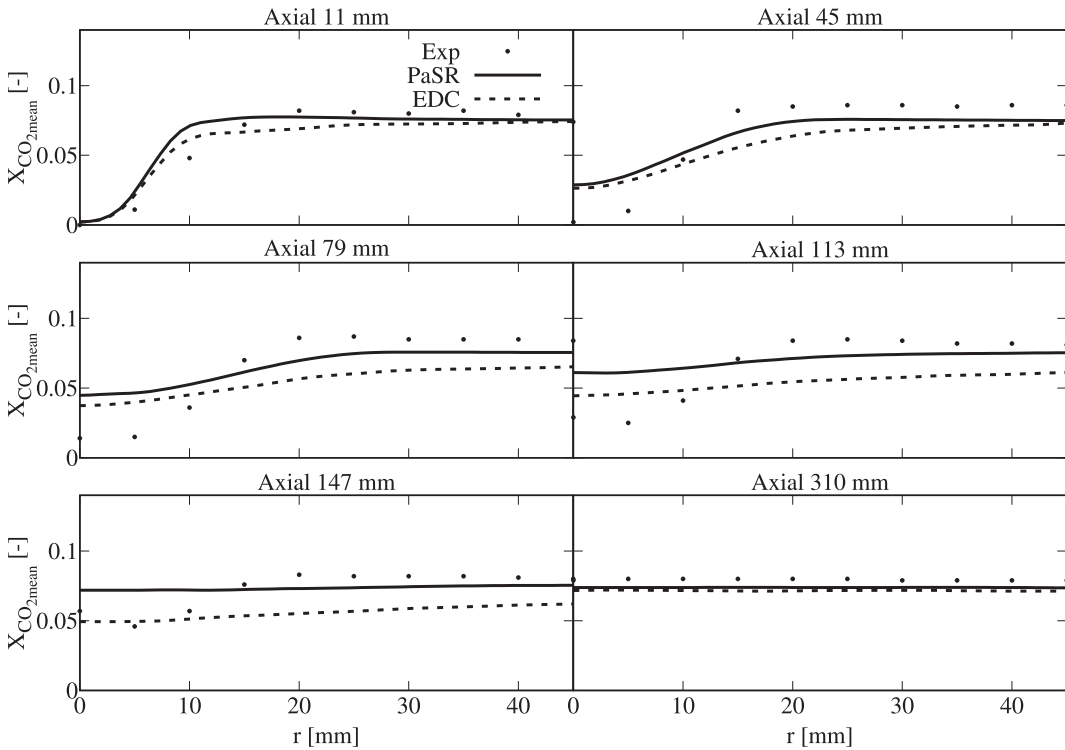


Fig. 6. Comparison of computed and measured mean CO₂ mole fraction for six axial locations.

tours for $\tilde{Q} = 10^8$ and 10^7 W/m³. The contours of normalised B are shown for three values to mark flame-like ($B^+ \sim 0$), ignition-like ($B^+ < 0$), and convective-diffusive regions. These contours for $x > 0.2$ m are not shown since combustion is almost complete by this axial location, see Fig. 3. Values of $\psi_{\tilde{\tau}} > 0$ indicate the tendency for the local mixture to react and this occurs before ignition begins. Large positive $\psi_{\tilde{\tau}}$ appears close to the shear layer between the air and fuel stream in the near-field. There is no substantial heat release in these regions and B^+ is positive. All of these signify convective-diffusive region which is consistent with expectation based on physical considerations. This region is also seen to be intermittent (see the difference between the top and bottom shear layers) because of the strong shear generated turbulence in these areas. After $x = 0.05$ m, larger negative $\psi_{\tilde{\tau}}$ values appear. Heat release rate larger than 10^7 W/m³ is observed in the regions where $\psi_{\tilde{\tau}}$ changes from positive to negative values (see the location at about $x = 0.05$ m and $r = -0.01$ m). The \tilde{Q} increase to 10^8 W/m³ by about $x = 0.1$ m where $\psi_{\tilde{\tau}} < 0$ start to appear suggesting that the ignition has occurred and these regions are dominated by reactions. Indeed, the values of B^+ are negative suggesting that these are reaction dominated regions. To see these phenomena clearly, these regions are

magnified in the insets of Fig. 7 depicting that negative B^+ appears in the middle of the \tilde{Q} contour of 10^8 W/m³, and it expands in the direction of relatively lower \tilde{Q} (10^7 W/m³), indicated by the white arrows. Hence, it is clear that the MILD combustion shares some conventional combustion features while having its own distinctive attributes, as observed in past DNS studies [12,13], which can be captured using the PaSR model.

From Fig. 7, different areas with varied features are identified. In order to better characterize the current flame with region-based post-processing tool, local PCA approach [14] is used here. In total eight clusters are used, each one representing a specific area of the system (see Fig. 8). In each cluster, one species contributing the most (showing the highest weight) to the first PC is identified. It is observed that cluster 2 marked with OH is located in the region where $B^+ = 0$ and $\tilde{Q} = 10^7$ W/m³. This area represents the flame region, which is consistent with the identification of a flame marker such as OH as principal variable. The region with positive $\psi_{\tilde{\tau}}$ value indicates the explosive region of the flame, where the radical pool (H, O and OH) is initiated, before ignition takes place. Cluster 5 in this region is characterised by H (followed by O) as the most contributing species, which is again consistent with what is observed in Fig. 7. H₂O₂ is the leading

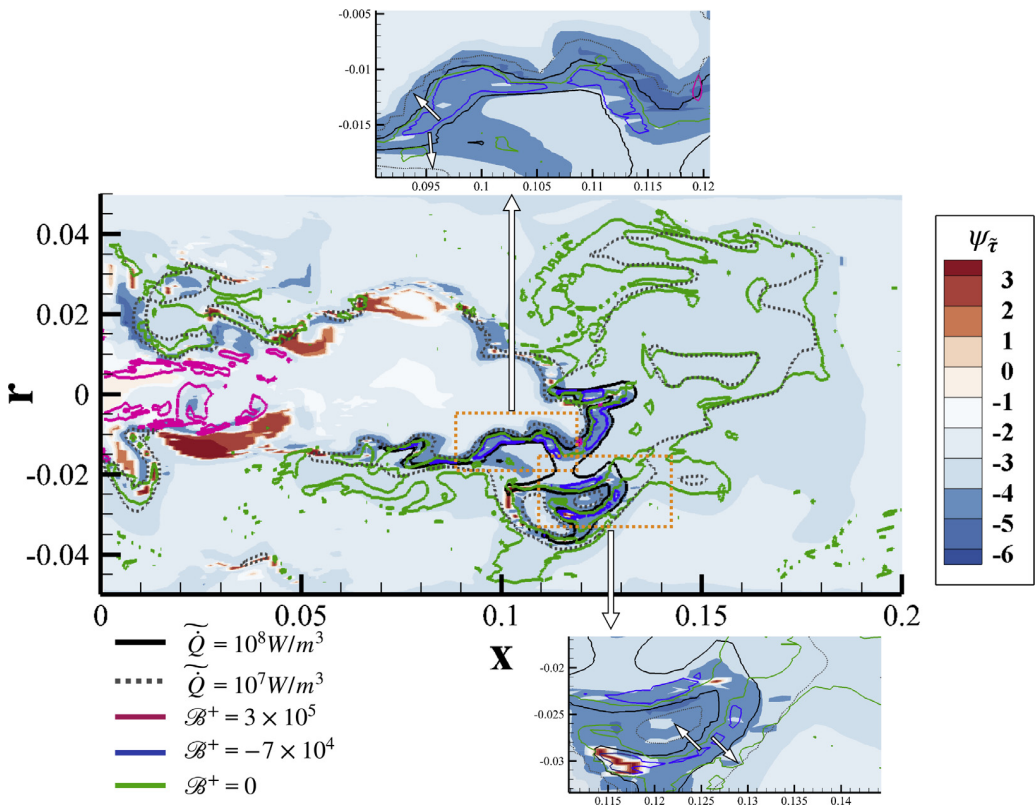


Fig. 7. Typical distribution of $\psi_{\tilde{z}} = (|\omega_{\tilde{z}}|/\omega_{\tilde{z}}) \log |\omega_{\tilde{z}}|$ in the mid-plane is shown along with heat release rate \tilde{Q} and B^+ contours. The unit of the axes is m.

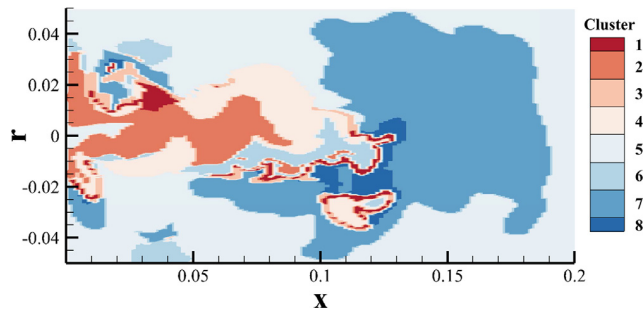


Fig. 8. The local PCA map of clusters. The unit of the axes is m.

species in cluster 8. This area overlaps with the region showing high heat release, as well as negative $\psi_{\tilde{z}}$ and B^+ value. H_2O_2 is considered as an ignition precursor and it well characterises the identified region.

7. Conclusions

Turbulent partially premixed combustion under MILD condition inside a cylindrical combustor with aerodynamically established recirculation

zone is studied using LES with the PaSR and EDC models for SGS combustion. The computed temperature and scalar mole fractions are compared to the measurements from [6]. A good overall agreement is observed for the PaSR model and it is comparable to those observed in past studies using FPV and homogenous reactor-based tabulation combustion models [9,10]. The averaged temperature and CO_2 mole fractions are generally under-estimated, leading to over-estimation of O_2 mole fraction by the EDC, which could be due to the model parameters (e.g. C_γ) chosen or

the value used for the canonical reactor residence time [28] since they are taken from past studies. Sensitivities of the EDC results to these parameters are to be explored in a future study. The LES data from PaSR model is analysed using TSR derived from computational singular perturbation theory and convective-diffusive-reactive balance in T transport equation to identify ignition- and flame-like regions. A good agreement between these analyses are observed. Potential chemical markers (CMs) that can be used in laser diagnostics of MILD combustion are identified using local PCA.

Declaration of Competing Interest

The authors declare that they have no known competing financial interests or personal relationships that could have appeared to influence the work reported in this paper.

Acknowledgments

This project is supported by EPSRC grant agreement no. EP/S025650/1. ST acknowledges funding from the Norwegian Research council, Climit programme, project no. 268368, OxyFun Fundamentals of pressurized oxy/fuel combustion. AP acknowledges the European Research Council, Starting Grant no. 714605. This work used the ARCHER UK National Supercomputing Service with the resources provided by the UKCTRF (e649). The software toolkit for the CSP and TSR analyses, CSPTk, can be obtained by sending a request to mauro.valorani@uniroma1.it.

Supplementary material

Supplementary material associated with this article can be found, in the online version, at doi:10.1016/j.proci.2020.06.298

References

- [1] J.A. Wüning, J.G. Wüning, *Prog. Energy Combust. Sci.* 23 (1997) 81–94.
- [2] A. Cavaliere, M. de Joannon, *Prog. Energy Combust. Sci.* 30 (2004) 329–366.
- [3] B.B. Dally, A.N. Karpetis, R.S. Barlow, *Proc. Combust. Inst.* 29 (2002) 1147–1154.
- [4] A. De, E. Oldenhof, P. Sathiah, D. Roekaerts, *Flow Turbul. Combust.* 87 (2011) 537–567.
- [5] M. Graça, A. Duarte, P.J. Coelho, M. Costa, *Fuel Process. Technol.* 107 (2013) 126–137, doi:10.1016/j.fuproc.2012.06.028.
- [6] A.S. Verissimo, A.M.A. Rocha, M. Costa, *Energy Fuels* 25 (6) (2011) 2469–2480, doi:10.1021/ef200258t.
- [7] M. Ihme, Y.C. See, *Proceeding Combust. Inst.* 33 (1) (2011) 1309–1317.
- [8] Z. Li, A. Cuoci, A. Parente, *Proc. Combust. Inst.* 37 (4) (2019) 4519–4529, doi:10.1016/j.proci.2018.09.033.
- [9] J. Lamouroux, M. Ihme, B. Fiorina, O. Gicquel, *Combust. Flame* 161 (8) (2014) 2120–2136, doi:10.1016/j.combustflame.2014.01.015.
- [10] C. Locci, O. Colin, J.B. Michel, et al., *Flow, Turbul. Combust.* 93 (2) (2014) 305–347, doi:10.1007/s10494-014-9548-2.
- [11] S.H. Lam, D.A. Coussis, *Symp. Combust.* 22 (1) (1989) 931–941, doi:10.1016/S0082-0784(89)80102-X.
- [12] Y. Minamoto, N. Swaminathan, R.S. Cant, T. Leung, *Combust. Sci. Technol.* 186 (8) (2014) 1075–1096.
- [13] N.A.K. Doan, N. Swaminathan, *Combust. Flame* 201 (2019) 234–243, doi:10.1016/j.combustflame.2018.12.025.
- [14] A. Parente, J. Sutherland, B. Dally, L. Tognotti, P. Smith, *Proc. Combust. Inst.* 33 (2011) 3333–3341.
- [15] N. Kornev, H. Kröger, E. Hassel, *Commun. Numer. Methods Eng.* 24 (2008) 875–877, doi:10.1002/cnm.1009.
- [16] H.G. Weller, G. Tabor, H. Jasak, C. Fureby, *Comput. Phys.* 12 (6) (1998) 620–631.
- [17] A. Cuoci, A. Frassoldati, T. Faravelli, E. Ranzi, *Comput. Phys. Commun.* 192 (2015) 237–264.
- [18] R.W. Bilger, S.H. Stårner, R.J. Kee, *Combust. Flame* 80 (2) (1990) 135–149.
- [19] Z. Li, R.M. Galassi, P.P. Ciottoli, A. Parente, M. Valorani, *Combust. Flame* 208 (2019) 281–298, doi:10.1016/j.combustflame.2019.06.023.
- [20] F.P. Kärrholm, *Numerical Modelling of Diesel Spray Injection, Turbulence Interaction and Combustion*, Chalmers University of Technology, Chalmers, Sweden, 2008 Phd thesis.
- [21] Z. Li, M. Ferrarotti, A. Cuoci, A. Parente, *Appl. Energy* 225 (2018) 637–655, doi:10.1016/j.apenergy.2018.04.085.
- [22] I.R. Gran, B.F. Magnussen, *Combust. Sci. Technol.* 119 (1–6) (1996) 191–217.
- [23] M. Valorani, P.P. Ciottoli, R.M. Galassi, *Proc. Combust. Inst.* 36 (1) (2017) 1357–1367, <https://www.scopus.com/inward/record.uri?eid=2-s2.0-85008967509&doi=10.1016%2fj.proci.2016.09.008&partnerID=40&md5=fd16de531952b1f9d746ff863c559bc>.
- [24] M. Valorani, S. Paolucci, E. Martelli, T. Grenga, P.P. Ciottoli, *Combust. Flame* 162 (8) (2015) 2963–2990.
- [25] M. Valorani, P.P. Ciottoli, R. Malpica Galassi, S. Paolucci, T. Grenga, E. Martelli, *Flow, Turbul. Combust.* 101 (4) (2018) 1023–1033, doi:10.1007/s10494-018-9942-2.
- [26] D.M. Manias, E.-A. Tingas, F.E. Hernández Pérez, R. Malpica Galassi, P. Paolo Ciottoli, M. Valorani, H.G. Im, *Combust. Flame* 200 (2019) 155–167.
- [27] J.C. Sutherland, A. Parente, *Proc. Combust. Inst.* 32 (1) (2009) 1563–1570, doi:10.1016/j.proci.2008.06.147.
- [28] D.A. Lysenko, I.S. Ertesvåg, *Flow Turbul. Combust.* 100 (3) (2018) 721–768, doi:10.1007/s10494-017-9880-4.

Paper II


Development of a turbulence dissipation based reaction rate model for progress variable in turbulent premixed flames.

Stefanie Tomasch; Nedunchezhian Swaminathan; Christoph Spijker; Ivar S. Ertesvåg

Combustion theory and modelling
DOI:10.1080/13647830.2022.2083525



Development of a turbulence dissipation based reaction rate model for progress variable in turbulent premixed flames

Stefanie Tomasch ^{a*}, Nedunchezhian Swaminathan^b, Christoph Spijker^c and Ivar S. Ertesvåg^a

^aDepartment of Energy and Process Engineering, NTNU Norwegian University of Science and Technology, Trondheim, Norway ^bDepartment of Engineering, University of Cambridge, Cambridge, UK ^cDepartment of Environmental and Energy Process Engineering, Montanuniversität Leoben, Leoben, Austria

(Received 11 October 2021; accepted 7 May 2022)

This study presents an algebraic combustion closure for Large eddy simulation (LES) exhibiting attributes of simplicity and simultaneous accuracy under realistic combustion conditions. The model makes use of the interlink between the reaction and dissipation rates in premixed turbulent combustion but relaxes the thin flame assumption by considering finite-rate chemistry effects in the small-scale turbulence structure. The core idea of the approach is to approximate the reaction progress in the unresolved spectrum of wave lengths and to use it within a filtered reaction rate expression. The model is implemented in OpenFOAM 4.0 and is tested on a turbulent, premixed flame behind a bluff-body, applying an LES approach for turbulence modelling. The cross comparison of velocity, temperature and composition data with experiments and a well-investigated combustion model in literature reveals competitive performance of the new model. Especially in the near-field of the bluff body flame, corresponding to thin and moderately thickened flame regions, its ability to capture the flame structure is highly promising. The chosen, partly explicit approach to recover the temperature from the transported sensible enthalpy, involving a strong coupling between filtered reaction and heat release rate, also shows advantages over obtaining the temperature from presumed probability density functions.

Keywords: CFD; combustion; LES; progress variable; subgrid scale

1. Introduction

Computational fluid dynamics (CFD) plays an important role to study turbulent flames of practical interest. Under premixed and partially-premixed conditions, the complex interactions between chemistry and turbulence are important, and capturing these interactions is a challenge for combustion models. Many models have been developed in past studies, and the advent of computational hardware and methods has helped to use sophisticated models with high fidelity for the interactions. These models were reviewed in many past studies to highlight their strengths and weaknesses, for example see [1–3] for such a review

*Corresponding author. Email: stefanie.tomasch@ntnu.no

specifically for premixed combustion. The presence of thin flames resembling laminar ones was shown in many past investigations, which were reviewed by Driscoll [4]. Also, the physical connections between the flame shape and premixed combustion models, and among the models, were discussed by Veynante and Vervisch [1]. The flame-sheet models assume that the chemical kinetics are faster than turbulent mixing [5], which implies that the flame thickness is almost zero. The Bray-Moss-Libby (BML) formalism, described in [6–9], is a good example for this approach, which assumes a thin flame by taking the burning mode PDF (probability density function), $\gamma f(c)$ [3], to be negligible. Alternatively, this assumption implies fast chemistry or a high Damköhler number limit, under which, the back-mixing of hot and fresh gases becomes a rate-determining step. This mixing is related to the turbulent dissipation in high Reynolds number flows with combustion. Spalding's Eddy Break Up model (EBU) [10] and Bray's algebraic reaction rate model [11] make use of the connection between reaction rate and turbulent dissipation rate. Both of these models involve scalar dissipation rate of a reaction progress variable.

Sabelnikov and Lipatnikov [12] suggested that the BML approach may be limited to moderate turbulence intensities because the burning mode PDF is non-negligible as a consequence of flame thickening at large turbulence intensities, which may be of interest to practical applications. Also, Pope and Anand [13] noted that the turbulent premixing of unburnt and burnt mixtures gains importance for the onset of reactions under low Damköhler number (Da) conditions.

Although the thin flame approximation holds quite well, it may not hold well for fuel-lean combustion, which is of high interest for future combustion systems. Thickening of the flame front has been observed in past experiments and high-fidelity combustion simulations, see for example [14] and [15]. These experimental studies were reviewed by Driscoll [4], and he showed that small-scale turbulence can penetrate preheat zones leading to thin reaction zones combustion as articulated by Peters [5]. This flame thickening may also be caused by curvature effects [16]. However, turbulent premixed combustion in many applications is likely to involve a wide range of conditions, from flamelets to thin reaction zones, and also to broken reaction zones, specified in turbulent combustion regime diagrams [17,18]. The broken reaction zones regime may also be called as distributed flamelets [19]. Hence, it is becoming clear that the combustion model should cater for these changes in sub-grid scale combustion conditions. One such model is proposed here, which makes use of the interlink between the reaction and dissipation rates but does not assume mixing-limited or fast chemistry combustion. This is achieved by making use of the difference between the computed subgrid-scale (SGS) variance using its transport equation and its maximum theoretical limit as explained in Section 2.2. Hence, the objective of this study is to test this novel SGS combustion closure, which is simple and of algebraic form, by conducting Large eddy simulation (LES) of a turbulent premixed flame established behind a bluff body and depicting combustion in various regimes, ranging from wrinkled flamelets to distributed reaction zones. This burner was studied before using laser diagnostics [20,21] and LES, applying other combustion models [19,22,23] and hence, there is good data for model validation and cross-comparison.

This paper is organised as follows. The modelling theory is presented and discussed in Section 2. The experimental test case along with its characteristic parameters are discussed in Section 3. The LES details are discussed in Section 4 and the results are presented in Section 5. The conclusions are summarised in the final section.

2. Combustion model

2.1. Modelling theory

The thermo-chemical state of a mixture in a turbulent flame can be expressed using two key quantities, the mixture fraction, Z , and the reaction progress variable, c , in a two-variable formulation. The mixture fraction represents the fuel-air mixing, and the reaction progress variable denotes the progress of chemical reaction towards the fully burnt state. A value of $Z = 0$ implies air stream and $Z = 1$ represents the fuel stream. For lean premixed combustion, the fuel and air are already mixed at the molecular level and thus, there is no need to use the mixture fraction for studying premixed combustion. For the sake of completeness, the transport equation for the filtered mixture fraction is given by

$$\bar{\rho} \frac{d\tilde{Z}}{dt} = \nabla \cdot \left[\left(\tilde{\mu} + \frac{\mu_t}{Sc_t} \right) \nabla \tilde{Z} \right], \quad (1)$$

where μ_t and Sc_t are the SGS eddy viscosity and Schmidt number, detailed later in Section 3. The filtered density of the mixture is denoted using $\bar{\rho}$ and, the over-bar and tilde represent LES filtering and Favre-filtering operations, respectively. In its simplest form, the mixture fraction may be defined as [1]

$$Z = \frac{\nu Y_F - Y_{O_2} + Y_{O_2,2}}{\nu Y_{F,1} + Y_{O_2,2}}, \quad (2)$$

where Y_i is the mass fraction of species i , and ν is the stoichiometric fuel to oxidiser mass ratio. The subscripts 1 and 2 refer to pure fuel and oxidiser streams respectively.

The progress variable used in this work is defined as [24]

$$c = \frac{(Y_{O_2,u} - Y_{O_2,b})(Y_{O_2,u} - Y_{O_2}) + (Y_{F,u})(Y_{F,u} - Y_F)}{(Y_{O_2,u} - Y_{O_2,b})^2 + (Y_{F,u})^2}, \quad (3)$$

and its Favre-filtered transport equation is [1]

$$\bar{\rho} \frac{d\tilde{c}}{dt} = \nabla \cdot \left[\left(\tilde{\mu} + \frac{\mu_t}{Sc_t} \right) \nabla \tilde{c} \right] + \bar{\omega}_c. \quad (4)$$

Chemical reactions occur at small scales, which typically are not resolved in LES and thus, $\bar{\omega}_c$ requires modelling. Many models were proposed in past studies, and their details may be found in [1–3]. The interest here is on a finite-rate chemistry eddy dissipation model because of its simplicity and ease of use. The filtered reaction rate, as per this model, is given by Dopazo et al. [3] $\bar{\omega}_c = \mathcal{A} \bar{\rho} \sigma_{c,sgs}^2 / \tau_f$, where τ_f is the SGS turbulence timescale, $\sigma_{c,sgs}^2$ is the SGS variance of c , and \mathcal{A} is a model parameter. In the mixing-controlled limit, the SGS variance becomes $\tilde{c}(1 - \tilde{c})$ and the segregation factor, defined as

$$g = \frac{\sigma_{c,sgs}^2}{\tilde{c}(1 - \tilde{c})}, \quad (5)$$

takes a value of unity. This implies that the SGS filtered density function (PDF) is bimodal with two delta functions located at $c = 0$ and $c = 1$. Hence, for $g = 1$, there is no need to solve a transport equation for SGS variance, as has been suggested by Bray [11] for RANS (Reynolds Averaged Navier-Stokes) modelling. One must consider the progress

variable variance if there is a departure from the mixing-controlled limit (known as finite-rate chemistry), as shown by Bray et al. [25] in the context of presumed PDF models. Here, we propose an alternative approach involving a simple algebraic closure for the filtered reaction rate involving the SGS variance. The transport equation for this variance, defined as $\sigma_{c,\text{sgs}}^2 = \tilde{c}^2 - \bar{c}^2$, is [1]

$$\bar{\rho} \frac{d\sigma_{c,\text{sgs}}^2}{dt} = \nabla \cdot \left[\left(\tilde{\mu} + \frac{\mu_t}{Sc_t} \right) \nabla \sigma_{c,\text{sgs}}^2 \right] + 2 \frac{\mu_t}{Sc_t} (\nabla \tilde{c} \cdot \nabla \tilde{c}) - 2 \bar{\rho} \tilde{\chi}_{c,\text{sgs}} + 2 [\overline{\dot{\omega}_c \tilde{c}} - \bar{\dot{\omega}_c} \bar{c}]. \quad (6)$$

The modelling of SGS scalar dissipation rate $\tilde{\chi}_{c,\text{sgs}}$ and a chemical contribution $\overline{\dot{\omega}_c \tilde{c}} = [\overline{\dot{\omega}_c \tilde{c}} - \bar{\dot{\omega}_c} \bar{c}]$ are discussed in Section 4.

2.2. Reaction rate model

The filtered reaction rate, used in this study, is formulated as

$$\bar{\dot{\omega}_c} = \bar{\rho} [a^* (c_+^* - \tilde{c}) + (1 - a^*) (\tilde{c} - c_-^*)] / \tau_f, \quad (7)$$

involving the SGS turbulence timescale $\tau_f = k_{\text{sgs}}/\epsilon_{\text{sgs}}$, where k_{sgs} and ϵ_{sgs} are the subgrid kinetic energy and its dissipation rate. All the quantities, except for the timescale, in the above equation are based on \tilde{c} and $\sigma_{c,\text{sgs}}^2$. The factor a^* , to be defined shortly, depends on the departure of $\sigma_{c,\text{sgs}}^2$ from the bimodal limit value of $\tilde{c}(1 - \tilde{c})$ because of the finite-rate chemistry effects or finite local Damköhler number.

Figure 1 illustrates graphically how the various quantities in Equation (7) are determined. The c_-^* and c_+^* are two plausible states of the reacting mixture at the SGS level, which are marked using a black circle and an asterisk in the figure.

The dashed line represents the maximum variance value, given by $\tilde{c}(1 - \tilde{c})$, and the solid line denotes the SGS variance, $\sigma_{c,\text{sgs}}^2$, when the segregation factor is $g = 0.8$, as an example for the variance obtained using its transport equation. The dash-dotted line shows

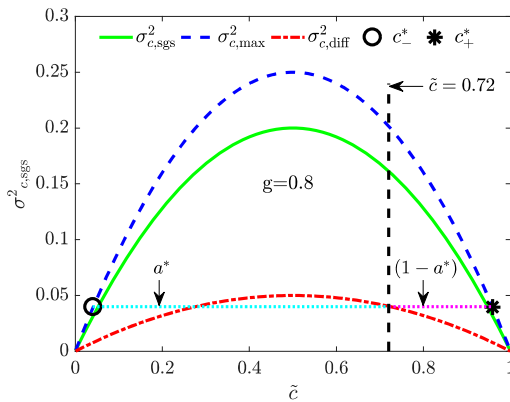


Figure 1. Graphical overview of the reaction rate expression presented for $\tilde{c} = 0.72$ as an example.

the difference between the maximum and calculated variances, which is given by

$$\sigma_{c,\text{diff}}^2 = \tilde{c}(1 - \tilde{c}) - \sigma_{c,\text{sgs}}^2 = \tilde{c}(1 - \tilde{c})(1 - g). \quad (8)$$

This quantity is called as mixing factor by Bray [26]. If one writes $\sigma_{c,\text{diff}}^2 = c^*(1 - c^*)$, the resulting quadratic equation gives two roots for c^* as

$$c_{-,+}^* = 0.5 \pm \sqrt{0.25 - \sigma_{c,\text{diff}}^2}. \quad (9)$$

This is consistent with the notion of Pope and Anand [13] suggesting that the mixing factor is related to premixing (of hot and cold gas) outside the fast reaction limits and thus, c^* must depart from 0 and 1 for the mixture, which will be reacting subsequently. In the limit of mixing controlled reaction, $\sigma_{c,\text{diff}}^2 = 0$ and thus c^* must take a value of either 0 or unity as indicated by Equation (9). When there are finite-rate chemistry effects, $\sigma_{c,\text{diff}}^2 \neq 0$ and hence c_-^* and c_+^* must deviate from 0 and 1, and the level of these deviations allows us to define the weighting factor a^* by using a lever rule, as

$$a^* = \frac{\tilde{c} - c_-^*}{c_+^* - c_-^*}. \quad (10)$$

It is straightforward to verify that the EBU reaction rate expression, $\bar{\omega}_c = \mathcal{A} \bar{\rho} [\tilde{c}(1 - \tilde{c})]/\tau_f$ with $\mathcal{A} = 2$, is recovered from Equation (7) when $\sigma_{c,\text{diff}}^2$ is zero. Following the arguments of Bray et al. [25], the factor $(1 - g)$ is inversely proportional to the local Damköhler number and hence the departure of c_-^* and c_+^* , respectively, from 0 and 1 will increase if the local chemical timescale is larger than τ_f (low Damköhler number or finite-rate chemistry). This directly influences the filtered reaction rate given by Equation (7). As stated earlier, the aim of this work is to test this model by conducting LES of lean premixed combustion with local combustion conditions spanning across corrugated flamelets to thickened reaction zones combustion regimes and comparing the simulation results with experimental measurements. Before presenting the simulation details, the experimental candidate considered for this study is described next.

3. Description of test case

A fuel-lean turbulent premixed flame of a methane-air mixture having an equivalence ratio of $\phi = 0.586$ at a temperature of 294 K, established behind a bluff body, is considered for this study. Despite this simple set-up, complex flow and flame conditions arise because of the shear layers, recirculation zones and their interactions with the flame as depicted in Figure 2, see [27] for elaborate discussions on these flow and flame attributes. The turbulence level at the bluff body base is known to affect the recirculation zone size [22] and combustion conditions in the wake region [19,28]. Hence, this experimental case serves as a good candidate to test the objectives of this study. Also, this flame has been investigated experimentally in [20,21] and using LES in [19,22,28] and thus cross-comparisons of statistics can also be made.

The various dimensions of the combustor relevant for the computational model are marked in Figure 2. The 284 mm long combustor has a square cross-section of $79 \times 79 \text{ mm}^2$. The characteristics of the incoming flow were measured at the base of the bluff body, marked as the axial location B in the figure. The bulk-mean velocity measured at this

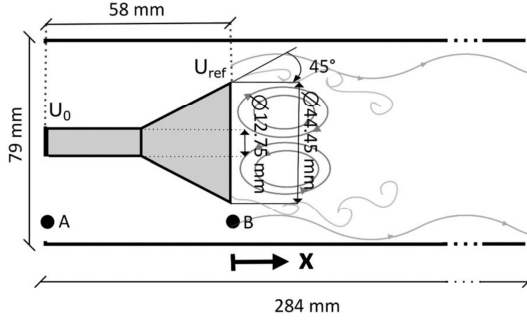


Figure 2. A schematic showing salient flow features and geometry attributes.

location was $U_{\text{ref}} = 15$ m/s, which is taken to be a reference value for discussing results in the later sections. The turbulence intensity at this location was $TI = u' / U_{\text{ref}} \approx 24\%$, where u' is the root-mean-square value of axial velocity fluctuations. The radial variations of measured statistics for temperature, axial velocity, and various species were reported for a few axial locations, up to $x = 2D$, where D is the bluff body diameter. These measurements are shown elaborately in [19,28] and were used for comparisons in this study. The reacting flow in this burner was computed using LES and its details are described next.

4. Large eddy simulation

4.1. Combustion closure

The philosophy of LES has been described in many books, see for example [29]. For premixed combustion, Favre-filtered transport equations for mass, momentum, sensible enthalpy, reaction progress variable and its SGS variance are solved along with SGS closures for sub-grid stresses, fluxes and reaction rates. The variance equation, Equation (6), also needs closures for its dissipation rate and for the influence of chemistry on its evolution. There are various approaches to model the sub-grid stresses, and the one-equation approach of Yoshizawa [30] involving the SGS kinetic energy, $k_{\text{sgs}} = (\widetilde{u_k u_k} - \widetilde{u_k} \widetilde{u_k}) / 2$, was used for this work. In this approach, the eddy viscosity is calculated using $\mu_t = C_k \bar{\rho} \Delta \sqrt{k_{\text{sgs}}}$, where $C_k = 0.094$ is a model parameter, and Δ is the filter width estimated as the cube root of the local numerical cell volume. The sub-grid scalar fluxes were obtained using gradient approximation involving the SGS eddy diffusivity, which was obtained as μ_t / Sc_t with a value of 0.7 for the sub-grid eddy Schmidt or Prandtl number.

The temperature was obtained using the transported sensible enthalpy h . The transport equation is given by

$$\bar{\rho} \frac{d\tilde{h}}{dt} = \nabla \cdot \left[\left(\bar{\mu} + \frac{\mu_t}{Pr_t} \right) \nabla \tilde{h} \right] + \bar{Q}, \quad (11)$$

Here, the heat release rate per unit volume, $\bar{Q} = \bar{\omega}_c Y_{f,u} \Delta h_{\text{LHV}}$, is related to the lower heating value of the fuel, unburnt fuel mass fraction and the reaction rate of the progress variable. The temperature calculation using h followed the approach described in [31].

Table 1. Parameters for the SGS scalar dissipation rate closure in Equation (12). $S_{L,0}$ is the laminar flame speed, δ_{th} the thermal flame thickness, $T_{ad} = 1637$ K the adiabatic flame temperature and $T_0 = 294$ K is the initial temperature, $Ka_{\Delta} = (\sqrt{2}k_{sgs}/3/S_{L,0})^{3/2}(\delta_{th}/\Delta)^{1/2}$.

Parameter	β'	K_c^*	τ	C_4	C_3	$S_{L,0}$	δ_{th}
Related to	–	thermo-chemistry	global heat release	–	Ka_{Δ}	–	laminar flamelet
Formula	–	$K_c^* = 0.79 \tau$	$\tau = \frac{(T_{ad}-T_0)}{T_0}$	$\frac{1.1}{(1+Ka_{\Delta})^{0.4}}$	$\frac{1.5\sqrt{Ka_{\Delta}}}{1+\sqrt{Ka_{\Delta}}}$	–	$\frac{(T_{ad}-T_0)}{\sqrt{I}_{max}}$
Dimensions	[]	[]	[]	[]	[]	[m/s]	[m]
Value	3.0	3.55	4.5	–	–	0.1	0.001

The SGS scalar dissipation rate, $\tilde{\chi}_{c,sgs}$, in Equation (6) for the progress variable variance was modelled using an algebraic expression

$$\tilde{\chi}_{c,sgs} \simeq [1 - \exp(-0.75\Delta/\delta_{th})] \left[(2K_c^* - \tau C_4) \frac{S_{L,0}}{\delta_{th}} + C_3 \frac{\epsilon_{sgs}}{k_{sgs}} \right] \frac{\sigma_{c,sgs}^2}{\beta'}. \quad (12)$$

This model was proposed by Dunstan et al. [32] and used in many past studies, see for example [19]. The various parameters appearing in the above model are defined along with their values in Table 1. The value of $\beta' = 3$ used here is close to the modal value of this parameter distribution obtained using a dynamic procedure in [19,28].

The variance equation, Equation (6), also needs a model for $\overline{\omega_c c}$, which is related to chemical reactions. Following the arguments in [11], a simple model used for this quantity is

$$[\overline{\omega_c c} - \overline{\omega_c} \tilde{c}] \approx (c_m - \tilde{c}) \overline{\omega_c}, \quad (13)$$

where c_m is a model parameter with a value ranging from 0.7 to 0.8. Although this model is strictly valid when the local Damköhler number is very large, it is shown to hold quite well for moderate and low Damköhler number situations as well [33,34].

4.2. Boundary conditions, numerical detail and grid

The computational volume used for this study is shown in Figure 3, which is the same as the one used in [19,22]. The flame was observed to extend beyond the 284 mm long combustor in the experiments and thus an additional domain of length 778 mm was included for the computations, so the boundary conditions at the exit could be specified unambiguously. A small co-flow velocity of $U_{Co} = 0.2$ m/s was specified to include the effects of room air (at 294 K) entrainment into the hot flow exiting the combustor. To track this entrainment, a fluid marker signifying the premixed mixture having a mixture fraction value of 0.0331 coming through the inlet was also carried in the simulation following the earlier studies [19,22]. This fluid marker had a value of 0 in the co-flowing air stream. The progress variable and its variance were specified to be zero for the co-flow, and the sensible enthalpy was specified to be consistent with this stream temperature and composition.

To allow a proper boundary layer development on the bluff body stem, which can affect the behaviour of the recirculation zone behind the bluff body, the inlet for the computation domain was specified to be at 296 mm upstream of the combustor exit. A uniform inflow velocity of $U_0 = 11.3$ m/s was set at this inlet so that the measured $U_{ref} = 15$ m/s was achieved at the bluff body base. Also, the measured TI at this location was achieved by

using the synthetic inflow turbulence generator described in [35]. An outflow boundary condition (zero gradient for all the quantities except pressure) was specified at the exit of the computational volume. The adiabatic walls were specified to be no-slip.

The open-source software OpenFOAM 4.0 [36] was employed for conducting LES using the above computational model. The spatial derivatives in the governing equations were discretised by a second-order accurate Gauss linear scheme, and these discretised equations were advanced in time using an Euler time-stepping algorithm. Adaptive time-stepping was used for simulations to keep the maximum CFL number below 0.2. Two different grids with cell count of 2.1 M and 3.1 M hexahedral cells were used to test for the grid dependency of the computed statistics. The distribution of cell sizes for these two grids are shown in Figure 4, and one can see that the majority of the cells in 2.1 M grid is 10% larger than the thermal thickness, whereas it is 20% smaller for the 3.1 M grid. Furthermore, both of these grids satisfy the grid requirement condition suggested by the Pope criterion [37]. Furthermore, no undue differences in the statistics, to be discussed in results section, computed using these two grids were observed. The 3.1 M grid was used for most of the results discussed in the results section.

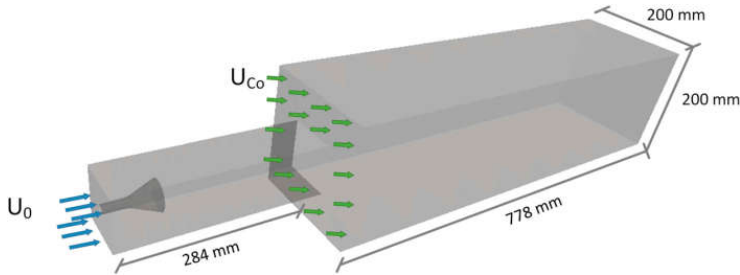


Figure 3. Computational geometry used for LES.

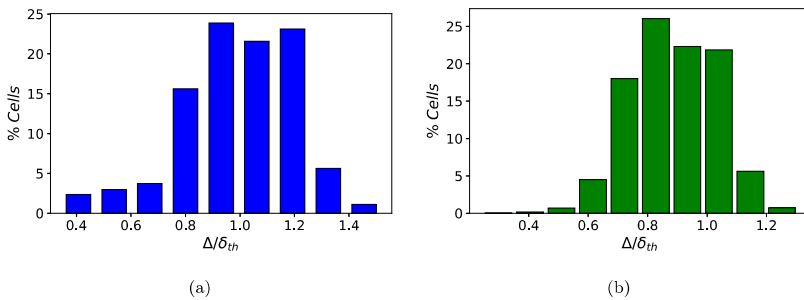


Figure 4. Histogram of numerical cell size normalised by the laminar flame thermal thickness for the (a) 2.1 M and (b) 3.1 M grids.

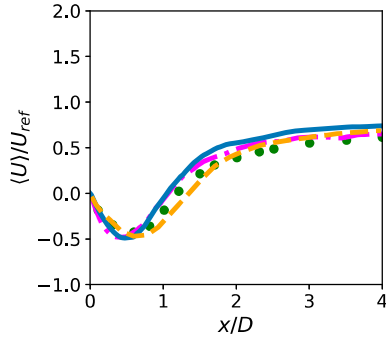


Figure 5. The centreline variation of normalised mean axial velocity in cold flow. Blue solid lines — and dot-dashed magenta lines - · - · denote the current results using the 3.1 M and 2.1 M grids, respectively. Orange dashed lines - - - denote the results of [19]. The symbols (•) are the measurements of Nandula, Pan and collaborators [20,21], used in [19].

5. Results

5.1. Cold flow

Cold flow simulations were performed first to assess the numerical grid, turbulence models and boundary conditions employed for the computational model. This was conducted by comparing the computed and measured centreline velocity variations. At the inlet of the computational volume, homogeneous turbulence with a characteristic length scale of $l_{BC} = 0.0035$ m was initialised using the inflow turbulence generator as noted earlier. This length scale corresponds to the spacing width of the turbulence grid used in the experiments. The turbulence intensity, TI , at the inlet was specified to be about 14%, which yielded the TI value at the bluff body base reported in the experimental studies [20,21]. Also, this procedure gave a good comparison between computed and measured centreline variation of axial velocity as shown in Figure 5. The experimental data is shown as green dots (also in the subsequent plots) along with results from another computational study [19,28]. It is clear the mesh did not influence these statistics, but the recirculation zone length is slightly underestimated in the current study, while the previous LES has slightly overestimated it. These differences are within about 0.5 to $0.6D$ while the experimental uncertainty for the recirculation zone length is typically about $\pm 0.5D$. Hence, one may say that both LES results are equally good, and differences between the two computations could arise from the SGS stress models used. The previous study [19,28] used the localised dynamic Smagorinsky model, whereas the current study employed the one-equation k_{sgs} -model.

5.2. Reacting flow

5.2.1. Flame specifics

The performance of the combustion model introduced earlier was tested using reacting flow simulations. For comparative evaluations, the measured and computed, using unstrained flamelet approach [19], velocity, temperature and species mass fraction data were available. The cold flow results discussed in the previous section showed that the computational model, in terms of boundary conditions, numerical methods, SGS models, etc., was good to capture the flow characteristics in this burner. Both experimental [20,21] and past

LES [19,22,28] studies showed that the turbulent flame considered for this study undergoes a structural change as it evolves from the flame anchoring point into the wake region behind the recirculation zone because of the changes in local combustion conditions. It was shown in the past LES studies [19,28] that the SGS flow timescale can increase by an order of magnitude from the bluff body base to about mid-length of the combustor, and hence, the local Damköhler number changes as one moves away from the bluff body base in the axial direction. This will alter the mixing factor given by Equation (8), and the filtered reaction rate will respond to this change as described in Section 2.2. This was tested by comparing the computed and measured statistics in the following discussion. The statistics computed directly from quantities transported in the LES are presented in Section 5.2.2 and those deduced from the computed quantities using a presumed PDF are presented in Section 5.2.3.

5.2.2. Comparison of velocity and temperature

The centreline variations of normalised axial velocity and temperature are shown in Figure 6. From the mean axial velocity variations in Figure 6a it can be seen that both modelling approaches overpredicted the recirculation zone length, L_r , compared to experiments. The unstrained flamelet model used in [28] yielded the recirculation zone length to be within the expected experimental uncertainty of $0.5D$. The length estimated in the present study was closer to the upper limit of experimental uncertainty for the 3.1 M grid, whereas the 2.1 M mesh showed improved agreement with experiments, which may arise from the differences in the resolution near the bluff body boundary. In addition to L_r , the negative velocity inside the recirculation zone, along the centreline, was captured well in the current study, within 5 – 10% deviation from measurements, compared to the unstrained flamelet model used in the earlier study.

It should be noted that both modelling approaches compared in Figure 6a used adiabatic wall boundary conditions, which is acceptable since the heat loss through the walls in the experiments was argued to be less 10% in [19]. From the normalised mean temperature variations in Figure 6b, a slight decrease of temperature $\langle T^+ \rangle \approx 0.94$, where the

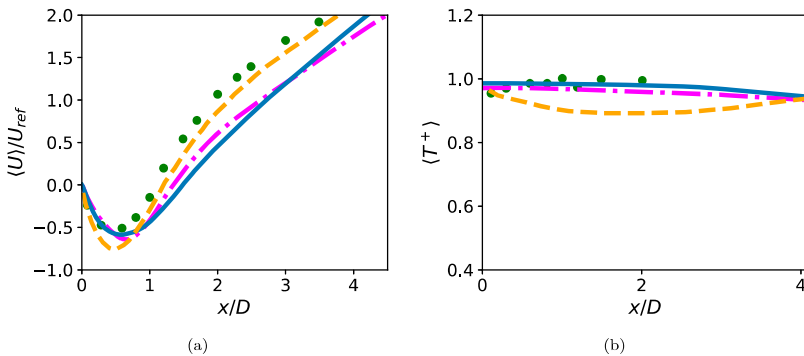


Figure 6. The centreline variations of time-averaged and normalised (a) axial velocity, $\langle U \rangle$, and (b) temperature, $\langle T^+ \rangle$. Blue solid lines — and dot-dashed magenta lines -.- denote the current results using the 3.1 M and 2.1 M grids, respectively. Orange dashed lines - - - denote the results of the unstrained flamelet model in [28]. The symbols (•) show experimental results from [20,21], which are used in [19] for comparison.

normalised temperature is defined as $\langle T^+ \rangle = (\langle \tilde{T} \rangle - T_0) / (T_{\text{ad}} - T_0)$ with $T_{\text{ad}} = 1637$ K, towards the bluff body is observed in the experimental data, suggesting some heat loss through the bluff body base. This heat loss influences the turbulence conditions in the boundary layer of the bluff body through the temperature-dependence of transport properties, increasing the importance of viscous effects. This could be relevant at the bluff body edge because the shape of the recirculation zone is strongly influenced by the boundary layer shedding.

Downstream of the recirculation zone, the confined turbulent flame causes an acceleration of the flow due to gas expansion [27], which is observable from all simulations and experiment. This can be seen by comparing Figures 5 and 6a. In the reacting case, the mean axial velocity shows a continuous increase along the centreline whereas it levels off and reaches almost a constant value in the non-reacting case shown in Figure 5. The results for our model indicate that it had difficulties to predict the onset and strength of the velocity increase measured by experiments and predicted by the unstrained flamelet model. One reason for the slightly delayed onset of velocity increase along the centreline is obviously the comparatively longer recirculation zone predicted by the current model. Another potential reason for a too slow and too weak acceleration of the centreline flow could be a slight underprediction of heat release in the downstream thickened regions of the flame.

The normalised mean temperature variation along the centreline is shown in Figure 6b, where the temperature is obtained using the sensible enthalpy transported in the LES. The mixture averaged specific heat capacity at constant pressure, required to calculate the temperature from the transported sensible enthalpy, was obtained using the procedure in [31] as noted earlier. Langella et al. [19] used the total (chemical + sensible) enthalpy to obtain the temperature in their unstrained flamelet model. The reason for the differences seen in Figure 6b is unclear at this time.

The experimental data suggests that the mixture in the recirculation zone is close to fully burnt state with the temperature almost equal to the adiabatic flame temperature. The centreline temperature variation computed in the current study showed a weak sensitivity to the numerical grid as seen in Figure 6b. A slight overestimate of the mean temperature in the region very close to the bluff body base may be due to the adiabatic condition used for the bluff body.

Radial profiles of the mean axial and radial velocity ($\langle U \rangle$, $\langle V \rangle$) are also available for comparison. The measurement region spans from $x/D = 0.1$ to 2.0 in the axial direction and from $r/D = 0$ to $0.8D$ in the radial direction. Good agreement is observed for the measured and computed normalised axial velocity for the near field as shown in Figure 7. There are also only minor differences with the unstrained flamelet results of Langella et al. [28] in this region. For $x/D = 0.3$ to 0.6, our model gave a slightly better prediction of the negative velocity variation in the recirculation zone, which matches the observations from Figure 6a. The different recirculation zone lengths between the simulations and experiments are expected to influence the discrepancies in the velocity profiles in the region downstream of $x/D = 1.0$. The recirculation zone length L_r from the experimental reacting flow measurements was around $1.1D$. The profiles of the radial velocity component are shown in Figure 8, and good to satisfactory agreement is observed depending on the axial location of interest.

The radial variations of normalised mean temperature are shown in Figure 9 and excellent agreement of our results with measurements is observed, which is better than for the

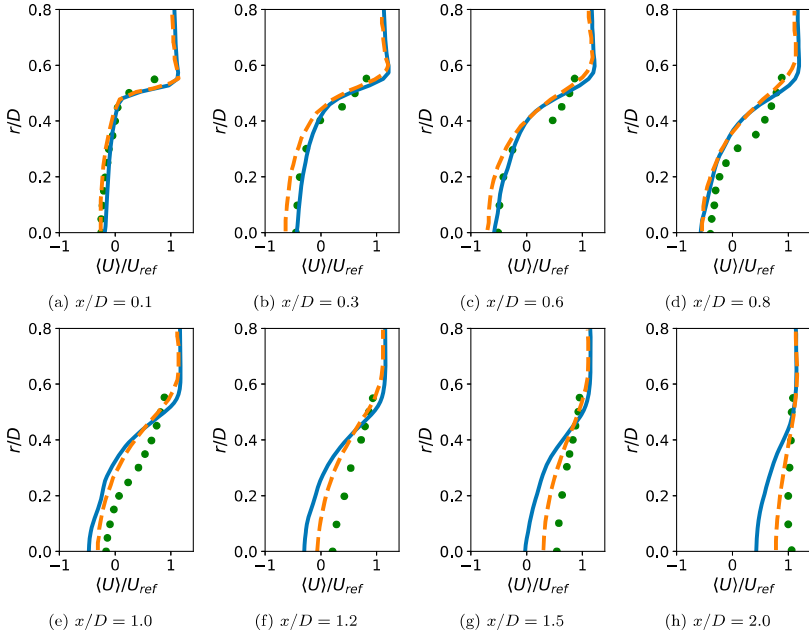


Figure 7. Normalized mean axial velocity profiles in radial direction in the flame and post-flame region. For legend, see Figure 6.

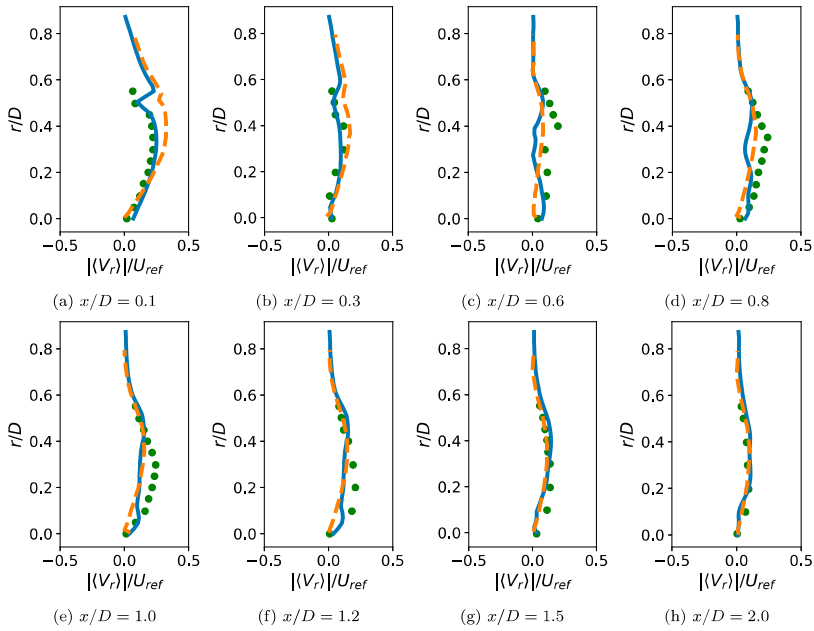


Figure 8. Normalized mean radial velocity profiles in radial direction in the flame and post-flame region. For legend, see Figure 6.

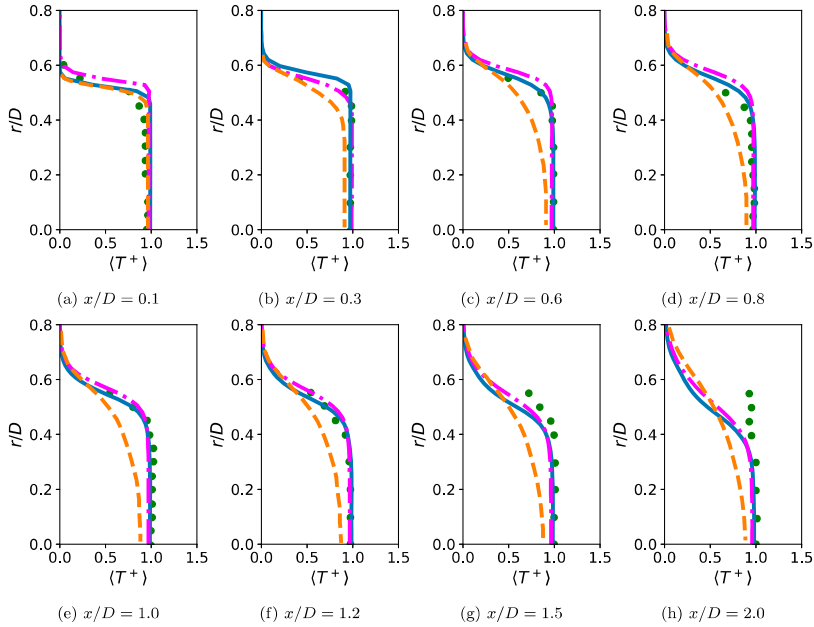


Figure 9. Normalized mean radial temperature profiles in the flame and post-flame region. For legend, see Figure 6.

unstrained flamelet model prediction. Also, a close observation of the results in this figure suggests that the unstrained flamelet model predicted a thicker flame brush, when defining the flame brush thickness as $\delta_T = \partial \langle T^+ \rangle / \partial r$ [21]. The computed temperatures for both models agree quite well with measurements in the near field, which may be because the combustion timescale is shorter than the turbulence timescale in these regions. Farther downstream, the unstrained flamelet model gave a slower increase of mean temperature in the radial direction compared to the current algebraic model. In comparison, our model captured the transition of the flame structure from the bluff body base $x/D = 0$ to the rear stagnation point $x/D < 1.5$ through various combustion regimes very well. However, a noticeable difference between measured and computed temperature is observed for outer radial positions at $x/D = 1.5$ and 2.

The growth of the flame brush downstream of the bluff body is shown in Figure 10 for the 2.1 M and 3.1 M mesh. It is based on the radial temperature gradient [21] as noted earlier. The black solid line shows the flame brush thickness δ_T normalised by laminar flame thickness δ_{th} . The two dotted lines are isolines of the normalised temperature $\langle T^+ \rangle$ at 0.1 and 0.9. In an analysis of the flame brush thickness in [19], it was noted that experimental measurements available for the flame indicated a growth of the flame brush thickness in the post-flame region to roughly 12 times its size at the bluff body base. For the simulations presented here, the ratio between δ_T close to the bluff body and at $x/D = 3$ was approximately 10. Quantitatively, the flame brush thickness shows slight differences between the used meshes, which is to a certain extent expected due to the mesh dependence of explicit LES filtering as applied in this study. Qualitatively, both simulations show very similar

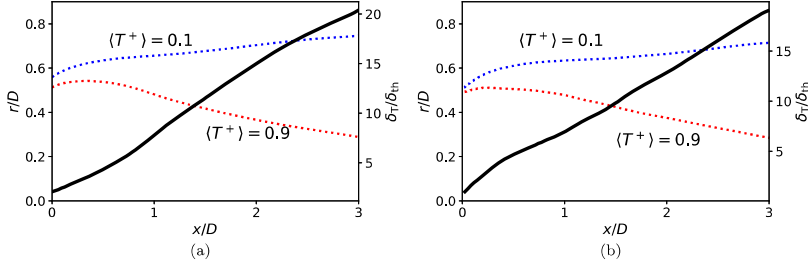


Figure 10. Estimation of the flame brush thickness δ_T by means of the radial temperature gradient for (a) the 2.1 M (b) the 3.2 M mesh.

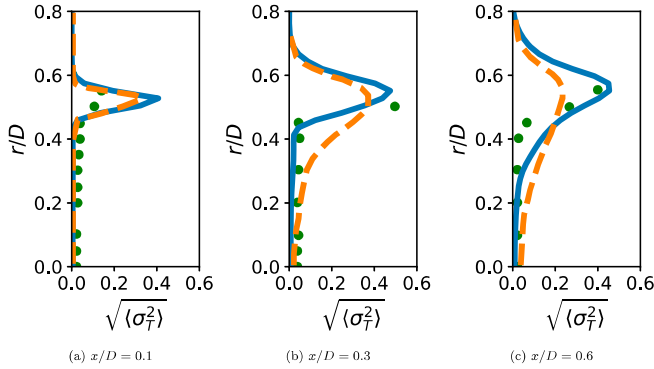


Figure 11. Normalized mean radial temperature variance profiles. For legend, see Figure 6.

trends for the flame brush thickness and no major differences in their behaviour, which is satisfactory.

The good performance of our model in the near field is also underpinned by results in Figure 11. The normalised temperature variance shown in this figure includes both the resolved and subgrid variances and is computed using $\langle \sigma_T^2 \rangle = \langle \sigma_{T,\text{res}}^2 \rangle + \langle \sigma_{T,\text{sgs}}^2 \rangle$. The mean resolved temperature variance $\langle \sigma_{T,\text{res}}^2 \rangle$ can be obtained using the computed temperature field where $\langle \sigma_{T,\text{sgs}}^2 \rangle$ is estimated using the SGS variance of the progress variable following the procedures described in [28], hence, $\langle \sigma_T^2 \rangle \approx \langle \sigma_{T,\text{res}}^2 \rangle + \langle \sigma_{c,\text{sgs}}^2 \rangle$. Both modelling approaches give very similar normalised temperature variance for the near field as shown in Figure 11a. The current model seems to give improved agreement for downstream locations as seen in Figure 11b,c. Unfortunately, no experimental data is available for axial location beyond $x/D = 0.6$ for further assessment and to draw a wider conclusion.

5.2.3. Comparison of mass fractions

A presumed PDF approach is used to obtain statistics of other thermo-chemical quantities. A Favre-filtered quantity of interest, $\tilde{\phi}$, is obtained from

$$\tilde{\phi}(X, t) = \int \int \phi(Z, c) \tilde{P}(Z, c; X, t) dZ dc, \quad (14)$$

where X denotes the position vector and t is time. This formulation is typically known as a two-variables approach. The PDF $\tilde{P}(Z, c; X, t)$ incorporates statistical information on the reacting flow and is determined from the resolved fields of mixture fraction, progress variable and the progress variable variance. Since a lean turbulent premixed flame is considered, the joint PDF becomes the marginal PDF, $\tilde{P}(c; X, t)$, of the reaction progress variable for which a bimodal interior flamelet PDF, as presented in [25], is presumed. The application of the interior flamelet PDF is limited to normalised variance values large enough to indicate bi-modal behaviour [25]. A detailed derivation for a one-step and a systematically reduced mechanism are given by Bray et al. [25] and Bray, Champion and Libby [24]. The mass-weighted PDF,

$$\tilde{P}(c; X, t) = \tilde{\alpha} \delta(c) + \tilde{\beta} \delta(1 - c) + \tilde{\gamma} \tilde{f}(c), \quad (15)$$

is based on two delta functions for fully burnt and unburnt state. The strength of the delta functions is described by $\tilde{\alpha}$ and $\tilde{\beta}$ respectively. The internal PDF $\tilde{f}(c)$ is determined from a premixed laminar flame and considers an intermediate reacting state due to finite-rate chemistry. The strength of the function $\tilde{f}(c)$ is given by $\tilde{\gamma}$. The strength of $\tilde{\gamma}$ and $\tilde{\beta}$ are determined based on functional relations with \tilde{c} and $\sigma_{c,sgs}^2$, and $\tilde{\alpha}$ is obtained using $\tilde{\alpha} + \tilde{\beta} + \tilde{\gamma} = 1$.

A comparison of radial variations of mass fractions is done for the major gas components CH_4 , CO_2 , H_2O , O_2 and CO , which are shown in Figures 12–15. The ability of the current modelling approach to predict the main species mass fractions is excellent for the region upstream of the rear stagnation point. It is interesting to note that the discrepancy between measurements and our simulations in the region downstream of the rear stagnation point is more pronounced for the species mass fractions than the temperature. A comparison to the unstrained flamelet results suggests that this might be related to the use of presumed PDF involving delta functions, as the unstrained flamelet results are also based on Equation (14) but with a Beta-PDF instead of Equation (15).

To investigate the influence of the used PDF on the results for mean species mass fractions, we have post-processed mean CO_2 mass fractions, shown as red dash-dotted lines in Figure 14, by means of Beta-PDFs generated from the first and second moment $\langle \tilde{c} \rangle$ and $\langle \sigma_c \rangle$ of the progress variable c . The Beta-PDF has the general form $\tilde{P}(c; X) = Cc^{(a-1)}(1-c)^{b-1}$, where a and b are functions of the first and second moment of c , and C is a constant ensuring that the integral of $\tilde{P}(c; X)$ is unity. A description of the Beta-PDF for progress variable is given in [25].

As becomes clear from Figure 14, the choice of PDF had a prominent effect on the predicted CO_2 mass fractions in the burnt regions of the flame. This could, to a certain extent, explain the differences in centreline temperature variation observed in Figure 6b between our and Langella's model, with the latter obtaining temperature data by means of the Beta-PDF. In Figure 14, the maximum CO_2 mass fraction post-processed from Beta-PDFs resulted in an approximately 7% reduced value compared to the result of the bimodal interior flamelet PDF. In the near-field of the flame $x/D \leq 0.6$, the predicted flame brush was not affected noticeably by the choice of PDF. Good agreement between the bimodal interior flamelet PDF and Beta-PDF results were achieved in this region. Farther away from the bluff body, the predicted burnt side ($\langle Y_{\text{CO}_2} \rangle > 0.5 \langle Y_{\text{CO}_2} \rangle_{\text{max}}$) of the flame brush was also noticeably changed by applying Beta-PDFs. The gradients characterising the flame brush became less steep departing considerably from experimental measurements and results using the bimodal interior flamelet PDF.

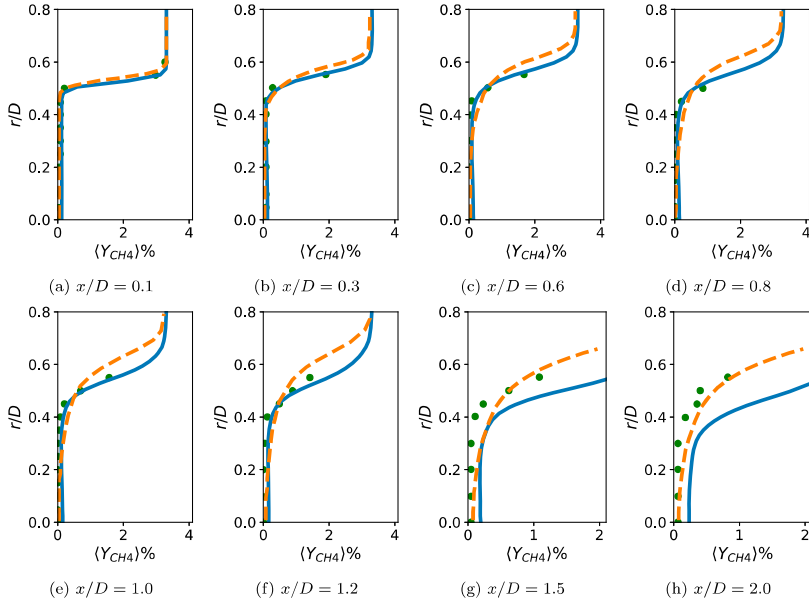


Figure 12. Radial mean CH_4 mass fraction profiles in the flame and post-flame region. Blue solid lines — denote the results of the current study using the 3.1 M grid. Orange dashed line — denote the results of the unstrained flamelet model [19]. The symbols (•) show experimental results [20,21], used in [19] for comparison.

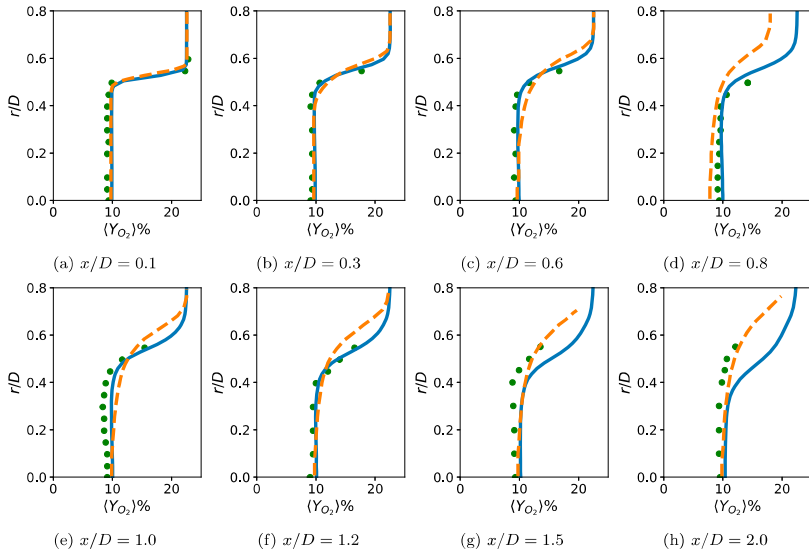


Figure 13. Radial mean O_2 mass fraction profiles. For legend, see Figure 12.

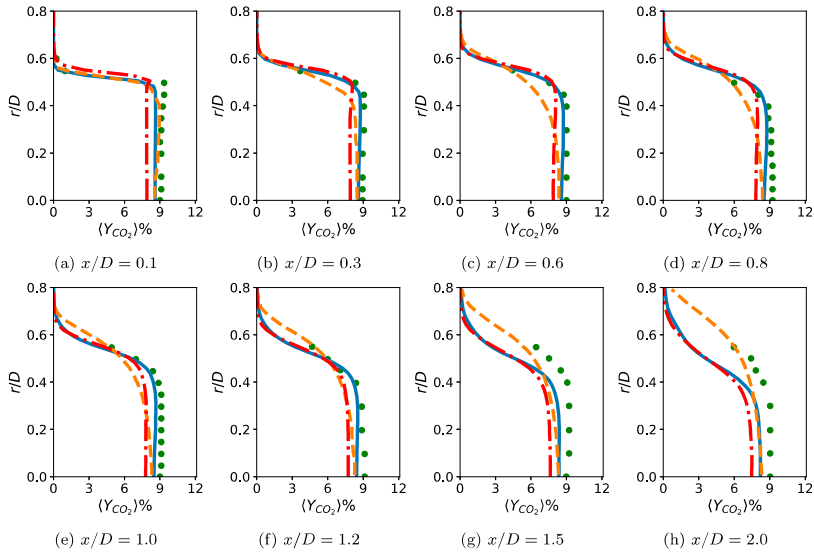


Figure 14. Radial mean CO_2 mass fraction profiles in the flame and post-flame region. Blue solid lines — denote the results of the 3.1 M mesh used for this study. Dash-dotted red-coloured lines — are post-processed results of the 3.1 M mesh using Beta-PDF. Orange dashed lines — denote the results of the unstrained flamelet model in [19]. The symbols (•) show experimental results from [20,21], used in [19] for comparison.

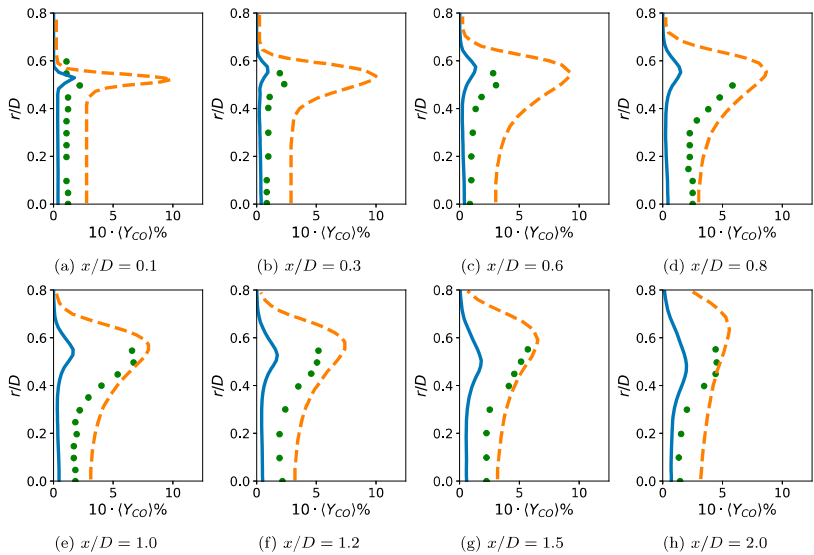


Figure 15. Radial mean CO mass fraction profiles in the flame and post-flame region. For legend, see Figure 12.

Finally, mean species mass fraction profiles for the minor species CO were available for comparison. The CO profiles close to the bluff body ($x/D = 0.1$ to $x/D = 0.6$) in Figure 15 show good agreement between experimental data and the results of our model. In this region, thin reaction zones of order of laminar flame thickness δ_{th} indicate fast chemistry largely uninfluenced by turbulence, for which the PDF used here provides very good results. Interestingly, while our model and the unstrained flamelet model performed equally well in this region for velocity, temperature and main species, very different variations between the two approaches can be observed for CO. A possible explanation could be the different choice of presumed PDF between our study and [19]. In Figure 14 it has been observed that the usage of the Beta-PDF resulted in lower predictions of CO₂ in burnt regions, which will naturally affect the presence of CO as well. The unstrained flamelet approach noticeably overestimated the presence of CO close to the bluff body, in the flame zone as well as in the burnt gas. Farther away from the bluff body, $x/D > 0.6$, the presence of large amounts of CO can be observed from experiment. For comparison, the equilibrium CO mass fraction for burnt gas at equivalence ratio 0.586 is approximately 6.8 ppm, its maximum value in a laminar unstrained premixed flame, reached at around $c = 0.81$ is approximately 1.5%. It is described in [20] that the intermediate species can be in super-equilibrium state in the investigated type of flame due to short residence times. The CO mass fraction in the region $x/D = 0.8$ to 1.5 is well captured by the unstrained flamelet model but not very well captured by our model. The influence of the choice of presumed PDF will have to be investigated further to better understand the different predictions of both compared models.

6. Conclusion

A simple algebraic closure for filtered reaction rate is proposed and tested for a lean turbulent premixed flame established behind a bluff body. The model is dissipation based but relaxed the thin flame assumption by including the finite-rate chemistry effects in small-scale turbulence structures. Statistically this corresponds to allowing for an intermediate state between the two extreme limits, unburnt and fully burnt states of the mixture. The test case is compared to measurements and to past numerical results for a careful analysis to assess the reaction rate closure proposed in this study.

The direct comparison with a well-investigated combustion model revealed competitive performance in terms of computational effort as well as the accuracy of the results. Especially along the recirculation zone, the ability of our model to capture the flame structure is quite well. The current model has a number of advantages that stood out in the comparison. First, for thin and moderately thickened flame brush the model provides excellent results. Second, the reaction rate closure has no tuneable constant. Third, the partly explicit approach to recover the temperature from the transported sensible enthalpy shows advantages over obtaining the temperature using presumed PDFs. Encouraging results are obtained for the near-field region behind the bluff body. The model yielded satisfactory results for the downstream regions, nevertheless, the comparison to the measured statistics is good showing the potential ability of this simple reaction rate closure. Further extensive tests using other flow and flame configurations with partial premixing and swirling flow conditions would be required to draw conclusions on the ability of this reaction rate closure in a wider context.

Disclosure statement

No potential conflict of interest was reported by the author(s).

Funding

The work has been funded by the Norwegian Research Council, Climit programme [project number 268368], OxyFun Fundamentals of pressurised oxy/fuel combustion. The simulations were performed on resources provided by Sigma2 - the National Infrastructure for High Performance Computing and Data Storage in Norway [project number NN9400K].

ORCID

Stefanie Tomasch  <http://orcid.org/0000-0002-9247-0418>

References

- [1] D. Veynante and L. Vervisch, *Turbulent combustion modeling*, Prog. Energy Combust. Sci. 28 (2002), pp. 193–266.
- [2] S. Cant, *RANS and LES modelling of premixed turbulent combustion*, in *Turbulent Combustion Modeling: Advances, New Trends and Perspectives*, T. Echekki and E. Mastorakos, eds., Springer Netherlands, Dordrecht, 2011, pp. 63–90.
- [3] C. Dopazo, N. Swaminathan, L. Cifuentes, and X.S. Bai, *Premixed combustion modeling*, in *Advanced Turbulent Combustion Physics and Applications*, C. Fureby, G. Brethouwer, N. Swaminathan, N.E.L. Haugen, and X.S. Bai, eds., Cambridge University Press, Cambridge, 2022, pp. 100–161.
- [4] J.F. Driscoll, *Turbulent premixed combustion: Flamelet structure and its effect on turbulent burning velocities*, Prog. Energy Combust. Sci. 34 (2008), pp. 91–134.
- [5] N. Peters, *Laminar flamelet concepts in turbulent combustion*, Proc. Combust. Inst. 21 (1988), pp. 1231–1250.
- [6] K.N.C. Bray, P.A. Libby, and J.B. Moss, *Unified modeling approach for premixed turbulent combustion-part I: General formulation*, Combust. Flame 61 (1985), pp. 87–102.
- [7] P.A. Libby and K. Bray, *Countergradient diffusion in premixed turbulent flames*, AIAA J. 19 (1981), pp. 205–213.
- [8] P.A. Libby, *Theory of normal premixed turbulent flames revisited*, Prog. Energy Combust. Sci. 11 (1985), pp. 83–96.
- [9] R.S. Cant and K.N.C. Bray, *A theoretical model of premixed turbulent combustion in closed vessels*, Combust. Flame 76 (1989), pp. 243–263.
- [10] D.B. Spalding, *Development of the eddy-break-up model of turbulent combustion*, Proc. Combust. Inst. 16 (1977), pp. 1657–1663.
- [11] K.N.C. Bray, *The interaction between turbulence and combustion*, Proc. Combust. Inst. 17 (1979), pp. 223–233.
- [12] V.A. Sabelnikov and A.N. Lipatnikov, *A new mathematical framework for describing thin-reaction-zone regime of turbulent reacting flows at low damköhler number*, Fluids 5 (2020), pp. 1–18.
- [13] S.B. Pope and M.S. Anand, *Flamelet and distributed combustion in premixed turbulent flames*, Proc. Combust. Inst. 20 (1985), pp. 403–410.
- [14] M.M. Kamal, R.S. Barlow, and S. Hochgreb, *Conditional analysis of turbulent premixed and stratified flames on local equivalence ratio and progress of reaction*, Combust. Flame 162 (2015), pp. 3896–3913.
- [15] F. Proch, P. Domingo, L. Vervisch, and A.M. Kempf, *Flame resolved simulation of a turbulent premixed bluff-body burner experiment. Part I: Analysis of the reaction zone dynamics with tabulated chemistry*, Combust. Flame 180 (2017), pp. 321–339.
- [16] P. Tamadonfar and O.L. Gülder, *Experimental investigation of the inner structure of premixed turbulent methane/air flames in the thin reaction zones regime*, Combust. Flame 162 (2015), pp. 115–128.

- [17] E. Giacomazzi and D. Cecere, *A combustion regime-based model for large eddy simulation*, *Energies* 14 (2021), pp. 1–23.
- [18] D. Butz, S. Hartl, S. Popp, S. Walther, R.S. Barlow, C. Hasse, A. Dreizler, and D. Geyer, *Local flame structure analysis in turbulent CH₄/air flames with multi-regime characteristics*, *Combust. Flame* 210 (2019), pp. 426–438.
- [19] I. Langella, N. Swaminathan, and R.W. Pitz, *Application of unstrained flamelet SGS closure for multi-regime premixed combustion*, *Combust. Flame* 173 (2016), pp. 161–178.
- [20] S. Nandula, R. Pitz, R. Barlow, and G. Fiechtner, *Rayleigh/Raman/LIF measurements in a turbulent lean premixed combustor*, in *34th Aerospace Sciences Meeting and Exhibit*, Reno, NV, 1996, 15 Jan.–18 Jan.
- [21] J.C. Pan, M.D. Vangsness, S.P. Heneghan, and D.R. Ballal, *Scalar measurements in bluff body stabilized flames using cars diagnostics*, in *ASME 1991 International Gas Turbine and Aero-engine Congress and Exposition*, Vol. 3: Coal, Biomass and Alternative Fuels; Combustion and Fuels; Oil and Gas Applications; Cycle Innovations. 1991.
- [22] J.C. Massey, I. Langella, and N. Swaminathan, *A scaling law for the recirculation zone length behind a bluff body in reacting flows*, *J. Fluid Mech.* 875 (2019), pp. 699–724.
- [23] A. Andreini, C. Bianchini, and A. Innocenti, *Large eddy simulation of a bluff body stabilized lean premixed flame*, *J. Combust.* 2014 (2014), pp. 1–18.
- [24] K. Bray, M. Champion, and P.A. Libby, *Systematically reduced rate mechanisms and presumed PDF models for premixed turbulent combustion*, *Combust. Flame* 157 (2010), pp. 455–464.
- [25] K.N.C. Bray, M. Champion, P.A. Libby, and N. Swaminathan, *Finite rate chemistry and presumed pdf models for premixed turbulent combustion*, *Combust. Flame* 146 (2006), pp. 665–673.
- [26] K.N.C. Bray, *Modelling methods*, in *Turbulent Premixed Flames*, K.N.C. Bray and N. Swaminathan, eds., Cambridge University Press, Cambridge, 2011, pp. 41–150.
- [27] T.C. Lieuwen, *Unsteady combustor physics*, Cambridge University Press, Cambridge, UK, 2012.
- [28] I. Langella, *Large eddy simulation of premixed combustion using flamelets*, Ph.D. diss., University of Cambridge, Cambridge, UK, 2016.
- [29] M. Lesieur, O. Métais, and P. Comte, *Large-Eddy simulations of turbulence*, Cambridge University Press, Cambridge, UK, 2005.
- [30] A. Yoshizawa, *Statistical theory for compressible turbulent shear flows, with the application to subgrid modeling*, *Phys. Fluids* 29 (1986), pp. 2152–2164.
- [31] S. Ruan, N. Swaminathan, and O. Darbyshire, *Modelling of turbulent lifted jet flames using flamelets: A priori assessment and a posteriori validation*, *Combust. Theory Model.* 18 (2014), pp. 295–329.
- [32] T.D. Dunstan, Y. Minamoto, N. Chakraborty, and N. Swaminathan, *Scalar dissipation rate modelling for large eddy simulation of turbulent premixed flames*, *Proc. Combust. Inst.* 34 (2013), pp. 1193–1201.
- [33] N. Chakraborty and N. Swaminathan, *Effects of lewis number on scalar variance transport in premixed flames*, *Flow Turbul. Combust.* 87 (2011), pp. 261–292.
- [34] T. Nilsson, I. Langella, N.A.K. Doan, N. Swaminathan, R. Yu, and X.S. Bai, *A priori analysis of sub-grid variance of a reactive scalar using dns data of high ka flames*, *Combust. Theory Model.* 23 (2019), pp. 885–906.
- [35] N.V. Kornev and E. Hassel, *Method of random spots for generation of synthetic turbulent fields with prescribed autocorrelation functions*, *Comm. Numer. Meth. Eng.* 23 (2006), pp. 35–43.
- [36] *OpenFOAM (field operation and manipulation)*. Available at www.openfoam.org.
- [37] S.B. Pope, *Turbulent Flows*, Cambridge University Press, Cambridge, UK, 2000.

Paper III

A numerical study of flow structures and flame shape transition in swirl-stabilized turbulent premixed flames subject to local extinction.

Stefanie Tomasch; Nedunchezhian Swaminathan; Christoph Spijker; Ivar S. Ertesvåg

To be submitted to a journal

This paper will be submitted for publication and is therefore not included.

Part III
Appendix

A Supplementary data

A.1 Cold Sydney swirl burner velocity variations

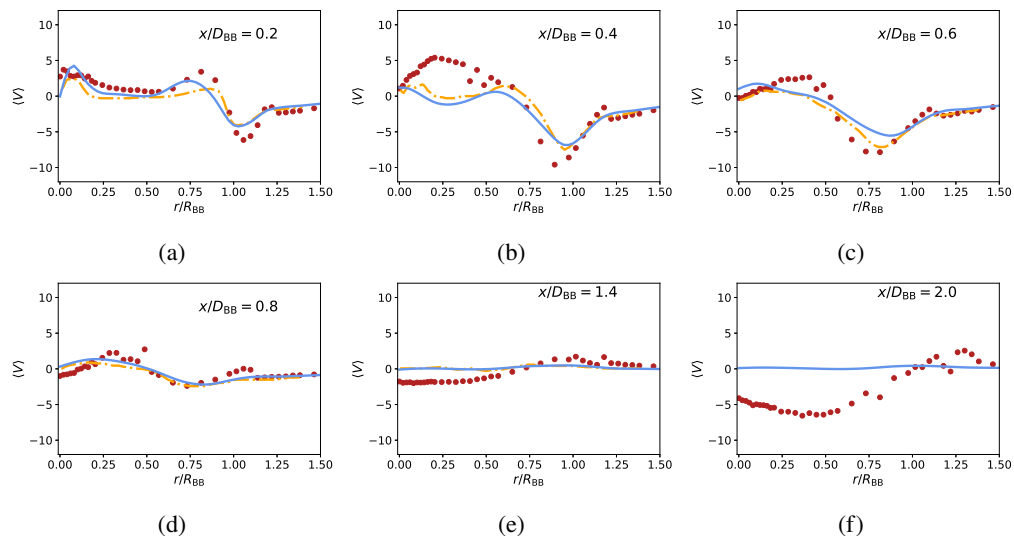


Fig. 21 Mean radial velocity variation. Red symbols \bullet denote measurement points from [98], solid blue lines — give results of the investigated $k-\omega$ SST-SAS model. Orange dash-dotted lines $\text{—}\cdot\text{—}$ represent LES results from Stein, Kempf and Janicka [105], green dashed lines --- RANS data from Yang and Kær [102].

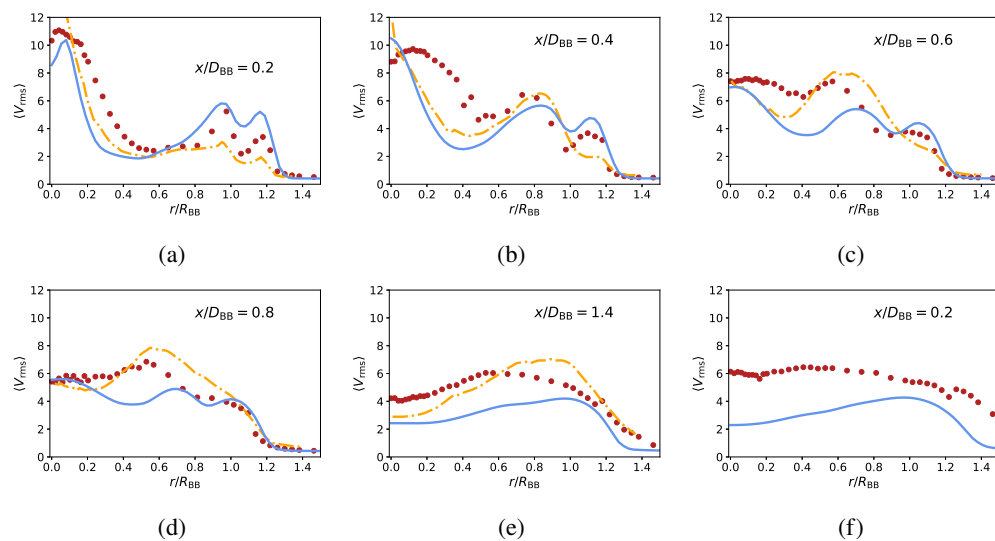


Fig. 22 RMS radial velocity variation, for legend see Fig. 21.

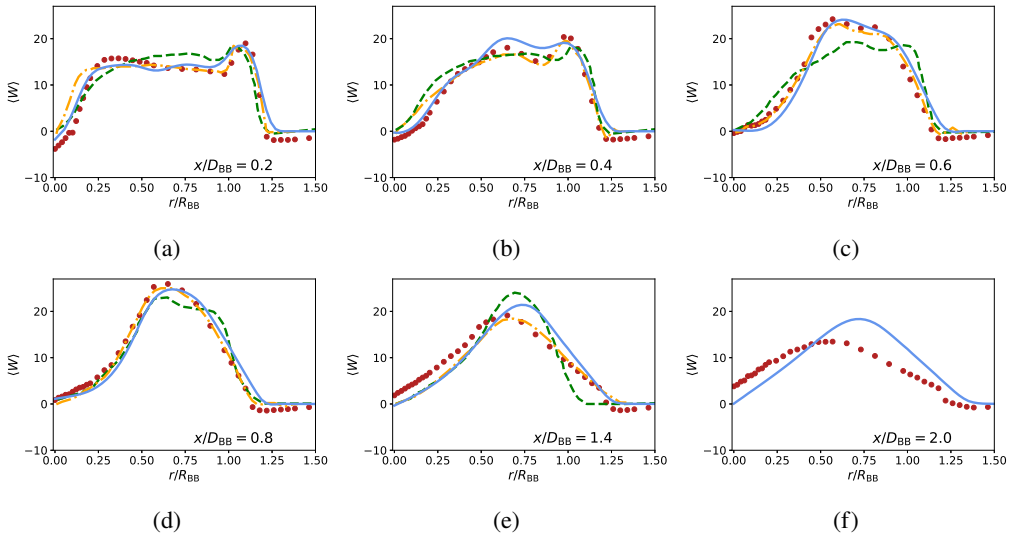


Fig. 23 Mean tangential velocity variation., for legend see Fig. 21.

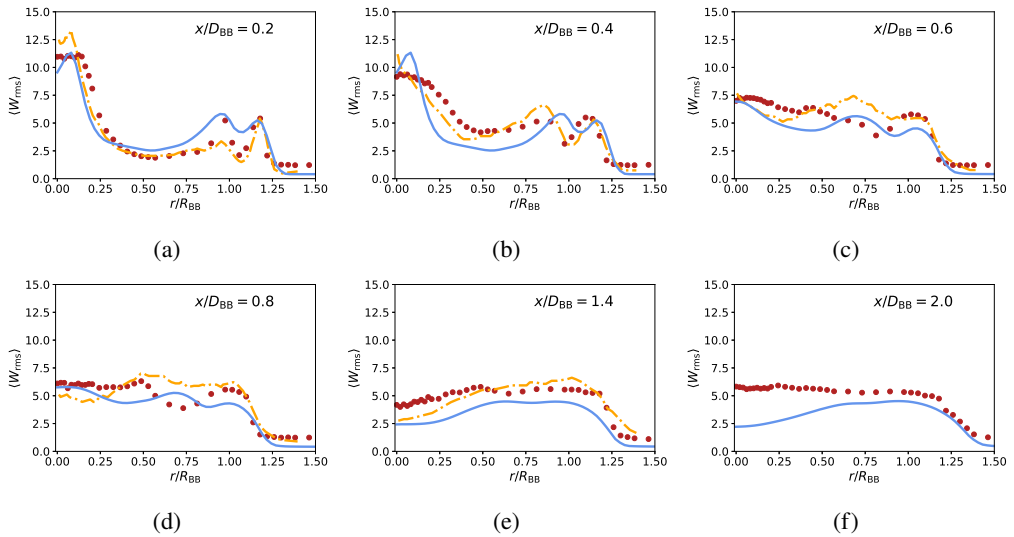


Fig. 24 RMS tangential velocity variation, for legend see Fig. 21.

A.2 Sandia Flames D

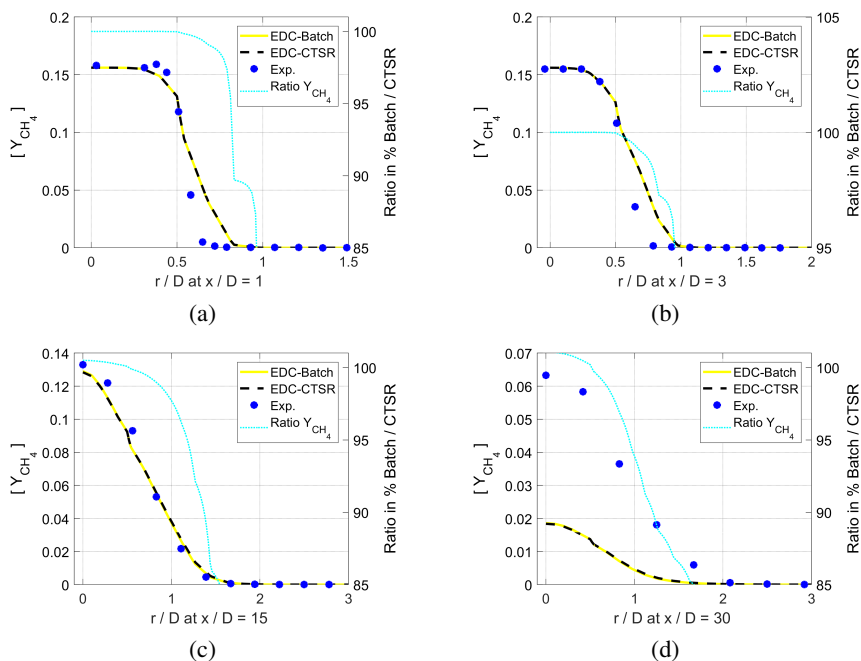


Fig. 25 Radial profiles of CH_4 mean mass fractions at varying axial positions in Flame D. Measurements are taken from [99].

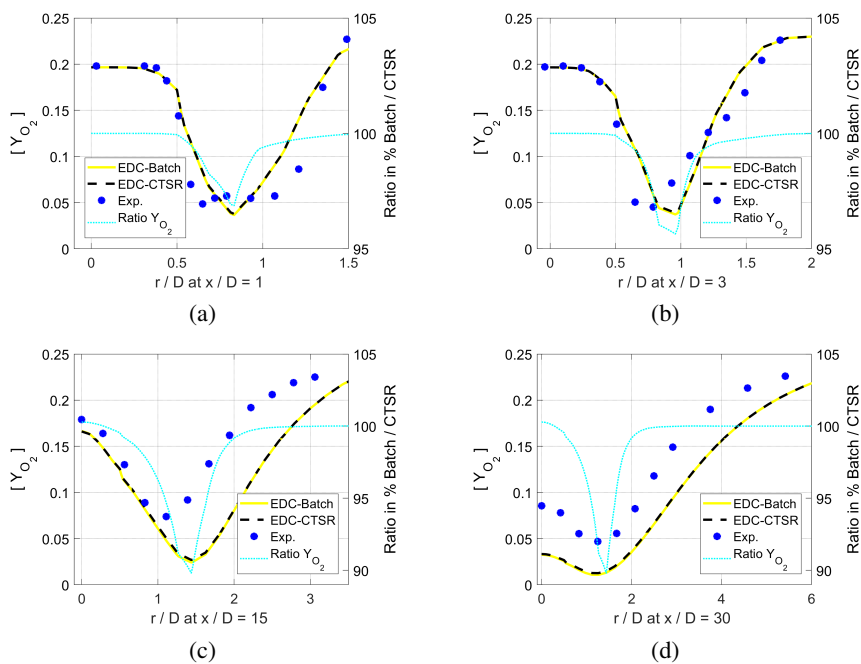


Fig. 26 Radial profiles of O_2 mean mass fractions at varying axial positions in Flame D. Measurements are taken from [99].

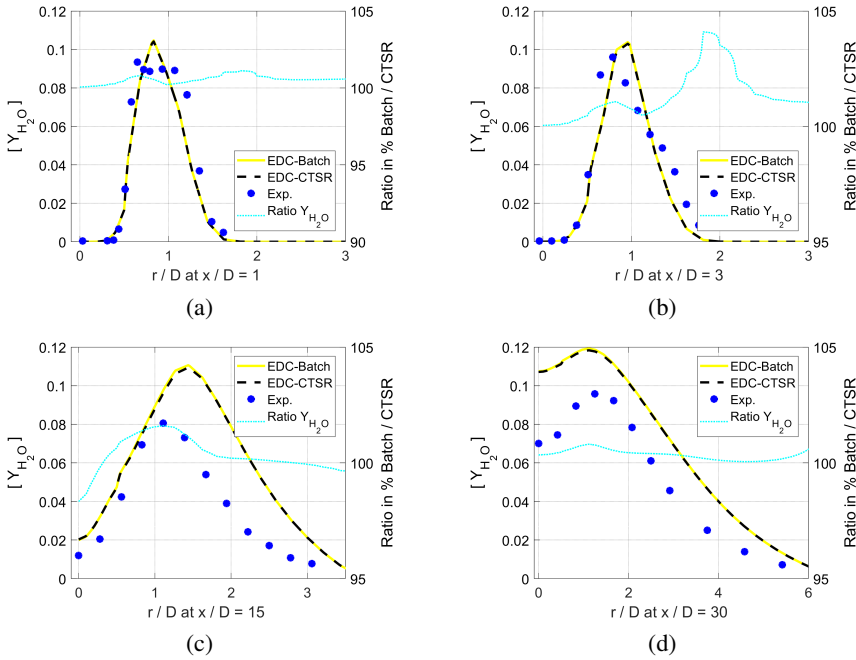


Fig. 27 Radial profiles of H_2O mean mass fractions at varying axial positions in Flame D. Measurements are taken from [99].

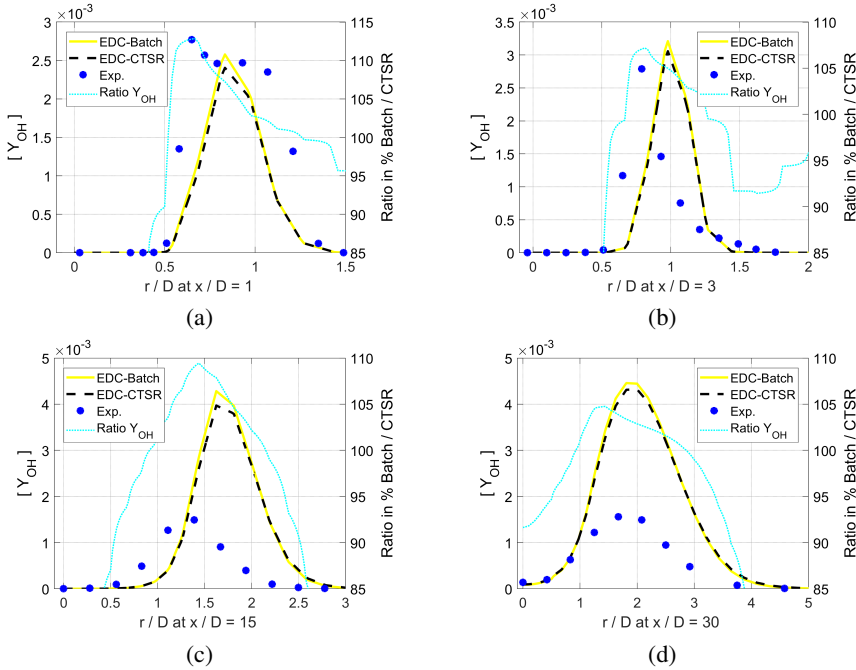


Fig. 28 Radial profiles of OH mean mass fractions at varying axial positions in Flame D. Measurements are taken from [99].

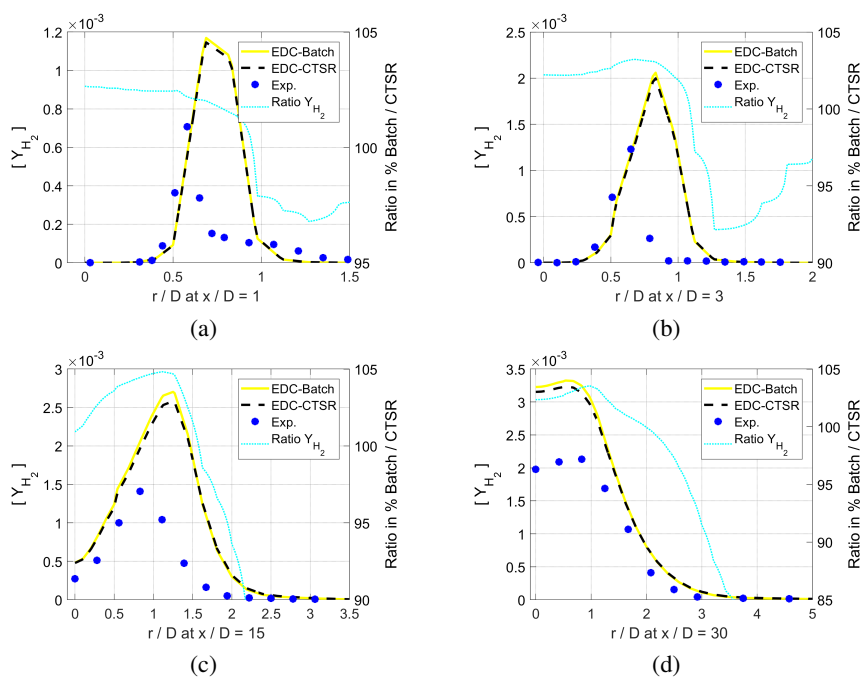


Fig. 29 Radial profiles of H_2 mean mass fractions at varying axial positions in Flame D. Measurements are taken from [99].

A.3 Swirl-stabilised oxy-fuel flame velocity variations

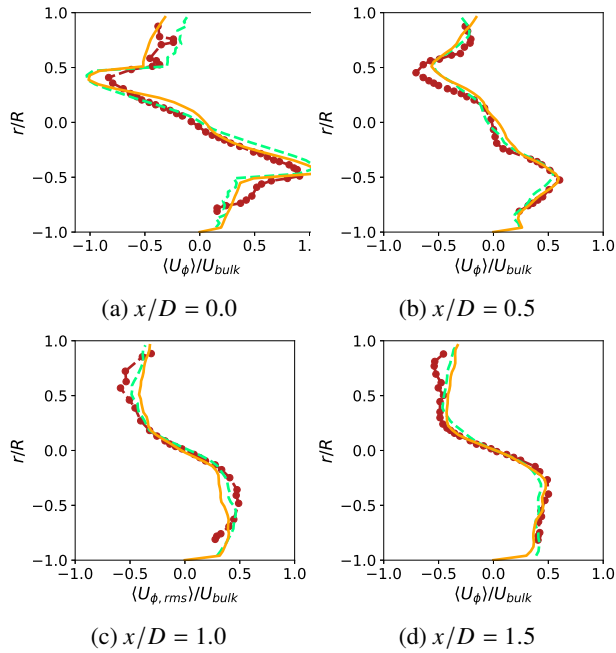


Fig. 30 Normalised mean axial velocity profiles in radial direction for the cold flow. Orange solid lines — and light green dashed lines --- denote the results for the cold flow with $\text{CH}_4/\text{O}_2/\text{CO}_2$ and CH_4/air composition. The dark red dots • connected by dashed lines are respective experimental results from [61].

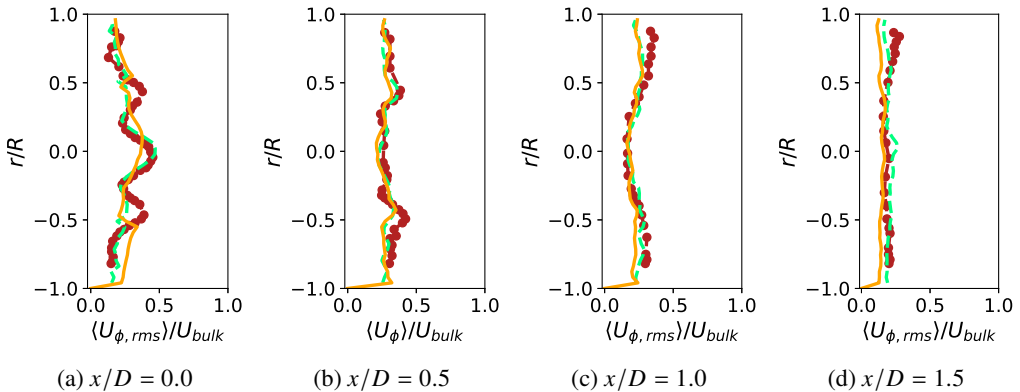


Fig. 31 Normalized rms tangential velocity variation in radial direction for the cold flow, for legend see Fig. 30.

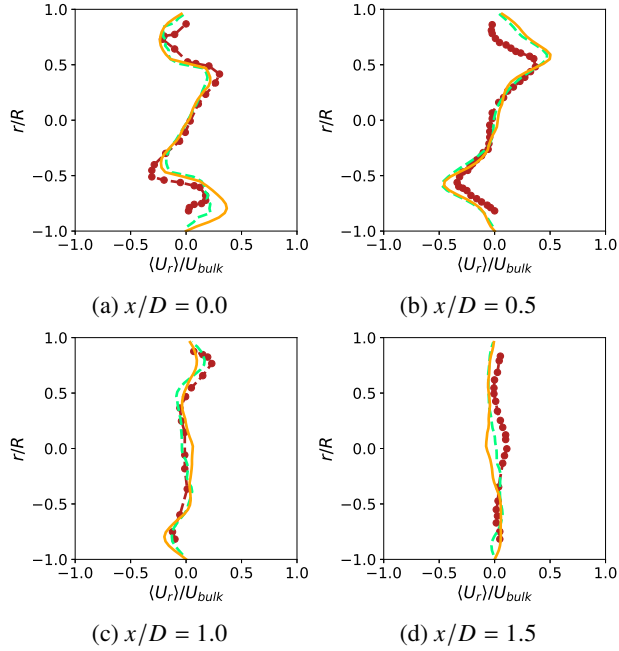


Fig. 32 Normalized mean radial velocity profiles in radial direction for the cold flow, for legend see Fig. 30.

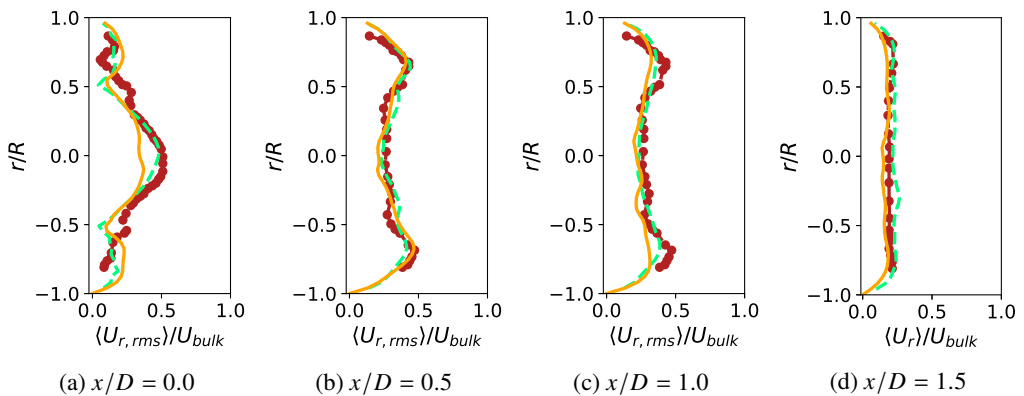


Fig. 33 Normalized rms radial velocity variation in radial direction for the cold flow, for legend see Fig. 30.

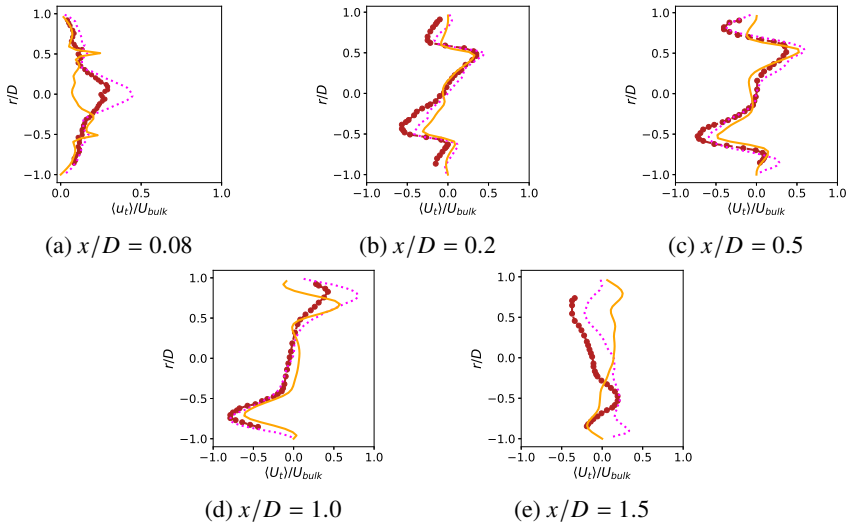


Fig. 34 Normalised mean tangential velocity profiles in radial direction for the hot flow with oxy-methane combustion at equivalence ratio $\phi = 0.65$. Orange solid lines represent simulation results of this study. The magenta dotted lines denote simulation results in [62] and the dark red dots connected by dashed lines are respective experimental results from [62].

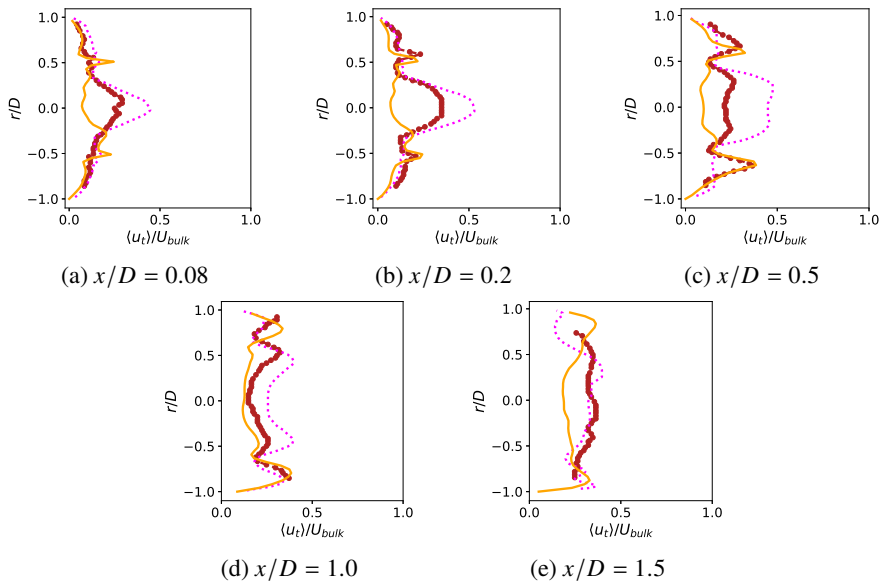


Fig. 35 Normalised rms tangential velocity profiles in radial direction for the hot flow with oxy-methane combustion at equivalence ratio $\phi = 0.65$. For legend see Figure 34.